理學博士學位論文

효모에서의 단백질 호모머 형성에 대한 글로벌 분석

Global analysis of protein homomerization in *Saccharomyces cerevisiae*

2018 年 **8** 月

서울大學校 大學院

生命科學部

김 연 수

ABSTRACT

Global analysis of protein homomerization in *Saccharomyces cerevisiae*.

Yeonsoo Kim

School of Biological Sciences

The Graduate School

Seoul National University

In vivo analyses of protein-protein interaction (PPI) occurrence, subcellular localization, and dynamics are important issues in functional proteomic researches and various PPI analyzing methods have been developed over the past decades. Bimolecular fluorescence complementation (BiFC) assay has many advantages over other research methods in that it can provide a reliable way to detect PPI in living cells with minimal perturbation of the structure and function of target proteins and it allow the visualization of subcellular localization where PPI occurs.

Previously, to facilitate the application of BiFC assay to the genome-wide analysis of PPIs, we generated a collection of yeast strains expressing full-length proteins tagged with the N-terminal fragment of Venus (VN), a yellow fluorescent protein variant, under the control of their own endogenous promoters. The VN fusion library consists of 5,911 *MAT***a** strains (representing ~95% of the yeast proteome) and was successfully exploited to screen SUMO interactome in *Saccharomyces cerevisiae*. In the present study, we constructed the VC (the C-terminal fragment of Venus) fusion library that consists of 5,671 *MAT*α strains expressing C-terminally VC-tagged proteins (representing ~91% of the yeast proteome) under their native promoters. The reliability of the constructed library was then proved by using it with VN fusion library to genome-widely detect protein

homomers in yeast. For a genome-wide analysis of protein homomer formation, we mated each strain of the VC fusion library with its cognate strain of the VN fusion library and performed BiFC assay. Through this analysis, we identified 186 homomer candidates, 104 of which are previously unknown homomers. Subcellular localization, highly enriched gene ontology (GO) and changes of homomeric interaction upon nitrogen starvation was further analyzed to characterize homomer population of yeast. Out of 186 protein homomers identified in this study, Pet10, a protein of unknown function which localize to lipid droplet, was further investigated for its functional relevance of homomerization and lipid accumulation. Our data set represents a useful resource for understanding the physiological roles of protein homomerization. Furthermore, thoroughly examined credibility and feasibility of the VC fusion library together with the VN fusion library in BiFC assay revealed that this system will provide a valuable platform to systematically analyze PPIs in the natural cellular context.

Key words: bimolecular fluorescence complementation, protein-protein interaction, protein homomerization, Saccharomyces cerevisiae, Pet10, lipid metabolism.

Student number : 2010-20309

CONTENTS

ABSTRACT ..... **i**

CONTENTS ..... **iii**

LIST OF FIGURES ..... **vi**

LIST OF TABLES ..... **viii**

ABBREVIATIONS ..... **ix**

CHAPTER I. Introduction **1**

1. Study of protein-protein interaction 2

1.1. Interaction study as a tool to understand biological phenomenon 2

1.2. Bimolecular fluorescence complementation (BiFC) assay 5

1.3. Advantages and disadvantages of BiFC assay 13

1.4. Application of BiFC assay for large-scale studies 16

2. Protein homomerization 22

2.1. Biological meaning of protein homomerization 22

2.2. Importance of protein homomerization study 23

3. Aim of this study 25

CHAPTER II. Construction of VC library to facilitate large-scale BiFC assay **27**

1. Introduction 28

2. Materials and Methods 30

2.1. Yeast strains and culture conditions 30

2.2. Construction of plasmids 30

2.3. Transformation of yeast cells 34

2.4. Mating type switching 34

2.5. Vector elimination 34

2.6. Western blot analysis 35
3. Results 36
3.1. Construction of VC fusion library *MAT***a** 36
3.2. Construction of VC fusion library *MAT*α 38
4. Discussion 43

CHAPTER III. Global analysis of protein homomerization in *S. cerevisiae* 45
1. Introduction 46
2. Materials and Methods 48
2.1. Yeast strains and culture conditions 48
2.2. Amplification of PCR fragment 48
2.3. Transformation of yeast cells 48
2.4. Microscopic analysis and fluorescence quantification 55
2.5. Spot assay 55
2.6. Western blot analysis 55
2.7. Co-immunoprecipitation assay 56
2.8. Flow cytometry 57
3. Results 58
3.1. Genome-wide screening of protein homomers by BiFC using the VC and VN fusion libraries 58
3.2. Characterization of protein homomers 70
3.3. Changes of homomerization signal upon nitrogen deprivation 82
4. Discussion 97

CHAPTER IV. Homomerization of Pet10 and its physiological effects 101
1. Introduction 102
2. Materials and Methods 104
2.1. Yeast strains and culture conditions 104
2.2. Amplification of PCR fragment 104

2.3. Construction of plasmids 104
2.4. Transformation of yeast cells 109
2.5. Microscopic analysis and fluorescence quantification 109
2.6. Western blot analysis 110
2.7. Co-immunoprecipitation assay 110
2.8. FCH and PCH 111
2.9. TAG quantification assay 112
3. Results 113
3.1. Increased homomerization of Pet10 upon nitrogen deprivation 113
3.2. Finding novel interactors 115
3.3. Involvement of Pet10 in lipid metabolism 124
4. Discussion 130
CHAPTER V. Conclusion 133
References 141

LIST OF FIGURES

Figure I-1. Principles of BiFC (Bimolecular fluorescence complementation) assay 6

Figure II-1. Scheme of construction of the *MAT*a and *MAT*α VC fusion library 37

Figure II-2. The number of yeast ORFs each type of VC library covers 39

Figure II-3. Confirmation of proper VC tagging and expression of tagged proteins by western blot analysis 41

Figure II-4. Strategy for genome-wide analysis of PPIs using the *MAT*α VC fusion library and the *MAT*a VN fusion library 42

Figure III-1. Scheme of genome-wide BiFC analysis of protein homomers 59

Figure III-2. Examples of self-assembly signals 60

Figure III-3. BiFC images of homomer candidates with diverse subcellular localizations and composition of homomer candidates 61

Figure III-4. Co-IP assay of homomer candidates 68

Figure III-5. Results of Co-IP verification and comparison of expression level 69

Figure III-6. BiFC analysis of Rad52 homomer 71

Figure III-7. Spot assay for growth phenotypes of VN/VC-tagged and VC/VC-tagged diploids 72

Figure III-8. Comparisons of protein homomer datasets 74

Figure III-9. Enrichments of subcellular localization with protein homomers 76

Figure III-10. BiFC and RFP images of homomer candidates and marker proteins 77

Figure III-11. Comparison of localization between BiFC and GFP signals 83

Figure III-12. Protein homomers showing increased BiFC signals upon nitrogen starvation 85

Figure III-13. Increased of homomerization upon nitrogen starvation 86

Figure III-14. Protein homomers showing decreased BiFC signals upon nitrogen starvation 87

Figure III-15. Decreased of homomerization upon nitrogen starvation 88

Figure III-16. Flow cytometry to detect fluorescence changes of homomer candidates 90

Figure III-17. Co-IP assays to determine homomeric states under two conditions 91

Figure III-18. Localization changes of homomers upon nitrogen starvation 92

Figure III-19. Localization changes of GFP signals upon nitrogen starvation 93

Figure IV-1. Homomerization of Pet10 under normal and nitrogen starvation condition 114

Figure IV-2. PCH analysis of Pet10-GFP and free GFP 116

Figure IV-3. PCH analysis of Pet10-GFP under normal and nitrogen starvation condition 117

Figure IV-4. Interaction of Pet10 with Fas1, Fas2 in normal and nitrogen-deprived condition detected by BiFC assay 119

Figure IV-5. Interaction of Pet10 with Fas1, Fas2 in normal and nitrogen-deprived condition detected by Co-IP assay 120

Figure IV-6. Interaction between Pet10 and Slc1 detected by BiFC 121

Figure IV-7. Increased homomeric signal of LZ-Pet10 125

Figure IV-8. Localization of LZ-Pet10 and Hsp104 126

Figure IV-9. Comparison of interacting signal of Pet10-Fas1/Fas2 and LZ-Pet10-Fas1/Fas2 127

Figure IV-10. Triacylglycerol quantification 129

LIST OF TABLES

TableI-1. Fluorescent proteins applied for BiFC assays 7

Table II-1. Strains used in this study 31

Table II-2. Oligonucleotide primers used in this study 32

Table II-3. Plasmids used in this study 33

Figure III-1. Strains used in this study 49

Figure III-2. Oligonucleotide primers used in this study 52

Figure III-3. Protein homomer candidates identified in this study 62

Figure III-4. Gene ontology analysis of protein homomers 78

Figure III-5. Protein homomers showing changes in the BiFC signal intensity upon N starvation 94

Figure III-6. Protein homomers showing changes in the BiFC signal localization upon N starvation 96

Figure IV-1. Strains used in this study 105

Figure IV-2. Oligonucleotide primers used in this study 107

Figure IV-3. Proteins analyzed for interaction with Pet10 by BiFC assay.....122

ABBREVIATION

BiFC	Bimolecular fluorescence complementation
PPI	Protein-protein interaction
PCA	Protein complementation assay
VC	C-terminal fragment of Venus
VN	N-terminal fragment of Venus
FN	N-terminal fragment of fluorescent protein
FC	C-terminal fragment of fluorescent protein
ORF	Open reading frame
LZ	Leucine zipper
TAG	Triacylglycerol
FAS	Fatty acid synthase
GFP	Green fluorescent protein
YFP	Yellow fluorescent protein
EYFP	Enhanced yellow fluorescent protein
RFP	Red fluorescent protein
IP	Immunoprecipitation
TAP	Tandem affinity purification
GO	Gene ontology
5-FOA	5-Fluoroorotic acid
HO	Homothallic switching endonuclease
DMSO	Dimethyl sulfoxide
FCS	Fluorescence correlation spectroscopy
PCH	Photon counting histogram
cpsm	Counts per second per molecule

a.u.	Arbitrary unit
SD	Standard deviation
IB	Immunoblot
Y2H	Yeast two hybrid
AP/MS	Affinity purification/Mass spectrometry
MYTH	Membrane yeast two hybrid
FRET	Fluorescence resonance energy transfer

Chapter I. Introduction

1.Study of protein-protein interaction

1.1. Interaction study as a tool to understand biological phenomenon

Genetic information preserved and transmitted in living organisms is ultimately expressed and function in forms of protein. Most phenomena that take place in living organism such as cytoskeletal organization, response to stimulation, various signal transduction are mediated by proteins, so uncovering function of protein is essential for understanding biological processes. Notably, most proteins do not act alone. They work with other proteins to form protein complexes and often their interactions are necessary for proper functions of the proteins. Thus, finding interaction partners of a target protein is a good way to find out what the target protein do and how they are regulated. the function of the target protein.

Because of this importance, experimental methods for analyzing protein-protein interactions (PPIs) have also been developed with the history of life sciences. Immunoprecipitation is one of the most popular analytical methods to be used on this purpose. Immunoprecipitation is based on the principle that, when an antibody is used to purify a specific protein, other proteins that form complexes with the target proteins are refined together. When protein X and Y interact each other, a complex precipitates of protein X, Y, and antibody can be obtained by using anti-protein X antibody. Obtained precipitates are then separated by electrophoresis and detailed information about protein Y can be analyzed. Because of this importance, experimental methods for analyzing protein interactions have also been developed with the history of life sciences. Immunoprecipitation is one of the most popular analytical methods to be used on this purpose. Immunoprecipitation is based on the principle that, when an antibody is used to purify a specific protein, other proteins that form complexes with the target proteins are

refined together. When protein X and Y interact each other, a complex precipitates of protein X, Y, and antibody can be obtained by using anti-protein X antibody. Obtained precipitates are then separated by electrophoresis and detailed information about protein Y can be analyzed. In recent years, mass spectrometric analysis technology of separated proteins became very precise, enabling hundreds to thousands of proteins which were separated by immunoprecipitation method to be analyzed for their interacting proteins as described in various studies. (Gavin et al. 2002; Ho et al. 2002; Krogan et al. 2006)

Yeast two-hybrid is another commonly used method in analyzing protein-protein interactions (Bruckner et al. 2009). Unlike the immunoprecipitation by which interactions are analyzed in extracellular environment, with yeast two-hybrid, it is possible to observe interactions in a living cell by checking whether reporter gene is transcribed or not. For example, Gal4 transcription factor is split into two fragments, DNA binding domain and activation domain, and each domain is fused to proteins of interest. When fused target proteins interact, then separated two domains of Gal4 transcription factor reconstituted because of close proximity induced by interaction. This reconstitution of transcription factor takes place upstream of promoter region of reporter gene where upstream activator sequence (UAS) is inserted, and as a result, reporter gene is expressed. In previous research, 4,549 interactions among 3,278 proteins were identified by using this analyzing system (Ito et al. 2001).

Another widely exploited analyzing method is fluorescence resonance energy transfer (FRET) (Clegg 1995). Fluorescent proteins absorb light of a specific wavelength range and are excited, and when the energy is radiated to light or heat, they restored to base states emitting light of a unique wavelength. In FRET, two different fluorescent proteins are fused to proteins of interest and if these fluorescent proteins are within a range of 10 to 100 Å because of interaction of their fused proteins, light emitted after excitation of a

short wavelength fluorescent protein induces excitation of a long wavelength fluorescent protein so we can detect fluorescence signal from the long wavelength fluorescent protein. For example, a fluorescent protein that is excited at a wavelength of 488 nm emits fluorescence at a wavelength of 520 nm, which in turn stimulates another fluorescent protein that is paired and emits fluorescence at a wavelength of 630 nm. Therefore, the interaction of the two proteins can be analyzed by exciting at 488 nm and detecting fluorescence at the 630 nm. This system was successfully used to analyze the interaction between calmodulin and calmodulin-binding peptides (Miyawaki et al. 1997).

All protein-protein interaction analyzing methods mentioned above have their limitations, however. In case of immunoprecipitation, since the assay is carried out in in vitro conditions, they often show different results from the actual interacting status presented in vivo. Also, there is a high possibility of loss in the process of protein purification, it is usually difficult to detect unless they are strongly bonded interactions. Yeast two-hybrid can observe protein interactions in living cells, but it uses transcription factor as an indicator of interaction occurrence, so it is not suitable for proteins that are localized outside of nucleus. Finally, FRET can be utilized to detect interactions in living cells independent of where proteins are localized, but it often requires overexpression of target protein to make subtle changes of fluorescence signal noticeable. In addition, this assay demands relatively high-cost equipment. all PPI detection methods have pros and cons. Because of pros and cons explained above, all PPI detection methods each favor different kinds of PPIs so interaction detected in one method did not show any positive result in different assay. Therefore, it is important to apply various methods to minimize missing PPIs. BiFC (Bimolecular fluorescence complementation) assay is one of good examples of PPI detection methods which have several advantages over others and thus enables revealing of novel PPIs that were not detectable in previous studies.

1.2. Bimolecular fluorescence complementation (BiFC) assay

Bimolecular fluorescence complementation (BiFC) assay is one of PCA (protein complementation assay) methods in which a reporter is cut in half and fused to two proteins of interest. When two proteins interact each other, the fused complementary fragments come close enough to recover proper folding or assembly and thus are able to reconstitute reporter activity. In BiFC assay, fluorescent proteins are used as reporter proteins as described in Figure I-1. Fluorescent protein is split into its N-terminal and C-terminal non-fluorescent fragments and each fragment are fused N- or C-terminally to target proteins. If target proteins interact and provide close proximity between the two fragments, then fragments can recover their intact structure of fluorescent proteins so we can detect fluorescence signal by appropriate detection equipment such as fluorescent microscope or flow cytometry. This is very unique and convenient tool because it allows direct visualization of PPIs in living cell without any other special treatment, and not only occurrence but also subcellular localization of interaction can be examined when proper fluorescent microscope is available.

Many different kinds of fluorescent proteins have been developed and proved to be suitable for BiFC assay in various model organisms to date, as summarized in Table I-1. GFP (Green fluorescent protein) is the first fluorescent protein applied for the BiFC assay (Ghosh et al. 2000). GFP split between residues 157 and 158 (NGFP and CGFP) were tested for their recovered folding and fluorescence and revealed that weak interactions with the minimum dissociation constant estimated KD ≈ 1 mM were detectable (Magliery et al. 2005). A GFP-based BiFC assay was also used to find interactor candidates of protein kinase B (PKB)/Akt (Remy and Michnick 2004a). A human brain cDNA library was fused to N-terminal GFP fragment (1-158) and PKB cDNA was fused to the C-terminal GFP (159-238), and physical interactions in COS-1 cells were screened by flow

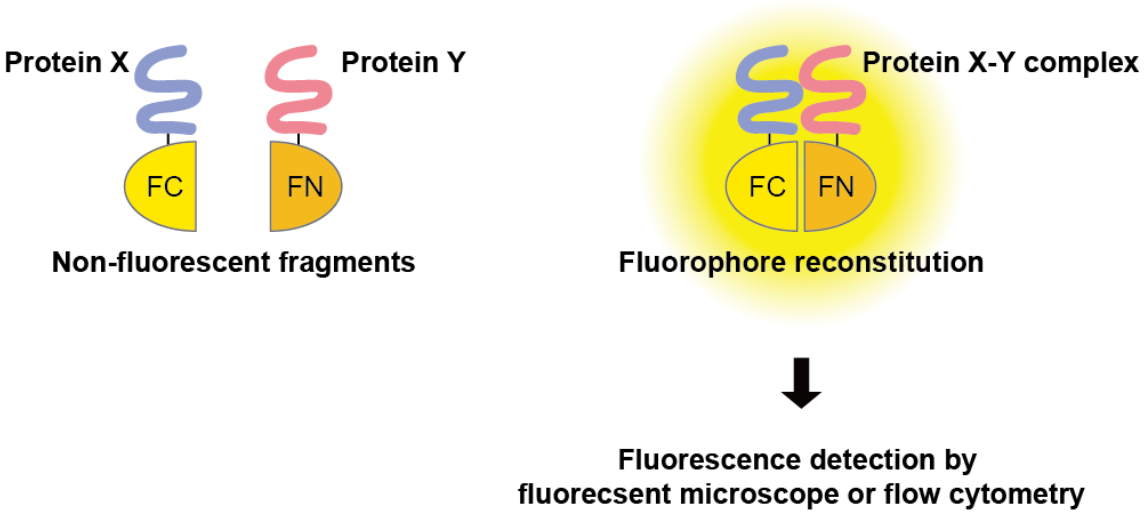

Figure I-1. Principles of BiFC (Bimolecular fluorescence complementation) assay.

The illustration describes basic principle of BiFC assay in the detection of protein-protein interaction. Non-fluorescent fragments generated by splitting fluorescent protein into N-terminal and C-terminal parts (which are designated as FN and FC in this figure) are fused to either N- or C-terminus of proteins of interest (which are designated as Protein X and Protein Y in this figure). When Protein X and Y do not interact each other, then distance between FN and FC is far enough so that they remain as non-fluorescent fragments. When Protein X and Y interact, FN and FC comes to each other and reconstitute a stable fluorophore, and the resulting fluorescence signal can be detected by proper equipment such as fluorescent microscope or flow cytometry. Any fragment pair of fluorescent proteins described in this chapter can be used as FN and FC and VN, VC fragments originated from Venus protein were used in this study.

Table I-1. Fluorescent proteins applied for BiFC assays.

Fluorescent protein	Excitation/ Emission (nm)	Split site	Temperature sensitivity of maturation	Interactions tested	Reference
EYFP	514/527	154/155	Poor maturation at 37°C	bJun-bFos ATF2-Jun p50-p65 p50-Jun p50-Fos p65-Jun p65-Fos p65-IκBα	(Hu et al. 2002)
Venus	514/529	154/155 172/173	-	bJun-bFos	(Shyu et al. 2006)
Citrine	516/528	154/155 172/173	-	bJun-bFos	(Shyu et al. 2006)
ECFP	452/478	154/155 172/173	Poor maturation at 37°C	bJun-bFos bATF2-bJun	(Hu and Kerppola 2003)
Cerulean	439/479	172/173	-	bJun-bFos	(Shyu et al. 2006)
EGFP	473/505	157/158	-	Z peptides TPR domains-Hsp90 TPR domains-Hsc70	(Ghosh et al. 2000; Magliery et al. 2005)
mRFP1-Q66T	549/570	168/169	Poor maturation at 37°C	hrGFP GC3-CPC BP/KNAT1-BLH7	(Jach et al. 2006)
mCherry	587/610	159/160	Poor maturation at 37°C	EGFP LTag-p53	(Fan et al. 2008)
mLumin	587/621	151/152	-	bJun-bFos EGFR-STAT5A EGFR-STAT5B	(Chu et al. 2009)
mNeptune	600/650	155/156	-	EGFP bJun-bFos	(Han et al. 2014)
Dronpa	503/518	164/165	-	hHus1-hRad1	(Lee et al. 2010)
iRFP	690/713	120/123	-	FRB-FKBP	(Filonov and Verkhusha 2013)

cytometry. In contrast, GFP fragments split between residues 154 and 155 did not properly reassemble and fluoresce when tested in mammalian cells (Hu and Kerppola 2003) or budding yeast (Sung and Huh, unpublished observation), indicating that fragments generated by cutting at appropriate site are crucial in BiFC application.

The first validation of YFP (Yellow fluorescent protein) fragments for a BiFC assay was demonstrated in a study of Ca^{2+}-dependent PPIs in living cells (Nagai et al. 2001). N-terminal fragment (1-144) of EYFP (V68L, Q69K) was fused to calmodulin and C-terminal fragment (145-238) was fused to M13 calmodulin binding peptide in HeLa cells, and fluorescent signals produced by them showed the reversible association in response to changes of intracellular Ca^{2+}. Kerppola and colleagues divided EYFP (S65G, S72A, T203Y) into two fragments at several non-conserved amino acid residues and fused them to bJun and bFos, the basic leucine zipper domains of Jun and Fos (Glover and Harrison 1995), and found out that YFP fragments split between amino acid 154 and 155 showed the brightest fluorescence (Hu et al. 2002). In spite of its brightness, EYFP was sensitive to pH and required pre-incubation at low temperatures before visualization (Llopis et al. 1998) and few YFP variants have been developed to resolve these weak points. Citrine, a YFP variant carrying Q69M mutation, showed relieved pH sensitivity (Griesbeck et al. 2001) and Venus, a YFP variant carrying F46L mutation, folds well even at 37°C (Nagai et al. 2002). Both were successfully applied for BiFC assays in COS-1 cells (Shyu et al. 2006), with Citrine split at D155 and Venus split at D173 showing significantly increased BiFC efficiency compared to EYFP. Venus is the most widely used fluorescent protein for BiFC assays to date, including this study.

There are also a series of CFP variants for use in BiFC assays. The N- and C-terminal fragments of CFP split between amino acids 154 and 155 showed fluorescence complementation when fused to bJun and bFos (Hu and Kerppola 2003). More

interestingly, C-terminal 155 fragment (CC155) can form complemental complex with YN155, and the fluorescent spectrum of this pair is different from those of YN155-YC155 and CN-155-CC155. Also, YC173 can complement with CN173 and in case of CC155, it can fluoresce with YN173 and CN173. This finding opened up the possibility to use different fluorescent proteins together for a multicolor BiFC assay, a method for simultaneous visualization of multiple protein interactions in living cells. Cerulean, an improved CFP variant with point mutations S72A, Y145A and H148D, showed increased quantum yield (Rizzo et al. 2004) and was successfully applied for BiFC assay (Shyu et al. 2006) in COS-1 cells.

Many proteins usually have several binding partners, so multicolor BiFC analysis can provide an effective assay to compare the subcellular distributions of protein complexes formed with different binding partners. Also, multicolor BiFC allows analysis of the competition between different binding partners for binding to a shared partner (Kerppola 2013). By combining single- and multi-color BiFC and co-localization analyses with proper markers, the previous study showed that Ypt1 interacts with Trs85, forming a few fluorescent puncta, one of which co-localizes with the Ypt1-Atg11 BiFC complex in the PAS, which appears as one dot per cell (Lipatova et al. 2012). Another study used multicolor BiFC analysis to determine the association preferences of b and g subunits of G protein in human embryonic kidney (HEK) 293 cells (Hynes et al. 2008). In plant cells, multicolor BiFC analysis was used to show the interaction between a protein kinase CIPK24 and its binding partners – CBL1 and CBL10, simultaneously in distinct subcellular localization (Waadt et al. 2008). Cerulean- and Venus-based BiFC systems have been also used in combination with an RFP-based BiFC system for multicolor BiFC assays. Despite of its usefulness for detection of multiple protein interactions, multicolor BiFC assay has some limitations. For example, it is possible that different fluorescent

protein fragments fused to alternative partners may affect efficiency of BiFC complex formation (Kerppola 2013). For this reason, it is important to choose appropriate fluorescent protein fragments which do not present significant difference in the rate of reconsituion. And because BiFC complex formation is generally irreversible, multicolor BiFC assay cannot represent binding affinity of alternative partners in equilibrium. Nevertherless, multicolor BiFC analysis can be cost-effective and timesaving because two interactions are examined simultaneously.

To extend the wavelength range for BiFC assays, a red fluorescent protein DsRed (Matz et al. 1999) became an object of attention after successful applications of YFP and CFP variants for BiFC assay. DsRed itself could not be used immediately because of its strong tendency to oligomerize (Baird et al. 2000), and an effort to compensate this problem resulted in the development of a monomeric RFP, mRFP1 (Campbell et al. 2002). But it was still not appropriate for BiFC assay because of its weak fluorescence intensity and low photostability, so mRFP1-Q66T with improved fluorescence intensity was first proved to be applicable for BiFC assay in tobacco protoplasts by using humanized Renilla GFP (hrGFP) as fused target protein. The mRFP1-Q66T-based BiFC assay was sensitive enough to catch weak and transient PPIs and shows a distinct increase in alkaline conditions. The mutant monomeric RFP mCherry (Shaner et al. 2004) with excitation and emission wavelength at 587/610 nm was also been studied for BiFC system. N-terminal fragment MN159 and C-terminal fragment MC160 could make fluorescence signal by dimerization of EGFP or interaction between SV40 large T antigen (LTag) and human p53 protein in Vero cells (Zacharias et al. 2002). In this study, the interaction between LTag and p53 as well as the interaction between sp100 and promyelocytic leukemia protein (PLM) were simultaneously visualized by co-expressing MN159, VN160-tagged LTag and p53 and VN172- and VC173-tagging PLM and sp100 in Vero cells. This

demonstrated the fact that mCherry-based BiFC system can be applied for multicolor BiFC assay when coupled with YFP-based BiFC, as mentioned above.

Although various kinds of fluorescent proteins have been developed and proved to be appropriate for the BiFC application, still fluorescent proteins with emission spectra in the far-red wavelengths are required to analyze images of deep tissues in animals. For this, mKate, a monomeric form of Katushka which is a far-red fluorescent protein with fast maturation and high photostability (Shcherbo et al. 2007), was studied to develop an RFP-based BiFC system that is applicable at higher temperature, but it turned out that mKate itself showed a relatively low fluorescence intensity, which was only about 25% of Venus protein. A S158A mutation of mKate was found to be increased in the brightness by 2-fold, so this variant was designated as mLumin, and it has an emission maximum of 621 nm of wavelength at 37°C, thus enabling BiFC assay in mammalian cells (Chu et al. 2009). N- and C-terminal fragments of mLumin were used to visualize interaction between EGFP and STAT4 in COS-7 cells. Also, mLumin could be combined with Ceruean- and Venus-based BiFC systems to simultaneously visualize multiple pairs of PPIs in the same study.

For a BiFC assay in animal tissue to work, fluorescent proteins need to meet particular criterion. Light below 600 nm of wavelength is absorbed by hemoglobin (Stamatas et al. 2006), and light above 1200 nm is absorbed by water molecules (Tromberg et al. 2000). To meet these conditions, fluorescent proteins having excitation wavelength above 600 nm, which is even longer than those of mCherry and mLumin described above, are required in animal tissues. So further mutations of mKate were tested and Neptune, the first fluorescent protein with excitation peak reaching 600 nm, was generated, and its monomeric variant mNeptune with excitation and emission wavelength of 600 and 650 nm was applied for BiFC assay in animal tissues (Lin et al. 2009). N-terminal and C-

terminal fragments of mNepture (MN155 and MC156, respectively) could successfully visualize dimerization of fragment-fused EGFP in HeLa cells by producing a bright red fluorescent signal, demonstrating the validity of mNeptune-based BiFC assay, and it was further exploited to detect interaction between bFos and bJun in living mice (Han et al. 2014).

A fluorescent protein that can be used as a BiFC reporter protein with even longer excitation and emission spectra which is optimal for animal imaging has been developed in a recent study (Filonov and Verkhusha 2013). The near-infrared fluorescent protein iRFP exhibits high fluorescence intensity and low cytotoxicity and uses endogenous concentrations of biliverdin chromophore to obtain its fluorescence. Then, iSplit with increased brightness compared to the split iRFP, was generated by introducing a polypeptide break into iRFP between the PAS domain (amino acids 1-120) and GAF domain (amino acids 119-315) with three substitutions. When PAS and GAF fragments were fused to FK506-rapamycin binding (FRB) domain of mTOR and FK506-binding protein 12 (FKBP), respectively, they could successfully visualize rapamycin-induced interaction between FRP and FKBP in both HeLa cells and living mice.

In addition to developments of various fluorescent protein fragment pairs to cover a wide range of spectrum, there also have been a series of trials to improve BiFC assay in respect of increased brightness and reduced background noise. For example, a new pair of Venus fragments was used to detect interactions occurring in Smad signaling in *Xenopus* embryos (Saka et al. 2007). Originally, Venus-based BiFC assay is not appropriate to visualization of protein-protein interactions in *Xenopus* embryos, because they have a large amount of yolk granule, thus generating high autofluorescence (de Maziere et al. 1996). To resolve this limitation, Venus fragments pairs 144/145, 154/155 were further subjected to point mutations and about 30 different kinds or pairs were tested.

As a result, Vm9, VN154 fragment with T153M mutation, was found to be able to produce interaction-induced fluorescence when complemented with VC155 with low background signal even in *Xenopus* embryos. By using this new pair of Venus fragments, Smad2-Smad4 heteromeric interaction was visualized. By the way, another pair of Venus fragments VN210 and VC210 was found to have low tendency of self-assembly and high fluorescence intensity, and was used to detect interaction between cofilin and actin in HeLa cells (Ohashi et al. 2012). Superfolder GFP (sfGFP), a GFP variant with enhanced folding robustness, has reduced possibility of misfolding that can be induced by fused target proteins (Pedelacq et al. 2006), but has a high risk of self-assembly. But sfGFPC(m12), a fragment carrying the deletion of R215 and substitution mutations V219A and L220A, was found to have an improved signal intensity with low background when complemented with sfGFPN, the study in which each fragment was fused to Bcl-xL and Bak (Zhou et al. 2011).

1.3. Advantages and disadvantages of BiFC assay

BiFC assay is highly sensitive with relatively low background because proteins of interest are fused to non-fluorescent, truncated fluorophores and so fluorescence can generally occur only in the presence of two fused proteins (Kerppola 2009). Through BiFC assay, direct visualization of protein interaction in living cell is easily possible and this is one of great advantages it has when compared to other fluorescence-based techniques. In case of FRET, for example, although it is a powerful PPI analyzing tool, it demands image capturing at two different wavelength and measurement as well as computation to properly analyze PPI information (Sekar and Periasamy 2003). Also this method has relatively low sensitivity when only small fractions of interactors associate with each other at a given time. And when compared to BiFC assay, fluorophores of the

two interactors should be retained in closer proximity, generally less than 10 nm, in FRET, making it fussy to generate interacting signal in many cases. This high sensitivity of BiFC assay, however, also works as a critical disadvantage. When two fused proteins are in the same macromolecular complex, fused fluorescent fragments can associate easily even without direct interaction between target proteins, thus may generate false-positive BiFC signal. Fortunately, this non selective association between fluorescent fragment was found to be inefficient unless there is direct contact induced by covalent or non-covalent bonds between the two fused proteins, no matter how they are closely located (Kerppola 2009).

Another greatness of BiFC assay is that because it uses fluorescent proteins as interaction reporters, which have intrinsic fluorescence at specific wavelength, it does not need any special treatment of cells with exogenous reagents before the detection of signal. It does not require fixation or lysis process of cells, so we can expect detection of PPIs in natural cellular environment with minimal perturbation, even with information about subcellular localization where PPIs occur. Developments of various fluorescent probes explained above enabled application of this assay in different cellular conditions, and the procedures required for this assay is relatively simple, and fluorescent images can easily be obtained by using a standard epifluorescence microscope.

One important issue we should consider when using BiFC assay is, as explained briefly in the previous context, fluorescent fragments used should not be able to reconstitute spontaneously and produce fluorescence signal in the absence of interaction between two fused proteins of interest. And although there is no requirement of additional reagents in the analyzing process, there still exist possibilities that fused fragments may induce disturbance and unexpected side effects in function of target proteins. And as importantly repeated above, proper development and use of fluorescent protein, not only that

excitation and emission wavelength is available in model organisms but also that fluorescence intensity of reconstituted fragments is comparable to that of intact fluorescent protein and bright enough when compared to background noises. And even with proper, optimized fluorescent proteins, it is still possible to make false positive BiFC signals and thus confirming interaction by using an appropriate control such as a binding partner carrying a mutation in the binding interface is usually recommended (Kodama and Hu 2012). When information about binding interface is not available, BiFC competition analysis by overexpressing untagged form of target protein or independent assays to ensure the interactions should be accompanied.

Another limiting factor for BiFC application is related to slow maturation of a chromophore (Tsien 1998). In general, fluorescent proteins require specific times to be matured after exposure to excitation wavelength and to produce detectable fluorescence, and in case of BiFC probes, additional times are needed for two split fragments to assemble and reconstitute a stable fluorophore. Because of this constraints, the subcellular location in which fluorescent signal is detected may not always reflect the actual interacting sites of two target proteins. Also, once the reconstitution has been completed, fluorescent fragments make stable assemblies and thus making it hard to tear off these fragments (Shyu and Hu 2008). This irreversibility may hamper the use of this assay in observing dynamic changes of PPIs because assembled fluorescent fragments may remain their complex and keep making interaction signals even in the environments that interactors which originally induced BiFC formation already finished their interactions.

Detection of BiFC signals by repeated capturing is usually limited because of photobleaching or low quantum yields. To compensate this limitation, a BiFC assay using Dronpa was developed. Dronpa is a genetically engineered monomeric GFP-like fluorescent protein obtained from a coral species, *Pectiniidae* (Ando et al. 2004). This

protein is unique in the fact that it has a reversible photo-switching activity between fluorescent and non-fluorescent states. Its split fragments, DN (amino acids 1-164) and DC (amino acids 165-224) were fused to hMYH and hHus1 to detect BiFC signal in HEK293 cells, and more importantly, the complemented Dronpa showed almost identical reversible photo-switching activity when compared to that of native Dronpa, indicating this strategy may allow trafficking of PPIs in living cells by BiFC assay (Lee et al. 2010). Meanwhile, limited resolution of BiFC analysis resulting from the use of fluorescent proteins as reporters can be greatly improved by combining BiFC with photoactivated localization microscopy (PALM) (Betzig et al. 2006; Hess et al. 2006). This strategy has allowed visualization of intracellular PPIs with resolution of nanometer and sensitivity of single molecule level. The fluorescent protein used for this purpose should be photoswitchable, for example, as fluorescent protein PAmCherry1. It was generated by introducing substituted mutation at ten different amino acid residues (E26V/A58T/K69N/L84F/N99K/S148L/I165V/Q167P/L169V/I203R) (Subach et al. 2009) to mCherry protein, and it can be used in BiFC assay when split between amino acid residues 159 and 160 (Nickerson et al. 2014). Reconstituted PAmCherry1 fragments could generate single molecule images by activation with 405 nm of wavelength and the brightness and signal to background ratio was found to be comparable to those of intact PAmCherry1. Also, the reconstitution of PAmCherry1 is highly efficient at 37°C in contrast to many other split fluorescent proteins such as mCherry requiring much lower temperature, so it allows nanoscale-resolved visualization of PPIs even under physiological conditions.

1.4. Application of BiFC assay for large-scale studies

Even with various limitations one should consider when using BiFC assay, large-scale

screens using BiFC assays have been performed in diverse species from yeast to mammalian cells, because of its definite advantages of simplicity and inexpensiveness. Various vector systems to tag fluorescent protein fragments to target proteins have been developed, and successfully used in high-throughput screening by BiFC assays usually with fluorescence microscopy or flow cytometry, as described below.

In yeast, it is particularly advantageous because fused proteins can easily be expressed under control of their endogenous promoters. This not only reduces risk of irreversibility induced by overexpression and also removes competition between tagged introduced proteins and untagged endogenous proteins. Irreversibility of BiFC complex is often mentioned as a major constraint of this assay, but in many cases, formation of bimolecular fluorescent complex was found to be reversible when it was expressed from its native promoter in budding yeast (Cole et al. 2007b; Sung and Huh 2007; Kang et al. 2010), although further investigation is necessary to clarify whether these are the results of actual reversibility or rapid turnover of the BiFC complex. Plasmids that allow for C-terminal tagging of the N-terminal (VN) or C-terminal (VC) fragments of Venus from native promoter of target protein and that allow for N-terminal tagging from the heterologous promoters of different strength were developed in *S. cerevisiae* (Sung and Huh 2007) and successfully validated for their application by testing known interactions including Pho2 and Pho4. To facilitate the application of BiFC assays to the genome-wide scale in budding yeast, a VN fusion library in which VN fragment is tagged to C-terminus of each gene under endogenous promoter was constructed (Sung et al. 2013). This library contains 5,911 VN-tagged strains, covering about 95% of all yeast ORFs and it was used to genome-widely screen interactor candidates of small ubiquitin-related modifier (SUMO) proteins in yeast. Out of the 5,911 proteins screened, 367 candidates were identified to have positive BiFC signals, adding 224 new protein candidates to the SUMO

interactome.

In another remarkable research, BiFC assay was applied to map the ATP-binding cassette (ABC) transporter interactome in *S. cerevisiae* (Snider et al. 2013). In this study, membrane yeast two-hybrid (MYTH) was firstly used to screen protein interactions and detected 285 interactions among 209 proteins tested. These PPIs were then verified by BiFC assay, and the results of this screen discovered 6 novel interactor candidates of ABC transporters, including a relationship between Snq2 and Pdr18. Several ABC transporters were found to interact with proteins involved in zinc homeostasis, and BiFC was used to detect the localization of these interactions, revealing their subcellular location at plasma membrane with some observed on the vacuolar membrane. Similar strategy was also taken to determine the interactome of Sho1, an integral membrane protein involved in the high-osmolarity glycerol (HOG) mitogen-activated protein kinase pathway in S. cerevisiae (Lam et al. 2015).

Unlikely as in budding yeast where chromosomally tagged fragments are used, many vector systems have been developed and exploited for BiFC assay in plants. For example, in a set of plasmids designated as pSATN, fusion proteins were expressed under a constitutive tandem cauliflower mosaic virus (CaMV) 35S promoter, a tobacco etch virus (TEV) translation leader, and a CaMV 35S poly(A) terminator to guarantee abundant expression levels in a broad range of plant species and tissues. This was successfully used to detect PPIs in the nucleus, plamodesmata, and chloroplasts of different plant species and cell types with N-terminal and C-terminal fragments of EYFP (Citovsky et al. 2006). This pSATN series of vectors were also tested for multicolor BiFC assay with C-terminal fragment of CFP and N-terminal fragment of either Venus or Cerulean (Lee et al. 2008).

In *A. thaliana*, BiFC assay was combined with yeast two-hybrid assay to find out PPIs between core cell cycle proteins (Boruc et al. 2010). BiFC vectors carrying the cell cycle

ORFs and GFP fragments under CaMV 35S promoter were generated by the MultiSite Gateway technology, and the constructs were co-expressed in leaf epidermal cells of tobacco. As a result, 917 interactions among 58 cell cycle regulatory proteins were tested and 341 interactions were identified. In different study, an *Arabidopsis* cDNA library colonies containing about $2x10^5$ cDNAs was screened for PPIs by BiFC assay, and interactor candidates of VirE2 and VirD2 were identified in *Arabidopsis* leaf or *N. tabacum* protoplasts (Lee et al. 2012). The same strategy was also exploited to detect interactors of VirE2 in orchid flowers, indicating the suitability of this assay in various plant model organisms.

A set of 12 GATEWAY-compatible BiFC vectors have been developed to readily produce combinations of candidate protein pairs tagged with N- or C-terminal fragments of Super cyan fluorescent protein 3A (SCFP3A) (Kremers et al. 2006) or Venus (Gehl et al. 2009). By using this vectors, interaction between Cnx6 and Cnx7, which are components of molybdopterin synthase complex, was detected. And because this vector set also permits the application of multicolor BiFC assay, the simultaneous formation of Cnx6-Cnx6 homomers and Cnx6-Cnx7 heteromers could be visualized in the same research.

BiFC assay can be quantified and analyzed in large scale when it is used in combination with flow cytometry. For example, *Arabidopsis* cDNA library was cloned into plasmids carrying C-terminal fragment of YFP (YC) to generate a random prey YC-cDNA library, and it was screened with a YN-bait fused partner in *Arabidopsis* protoplasts (Berendzen et al. 2012). Positive candidates presenting fluorescence above background were sorted by flow cytometry, and further confirmed by FRET-FLIM (fluorescence-lifetime imaging microscopy) assays, leading to the discovery of 4 interactor candidates of calcium-dependent protein kinase 3 (CPK3). In another research, BiFC assay was used in

combination with yeast two-hybrid to find interactions between *Arabidopsis* G-protein regulators and effectors (Klopffleisch et al. 2011). A high validation rate, confirmation of 74 out of 78 potential interactions, was obtained by BiFC, suggesting that BiFC assay cooperatively used with yeast two-hybrid can be a robust method to search protein interactions. BiFC signals detected in this study appeared in various subcellular organelles, proposing high possibility of functional differences between them. And also, several novel interactions uncovered by this approach may reflect involvement of G-proteins in cellular processes such as cell wall biogenesis or morphogenesis which were not on the focus in previous researches.

PPI study is difficult in wheat since the complete genome sequence is not available, while protein interactome involved in defense response in rice was well studied. By using BiFC assay, rice proteins were tested with wheat protein in cross-species manner to find out possible regulator candidates of defense response in wheat and simultaneously to estimate the conservation of proteins involved between two species (Cantu et al. 2013). It was revealed that PPIs in defense response were highly conserved between rice and wheat proteins and so that it is reasonable to use the rice interactome dataset to predict protein interactions involved in defense response of the wheat. This study again showed feasibility of BiFC assay for detecting any protein interactions, even with proteins obtained from different species.

BiFC assay was used to screen PPIs in large-scale in mammalian cells as well. One of the earliest was a trial to detect interactors of protein kinase B (PKB)/Akt, with use of split GFP fragments in COS-1 cells (Remy and Michnick 2004b). Fluorescence-activated cell sorting (FACS) was combined to detect BiFC signals in this study and a novel PKB binding protein hFt1 was identified. BiFC-based high-throughput screen in combination with flow cytometry was also exploited to find regulators of telomere signaling in human

cells (Lee et al. 2011). Telomeric proteins were tagged with VN fragment at either N- or C-terminus and VC fragment was fused to prey at either N- or C-terminus of 11,880 ORFs in the retroviral array library obtained by Gateway cloning process. Four combinations of VN- and VC-fused protein pairs were analyzed and as a result, low affinity or transient interactions including over 300 proteins between six core telomeric proteins were successfully visualized. Remarkably, BiFC signal obtained by flow cytometry was analyzed by CytoArray, an automated data analysis program developed in the same research. Subsequently performed GST-pull down assay showed 70% of overlaps with the results obtained by BiFC, demonstrating the reliability and effectiveness of this approach.

Recently, adenoviral BiFC vectors have been developed to facilitate BiFC assay in mammalian cells. Although adenovirus has benefits that it can transfect various types of cells with consistent expression of transgene, it was not able to be used in a large-scale study because of the difficulty of recombination process (Wang and Huang 2000). A recently developed AdHTS (adenovirus high-throughput system) utilizing Gateway in vitro site-specific recombination technology and terminal protein (TP)-coupled adenoviral vectors (Choi et al. 2012), however, enables simultaneous recombination of adenoviruses in 96-well plates without additional cloning steps in bacteria or mammalian cells. With this system, G protein-coupled receptor (GPCR) activation was monitored by an adenovirus-based β-arrestin BiFC assay in human cells, with the use of VN and VC fragments as BiFC probes (Song et al. 2014). 33 GPCRs within various classes showed increased BiFC signals upon appropriate agonist treatments.

2. Protein homomerization

2.1. Biological meaning of protein homomerization

As explained at the beginning of the introduction chapter, proteins in biological systems rarely act alone. They bind other biomolecules to elicit specific, required cellular responses. In most cases, these biomolecules are other proteins and they form protein complexes carrying at least more than one protein-protein interaction. Among several kinds of PPIs, protein homomerization takes a special place. Protein homomer means that a complex is formed by two or more identical subunits. This includes homo-dimers (complexes formed by two identical proteins), homo-trimers (complexes formed by three identical proteins), homo-tetramers (complexes formed by four identical proteins), and homo-oligomers (complexes formed by more than 5 identical proteins). In contrary, protein complexes consisting of more than two different subunits can be referred as heteromers.

The homomerization of proteins is a very common phenomenon detected in living cells and it is believed that vast majority of enzymes form homomers. Based on the Brenda enzyme database, only a third of 452 human enzymes act as monomers (Marianayagam et al. 2004). Among the remaining 311 multimeric enzymes found on the database, 199 were known as homomultimers and most highly represented populations are homodimers and homotetramers, 125 and 50 enzymes reported, respectively. This large population of homomeric enzymes reflects their involvement in the regulation of enzymatic activity. Homomers are also widely distributed in protein channels and vesicles because it can easily provide cavity required for transport of cargos. DNA binding proteins involved in diverse process such as DNA repair and DNA replication are another well-studied examples of homomers. Because homomerization is one of most widely used strategies

by cells to generate various effects as explained below, finding homomer candidates and understanding of their roles as homomers are crucial to extend our insights about protein interactome. Every PPI analyzing tool introduced in the previous chapter can be exploited to detect protein homomerization, including BiFC assay. If biochemical assays in which proteins are separated based on size difference such as cross-linking or Co-IP are used to analyze homomers, it is important to use proper two kinds of epitopes which are significantly different in their molecular sizes as presented in the current study. And when applying BiFC assay to detect homomer candidates, one should consider the possibility of false positive signals. This is because fluorescent fragments are required to be tagged to the same proteins in this purpose, and same proteins tend to be concentrated to relatively small area thus resulting in self-assembly of fused fluorescent fragments without actual homomrization.

2.2. Importance of protein homomerization study

The reason why so many proteins form homomers can be explained by various different effects cells can obtain by this process. In fact, it is one of the simplest and efficient ways cells can use to regulate function, concentration and structure of proteins. It can also help to minimize genome size, while providing the advantages of modular complex formation. Several benefits offered by protein homomerization were revealed in the researches about different protein functions. First, proteins can obtain new binding sites with increased specificity in a homomeric state. For example, many DNA-binding proteins in *S. cerevisiae* are known to bind DNA through binding sites expanded by their homomerization (Ellenberger et al. 1992; Hong et al. 2008; Grimme et al. 2010; Sung et al. 2014). Another well-known example is orthodox type II restriction enzyme, a protein that bind to palindromic DNA sequences and essential in DNA recombinant technologies

(Pingoud and Jeltsch 2001). Two of this protein form homomer, each subunit contacting one-half of the palindrome to form as a result a symmetric protein-DNA complex. Homomerization of this protein increase both binding affinity and specificity for DNA by doubling the length of interacting interface of DNA.

Second, cells can build up large protein complexes by homomerization with relatively small number of genes (Goodsell and Olson 2000). Making large homomeric complexes composed of multiple, identical subunits is relatively simple, and both structures with high stability required for long fibrous extracellular matrix proteins myosin or collagen and structures which should be highly dynamic such as tubulins in the cytoskeleton (Job et al. 2003). Proteins involved in correct protein folding and unfolding such as calreticulin (Jorgensen et al. 2003) and heat-shock protein 90 (Hsp90) (Yonehara et al. 1996) also use homomerization for structural and functional reason in this context (Zhang et al. 2002).

In addition, proteins can easily go through functional transitions depending on their homomeric states. For example, SF1 helicases, *Escherichia coli* UvrD, and *Bacillus stearothermophilus* PcrA all act as either helicase or translocase depending on whether they are homomers or monomers, respectively (Maluf et al. 2003; Niedziela-Majka et al. 2007; Yang et al. 2008). Homomerization can also influence protein modification. For example, *S. cerevisiae* Hxk2 exists in either monomeric or dimeric form but only monomeric Hxk2 is phosphorylated in response to carbon source (Randez-Gil et al. 1998). Despite profound physiological importance of protein homomerization, however, there has been no attempt to systematically identify protein homomers at a genome-wide level to date.

3. Aim of this study

As describe above, BiFC assay carries many advantages as PPIs analyzing tool when compared to other various methods. It is especially useful in yeast because replacing wild-type genes on the chromosomes with modified copies of the genes is capable in this model organism. Fluorescent fragment-fused proteins can be readily expressed under controls of their endogenous promoters and there is no competition between tagged and untagged proteins which can hamper the detection of BiFC signal. And irreversible characteristics of BiFC complex is usually enhanced by overexpression of fused proteins, and in many cases, with fusion proteins expressed from its native promoter at the chromosomal locus in budding yeast, BiFC signal was found to be reversible.

To facilitate a large-scale PPIs analysis by using BiFC, our laboratory has constructed the VN fusion library in a previous study (Sung et al. 2013). The VN fusion library contains 5,911 yeast strains in which N-terminal fragment of the Venus protein (Nagai et al. 2002), VN, is tagged to the C-termini of all yeast open reading frames (ORFs). This library was successfully used to map interactors of the small ubiquitin-related modified (SUMO) by screening candidates which showed BiFC signal when mated with yeast cells carrying N-terminally VC-tagged Smt3, a yeast ubiquitin-like (SUMO) modifier. In the current study, we construct VC fusion library to make BiFC assay more applicable. Firstly, we generated a collection of yeast strains in which VC fragment, a C-terminal region of the Venus protein, is tagged at the C-termini of yeast ORFs by epitope switching strains originated from TAP fusion library (Ghaemmaghami et al. 2003). Then we exchanged mating type of yeast strains from *MAT***a** to *MAT*α in order that this library can be immediately mated with strains of VN fusion library before application for BiFC analysis.

After the construction of two types of VC fusion library, *MAT*α VC library was tested

for its appropriate working by mating each strain with VN strain obtained from the same well of the same plate, and then resulting diploid cells were selected by media selection. Protein homomerization takes significant place in protein-protein interactions and large population of proteome is found to form various status of homomers, but no genome-wide scale of protein homomerization was studied so far. To map homomer candidates existing in budding yeast, we screened the diploid cells obtained by mating VN and VC fusion library by BiFC assay using fluorescent microscope. It is noteworthy that many homomer candidates were identified in many different subcellular localizations. The obtained homomer population was analyzed in various aspects such as their overlaps with previously reported localization, highly enriched gene ontologies, and their signal changes detected upon nitrogen starvation. These results will give new insights in understanding characteristics of homomers in budding yeast. Also, the VC fusion library was proved to be a powerful PPIs analyzing tool with many strong points as it will be explained in the following chapters. We are expecting that it will help us to strengthen and extend our knowledge about protein interactome by unraveling fussy, non-detectable interactions.

Chapter II. Construction of VC library to facilitate large-scale BiFC assay

1. Introduction

In previous study in our laboratory (Sung et al. 2008), a series of plasmids were designed and constructed to efficiently switch epitope tags of yeast strains from TAP fusion library (Ghaemmaghami et al. 2003). TAP tag integrated to the C-termini of yeast ORFs in TAP fusion library was designed to have same upstream and downstream flanking sequence. And the plasmids mentioned above were also designed to carry same flanking sequence, so now it is possible to switch TAP tags to different fluorescent or immune tags by one-step PCR-mediated epitope switching (Longtine et al. 1998) with PCR products generated with use of F2/R1 CORE primers. Among the plasmids constructed, pFA6a-VN-KlURA3 carries VN gene which can express VN fragment, N-terminal fragment of Venus protein, with selective marker gene and it can be used to generate yeast strains for PPI study by BiFC assay. It was successfully used to visualize previously reported interactions such as interaction between Pho2 and Pho4 in living yeast cells, and not only the occurrence of interaction but also subcellular localization of that interaction could be detected.

BiFC assay is a method for investigation of PPI by using fluorescent proteins as probes. (Kerppola 2008). In BiFC assay, a fluorescent protein is split into two non-fluorescent fragments that cannot make fluorescence signal themselves. Fragments are tagged to proteins of interest and if two target proteins come close to each other by physical interaction, then two tagged fragments also get close. When they are in close proximity, they assemble and reconstitute fluorophore so fluorescence can be detected after proper excitation wavelength is provided. BiFC assay is a good way to detect PPI with minimal disturbance in the cellular context. Furthermore, not only the occurrence but also subcellular localization of PPI can be examined by BiFC assay. Because of these

advantages, BiFC assay has been used for large-scale PPI studies in various species. In *S. cerevisiae*, BiFC assay was exploited to confirm ABC transporter interactome detected by MYTH (Snider et al. 2013). In *Arabidopsis thaliana*, 58 core cell cycle proteins were analyzed by BiFC assay and 342 interactions were found (Boruc et al. 2010). In addition, 74 interactions between *Arabidopsis* G protein complexes were observed by BiFC assay (Klopffleisch et al. 2011). Through these researches, BiFC assay has been proved as a reliable and convenient tool to investigate PPIs at a genome-wide scale.

The VN-carrying plasmid was used to construct VN fusion library, in which VN fragment is tagged to C-termini of yeast ORFs, and the library has been successfully identified SUMO interactor candidates. Out of the 5,911 yeast strains screened with VC-tagged Smt3, 367 strains showed bright BiFC signals above background and 224 of them are novel SUMO interactors. Previous studies have used TAP-MS or yeast two-hybrid assays to determine the SUMO interactome, and the large number of novel interactome found by BiFC revealed its strength in detecting transient or weak protein interactions. Meanwhile, many known SUMO interactors were not screened in BiFC assay for some unknown reason, and these non-overlapping candidates obtained from different studies propose the importance of applying various methods to minimize missing interactions. In this study, we constructed VC-fusion library of MATa and MATa for efficient and convenient BiFC assay with the VN-fusion library and for more broad range of PPI study.

2. Materials and Methods

2.1. Yeast strains and culture conditions

Yeast strains used in this study are listed in Table II-1. All *S. cerevisiae* strains were derived from BY4741 (*MAT***a** *his3*Δ*1 leu2*Δ*0 met15*Δ0 *ura3*Δ*0*). Yeast cells were grown at 30ºC in rich medium (YPD; 1% yeast extract, 2% peptone, 2% glucose), synthetic complete medium (SC; 0.67% yeast nitrogen base without amino acids, 2% glucose, appropriate amino acids) (Sherman 2002). For the overexpression of HO endonuclease gene under the inducible *GAL* promoter, SC medium with raffinose or galactose as a C-source instead of glucose was used. For plasmid elimination, SC medium containing 5-fluoroorotic acid (5-FOA) was dissolved to final concentration of 1mg/1ml.

2.2. Construction of plasmids

The oligonucleotide primers and plasmids used in this study are listed in Table II-2 and Table II-3, respectively. For the construction of pFA6a-VC-LEU2 vector, the ~1,900 bp PCR product of *LEU2* was obtained using pCgLEU2 as a template, forward primer CgLEU2-600 (BamHI), and reverse primer CgLEU2+1320R (TEF). In addition, the ~250 bp PCR product of *Ashbya gossypii* TEF terminator was obtained using pFA6a-GFP-His3MX6 as a template, forward primer T (TEF)-F3-L, and reverse primer T (TEF)-R. Using the two PCR products as templates, the ~2,150 bp PCR product was obtained using forward primer pCgLEU2-600 (BamHI) and reverse primer T (TEF)-R as previously described (Horton, 1997). Next, the obtained ~2,150 bp PCR product was digested with BamHI and PmeI and ligated into the BglII-PmeI-digested pFA6a-VC-KlURA3 (Sung et al. 2008), generating pFA6a-VC-LEU2.

Table II-1. Strains used in this study

Strain	Genotype	Reference
BY4741	*MAT***a** *his3Δ1 leu2Δ0 met15Δ0 ura3Δ0*	Research genetics
BY4742	*MATα his3Δ1leu2Δ0 lys2Δ0 ura3Δ0*	Research genetics
TAP strains	*MAT***a** *his3Δ1 leu2Δ0 met15Δ0 ura3Δ0 GENE-TAP::His3MX6*	(Ghaemmaghami et al., 2003)
VN strains	*MAT***a** *his3Δ1 leu2Δ0 met15Δ0 ura3Δ0 GENE-VN::KlURA3*	(Sung et al., 2013)
VC strains *MAT*a	*MAT***a** *his3Δ1 leu2Δ0 met15Δ0 ura3Δ0 GENE-VC::LEU2*	This study
VC strains *MAT*α	*MATα his3Δ1 leu2Δ0 met15Δ0 ura3Δ0 GENE-VC::LEU2*	This study

Table II-2. Oligonucleotide primers used in this study

Primer	Sequence (5' to 3')
F2CORE	GGTCGACGGATCCCCGGGTT
R1CORE	TCGATGAATTCGAGCTCGTT
CgLEU2-600 (BamHI)	GTCA**GGATCC**AAGGCTTCAAGTCATATAGC
CgLEU2+1320R (TEF)	CGTCATTGGTAGTCATTATGCGGATTTACG
T(TEF)-F3-L	CGTAAATCCGCATAATGACTACCAATGACGTTCCCTCAAC
T(TEF)-R	CATCGATGAATTCGAGCTCG
VC+20R	TTTCTGTTTCAGGTCGTTCG
F2 CHK	AACCCGGGGATCCGTCGACC

Restriction enzyme sites are indicated in bold.

Table II-3. Plasmids used in this study

Plasmid	Genotype	Source
HB0400	pCgLEU2	This study
HB0019	pFA6a-GFP(S65T)-His3MX6	(Huh et al. 2003)
HB0082	pFA6a-VC-KlURA3	(Sung and Huh 2007)
HB0172	pFA6a-VC-LEU2	This study
HB0129	pJH132-PGAL-HO-URA3	(Herskowitz and Jensen 1991)
HB0084	pRS413	(ATCC® 87518™)

2.3. Transformation of yeast cells

Yeast transformation was performed based on lithium acetate method previously describe (Gietz et al. 1995). Usually, 96 strains were transformed simultaneously using a 96-deep well plate for both epitope switching and plasmid transformation. Transformed cells were spread on SC agar medium without leucine (SC-Leu) or without uracil (SC-Ura), for epitope switching or plasmid transformation, respectively.

2.4. Mating type switching

pJH132 (Herskowitz and Jensen 1991), a plasmid carrying HO endonuclease and URA3 gene was introduced to yeast strains of MATa VC fusion library as explained above. To induce the expression of HO endonuclease that is under *GAL* promoter, the transformed cells were grown in SC medium containing 2% of raffinose as a carbon sourse instead of glucose for 12 hours. Then grown cells were washed and transferred to SC medium containing 2% of galactose as a carbon source and incubated at 30℃ in shaking incubator for more than 4 hours for galactose induction. After galactose induction, 2 μl of cell culture was streaked on YPD agar medium to obtain single colonies. 6 independent colonies from each strain were tested for their mating type by mating them with *MAT***a** yeast cells carrying His3MX6 gene, and only mating type switched cells formed diploid cells and grown on SC agar medium without histidine and leucine histidine (SC-HL).

2.5. Vector elimination

Cells that were switched from *MAT***a** to *MAT*α were incubated in SC medium containing 5-FOA to eliminate yeast cells carrying pJH132, as described in the previous study (Boeke et al. 1987). 5-FOA stock was prepared by dissolving 5-FOA in DMSO at

the concentration of 500 mg/ml and filter autoclaved, and then the stock was added to autoclaved media to final concentration of 1 mg/ml.

2.6. Western blot analysis

For western blot analysis, yeast cells grown to logarithmic phase in YPD medium were harvested and washed twice with phosphate-buffered saline. Cells then were disrupted by bead beating in lysis buffer (50 mM tris-Cl, pH 7.5, 150 mM NaCl, 0.15% NP-40, 1 mM EDTA) with protease inhibitors (10 mM phenylmethylsulfonyl fluoride, 1 mM benzamidine, 1 mM leupeptin, 1 mM pepstatin). Cell debris was eliminated by centrifugation at 13,000 rpm for 10 min at 4℃, and the extracts in the supernatant were collected and mixed with 6X SDS (sodium dodecyl sulfate) sample buffer. SDS-PAGE and Western blot analysis were performed using standard methods with a HRP-conjugated anti-mouse IgG antibody (A9044, Sigma), a HRP-conjugated anti-rabbit IgG antibody (A6154, Sigma), a HRP-conjugated anti-GFP antibody (600-103-215, Rockland) and an anti-hexokinase antibody (H2035-02, United States Biological).

3. Results

3.1. Construction of VC fusion library MATa

To construct the VC fusion library, we employed the same method used in the previous study (Sung et al. 2013) with some modifications. Basic scheme of this process is depicted in Figure II-1. First, we constructed a plasmid pFA6a-VC-LEU2 that can be used for switching C-terminally tagged epitopes to the VC tag, based on an epitope switching strategy (Sung et al. 2008) with primers described in Materials and Methods section. The plasmid should be designed to carry *S. cerevisiae* ACT1 terminator sequence downstream of *VC* gene, instead of *S. cerevisiae* ADH1 terminator which is integrated downstream of *TAP* gene in TAP fusion library to inhibit homologous recombination in unexpected regions. *LEU2* gene was incorporated to the plasmid in combination of promoter and terminator of itself which was originated from *Candida glabrata*. Upstream of *VC* gene and downstream of *LEU2* gene are flanked with sequence that can be annealed by CORE primers and thus can act as sites of homologous recombination.

A DNA fragment containing the VC tag and *LEU2* marker sequences was then amplified by PCR using pFA6a-VC-LEU2 as a template and a set of universal primers F2CORE and R1CORE. The resulting PCR products were transformed into each strain of the TAP fusion library (Ghaemmaghami et al. 2003), which consists of 6,097 *MAT***a** strains with chromosomal C-terminally TAP-tagged ORFs that encompass 98% of all ORFs. Since strains of the TAP fusion library carry *His3MX6* gene as selective marker while introduced VC tagging fragment having *LEU2* gene, transformants were subjected to selection medium (SC-Leu) and then to verify successful epitope switching from the TAP tag to VC tag at the corresponding locus, obtained colonies were confirmed by impaired grown on counter-selection medium (SC-His). Following this procedure, we

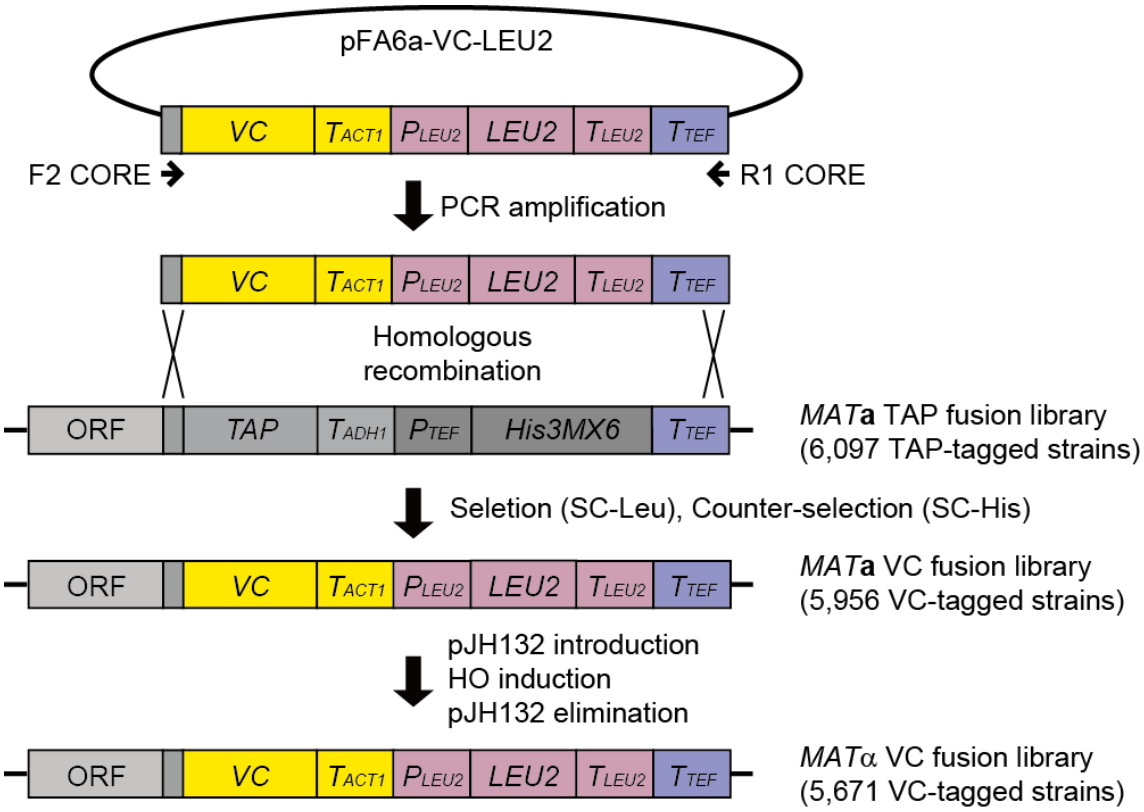

Figure II-1. Scheme of construction of the *MAT*a and *MAT*α VC fusion library.

A DNA fragment containing the VC tag and *LEU2* marker sequences was amplified by PCR using the pFA6a-VC-LEU2 vector as the template and the primers F2CORE and R1CORE and substituted for the C-terminal TAP tag sequence in the chromosome of each strain of the TAP fusion library by homologous recombination. To obtain a chromosomally VC-tagged *MAT*α strain collection, the HO gene was expressed by transforming pJH132 vector into each strain of the *MAT***a** VC fusion library. After confirming correct mating type switching, pJH132 vector was eliminated by 5-FOA treatment. *LEU2*, P_{LEU2}, T_{LEU2}, T_{ACT1}, T_{ADH1}, and T_{TEF} represent *Candida glabrata LEU2*, *C. glabrata LEU2* promoter, *C. glabrata LEU2* terminator, *S. cerevisiae ACT1* terminator, *S. cerevisiae ADH1* terminator, and *Ashbya gossypii TEF* terminator, respectively.

obtained 5,956 VC-tagged *MAT***a** strains with a coverage of 95% of all ORFs as indicated in Figure II-2.

3.2. Construction of VC fusion library MATa

Since the VN fusion library (Sung et al. 2013) was also constructed by using strains from TAP fusion library, it consists of *MAT***a** strains just as the VC library made by the process explained above. The purpose of VC library construction is to use BiFC assay more easily with VN fusion library, and VC-tagged *MAT***a** strains should be switched to MATa so they can be mated VN strains to generate diploid cells carrying both VN and VC fragments. To switch the mating type of VC-tagged strains from *MAT***a** to *MAT*α, we introduced a plasmid pJH132 carrying a galactose-inducible homothallic switching endonuclease (HO) gene (Herskowitz and Jensen 1991) into each VC-tagged strain. pJH132 carries URA3 gene as selective marker and HO gene under *GAL* promoter, so VC-tagged strains successfully transformed with the plasmid were selectively grown on SC-Ura medium and then HO endonuclease was induced by galactose treatment as described in the Materials and Methods section. After confirming successful mating-type switching, pJH132 was removed from cells by 5-FOA treatment to prevent further unintended mating-type switching. Through these steps, we finally obtained the VC fusion library consisting of 5,671 VC-tagged *MAT*α strains that cover 91% of all ORFs.

Although properly epitope switched strains from TAP tag to VC tag were obtained by growth on selection and counter-selection medium, it is necessary to confirm that VC gene is integrated at the chromosomal locus as we intended and that the resulting C-terminally VC tagged genes are normally expressed showing intact size of chimeric proteins. To test this, proteins which were reported to have high expression levels were selected from *MAT*α VC fusion library and TAP fusion library and the size of the epitope-

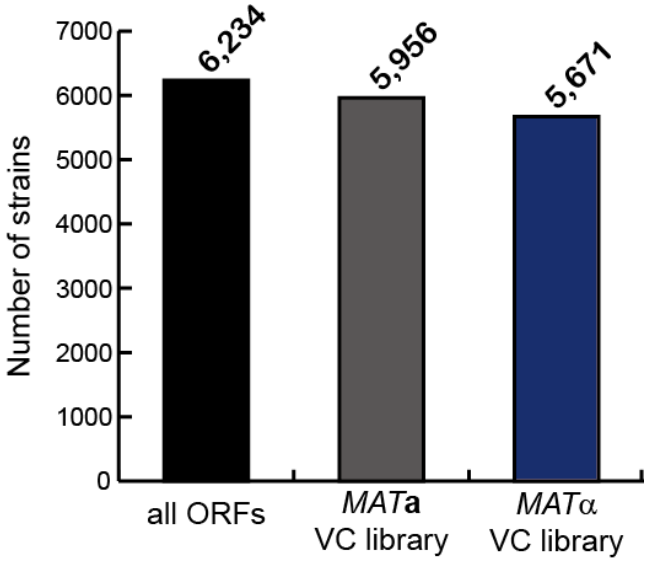

Figure II-2. The number of yeast ORFs each type of VC library covers

VC fusion library *MAT***a** contains 5,956 mating type a strains in which VC is C-terminally tagged to each gene. VC fusion library *MAT*α has 5,671 mating type alpha strains. Each library covers 95.54% and 90.96% of all yeast ORFs

tagged proteins was checked by western blot analysis. As depicted in Figure II-3, every tested *MAT*α VC strain showed smaller size of protein band when compared to that of TAP strains as expected. This results demonstrate that the appropriate epitope exchange occurred from TAP to VC with no detectable disturbance of expression, and tagged VC is properly fold into structure of part of Venus protein so that it can easily be blotted by anti-GFP antibody. If 5,671 VC-tagged *MAT*α strains are mated with 5,911 VN-tagged *MAT***a** strains (Sung et al. 2013) and subjected to BiFC assay, theoretically more than 33 million of PPIs can be analyzed, as describe in Figure II-4. This number represents most of possible interactions in the yeast proteome. And more importantly, steps required for this analysis are simple and of relatively low cost – only mating of two strains from each library and fluorescence detection of the resulting diploid cells are required. Thus, we are expecting the VC and VN fusion library can be exploited as a powerful tool to study PPIs in yeast in vivo.

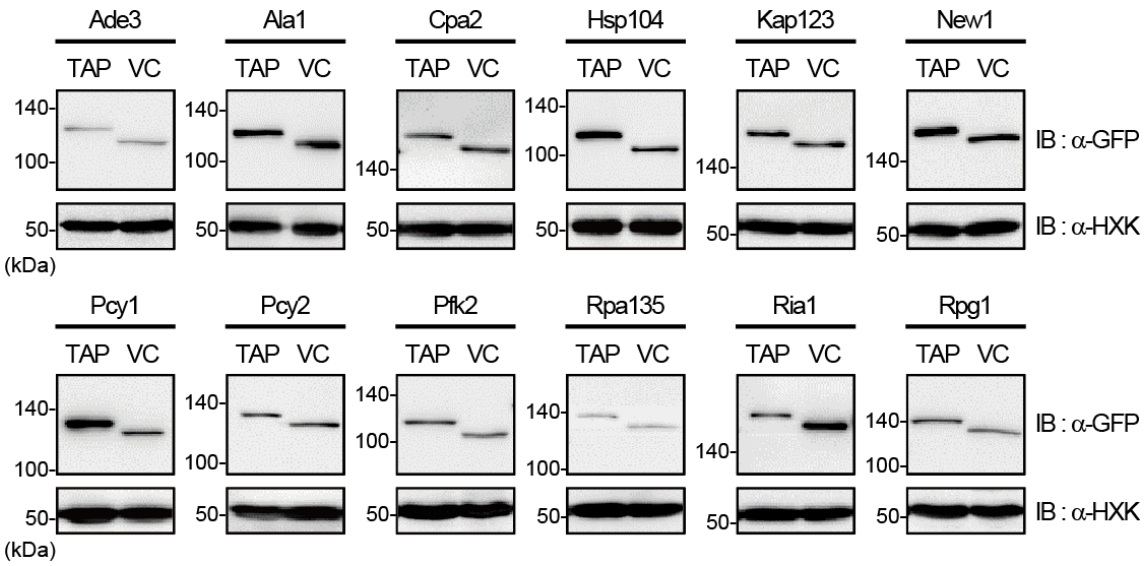

Figure II-3. Confirmation of proper VC tagging and expression of tagged proteins by western blot analysis.

Cells from TAP fusion library and VC fusion library with tags were lysed and immunoblotted using an anti-GFP antibody. Hexokinase was used as a loading control. Names of proteins tested and tagged epitopes are indicated at the *top* of each panel. The positions of molecular weight markers (in kDa) are indicated on the *left* of each blot.

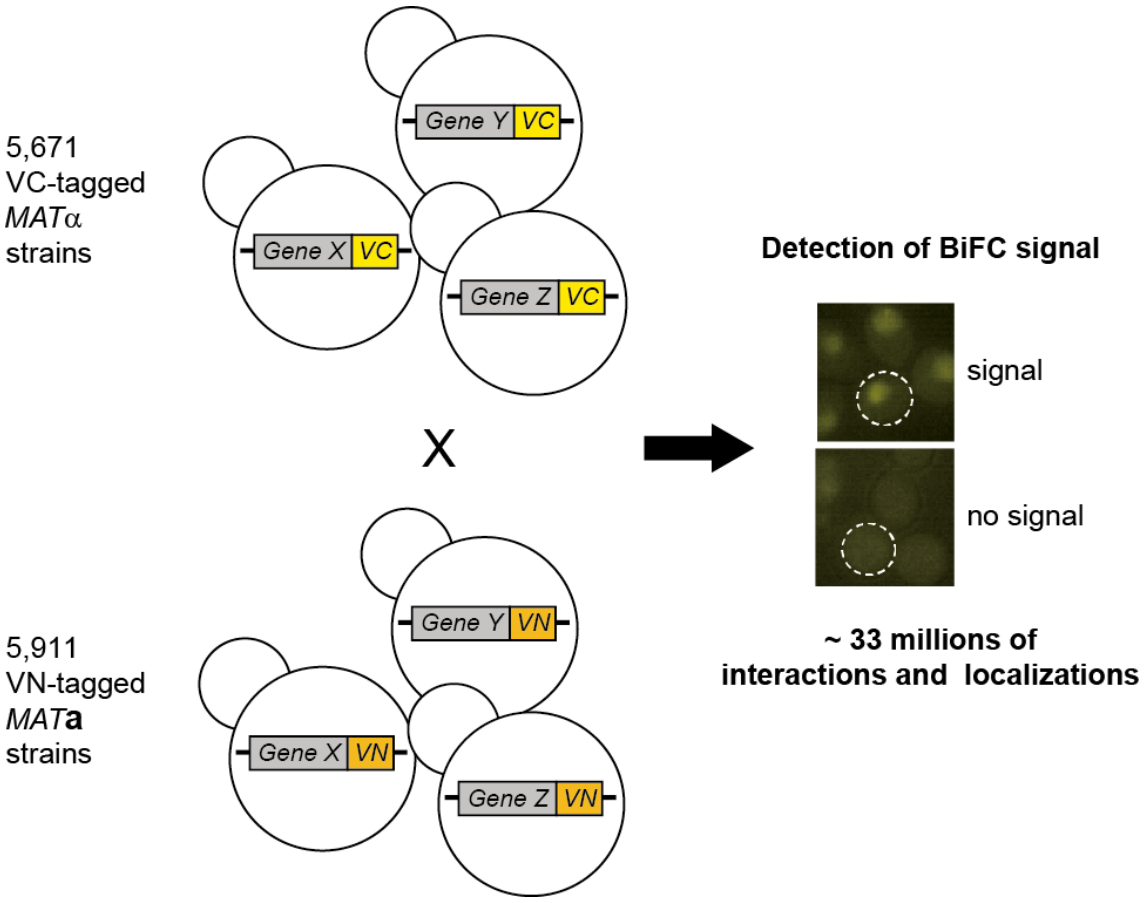

Figure II-4. Strategy for genome-wide analysis of PPIs using the *MAT*α VC fusion library and the *MAT*a VN fusion library.

Strains of the *MAT*α VC fusion library are mated with those of the *MAT***a** VN fusion library, thus generating a diploid collection. Then, each strain of the diploid collection expressing both the VC fusion protein and the VN fusion protein is analyzed by fluorescence microscopy. Theoretically, 33,521,281 PPIs can be analyzed in this way.

4. Discussion

In the current study, we constructed two kinds of VC fusion libraries composed of different mating types by using efficient epitope tagging and mating type switching procedures in genome-wide scale. Both libraries cover more than 90% of all ORFs in *S. cerevisiae*. Of the two libraries, the *MAT*α VC fusion library can be used together with the *MAT***a** VN fusion library to examine about 33 million of PPIs through BiFC assay. This number represents most of possible interactions in the yeast proteome, proposing its capability in mapping PPIs by various target proteins in various conditions.

Even though we are expecting this system will provide great feasibility in finding novel protein function and network, there are some caveats that are should be considered for using the VC fusion library. First, unlike the *MAT***a** VN fusion library, construction of the *MAT*α VC fusion library required an additional process of mating type switching. This includes several experimental steps during which relatively large number of strains were lost due to technical issues. As a results, the *MAT*α VC fusion library consists of fewer strains than the *MAT***a** VN fusion library (5,911 strains), and this ultimately limits possible interactions to be checked to fewer numbers than we expected.

More importantly, *MAT*α VC fusion library contains 5,671 strains chromosomally tagged with VC gene, but we cannot say that this number directly reflect the actual number of proteins that can be assessed for their interactors for some reasons. For example, there is possibility that interactions between two proteins cannot make two fused fragments close enough to recover their fluorescence because of topological problems. When finding novel interactors by BiFC assay, it is usually recommended that both fluorescent fragments should be tagged to either N-terminus of C-terminus of proteins of interest and the resulting 8 pairs with different combination of fragment

tagging should be tested for their fluorescence to rule out the false negatives caused by topological hindrance. But we only have C-terminally VN- and VC-tagged libraries, so we can test only 2 combinations out of 8 and some true interactors will be inevitably classified as negatives. Also, our tagging strategy allows efficient construction and endogenous level of expression, but does not give much consideration for proteins whose properties such as folding or post-translational modification can be disturbed by C-terminal tagging. And some proteins may be expressed as precursor forms and need to be cleaved for complete maturation by which tagged VC proteins are eliminated. In both cases, proteins cannot make BiFC signal even though they exist in sufficient amounts and form actual interactions. Indeed, it was reported that GFP strains showing signals and TAP strains detected by western blot analysis overlap more than 90% (Huh et al. 2003), which raises high possibility that unrevealed obstacles induced in the process of library construction may exist. The future construction of N-terminally VN- and VC-tagged strain collections and their utilization will help to resolve this unanswered question and also alleviate topological problems in genome-wide BiFC screens and greatly reduce false-negative results.

Chapter III. Global analysis of protein homomerization in *S. cerevisiae*

1. Introduction

Only a small portion of whole proteome function in isolation while the rest – both soluble and membrane bound proteins- form protein complexes. These complexes can be defined as homomers or heteromers based on the subunits that comprise them. Homomers are formed by more than two identical proteins and it is hard to overestimate the functional importance and biological meanings that homomerization have in living cells. Cells can obtain diverse physiological effects by regulating homomeric states of proteins. For example, it can provide increased affinity or fine-tunes specificity for binding interfaces in complexes. In other words, homomers can readily decrease their binding affinity by escaping from homomeric states in response to various environmental signals. Similarly, homomerization can also be used for allosteric regulation of enzymes, generating new binding sites at interfaces. In addition, homomerization allows proteins to form large assemblies without increasing genome size. And large complexes generated by homomerization can obtain enhanced stability because of repeating of binding interfaces from the identical subunits meanwhile the reduced surface area offering protection for the complexes against denaturation. It is not surprising that many chaperone proteins that usually their activities are required for in stressed conditions act as homomers (Miller et al. 1987; Jones and Thornton 1995; Goodsell and Olson 2000). Some proteins can exist in dynamic equilibrium between different homomeric states, and the equilibrium is affected by physiological conditions such as intracellular pH, ionic concentration, temperature, and posttranslational modifications (Nooren and Thornton 2003). Phosphorylation is one of most widely adopted mechanism by cells to control protein activity through homomerization. In these cases, changes of protein activity are usually accompanied by changes of homomeric states induced in a given condition.

Many characteristic protein regions – domains or sequences - have been revealed to be important for homomeric interactions, and it was found that some protein regions responsible for homomerization may be evolutionary preserved in specific protein subfamilies. And it was reported that, based on the Brenda enzyme database, only a third of 452 human enzymes act as monomers (Marianayagam et al. 2004). Very similar results were obtained from other proteomic research done by different group; based on a non-redundant set of Protein Data Bank (PDB), only 40% of analyzed protein was annotated as monomer and 38%, 4%, and 10% were categorized as dimeric, trimeric, tetrameric forms of homomer, respectively (Hashimoto et al. 2011; Nishi et al. 2013). These reports about evolutionary conserved characteristics of homomerization and vast amounts of proteins that form homomers emphasize the physiological importance of protein homomerization. However, as far as we know, there has been no attempt to systematically identify protein homomers at a genome-wide level to date. In this study, we screened homomer candidates in *S. cerevisiae* by BiFC assay with the use of VC fusion library constructed in the previous chapter. This research revealed many novel homomer candidates and interesting changes of homomeric states presented by some candidates upon nutrient-deprived condition.

2. Materials and Methods

2.1. Yeast strains and culture conditions

Yeast strains used in this study are listed in Table III-1. Yeast cells were grown at 30°C in YPD (1% yeast extract, 2% peptone, and 2% glucose) or synthetic complete (SC) medium lacking appropriate amino acids for selection (Sherman 2002). For solid media, 2% agar was added. For nitrogen starvation, cells grown to mid-logarithmic phase in SC medium were washed twice with and incubated in SD-N medium (0.17% yeast nitrogen base without amino acids and ammonium sulfate, 2% glucose) for 90 min at 30°C. For media change after starvation, cells incubated in SD-N medium were washed twice with and incubated in SC medium for 30 min at 30°C.

2.2. Amplification of PCR fragments

Oligonucleotide primers used in this study are listed in Table III-2. PCR amplification was performed in a 50 μl reaction mixture that contained 5 μl 10x Taq buffer, 5 μl of 2 mM each dNTP, 5 μl of 5 μM each oligonucleotide primer, 10 ng template plasmid DNA and 2.5 U Taq polymerase. The PCR cycle was initiated by denaturing at 95℃ for 5 min, followed by 40 cycles of 30 s at 95℃, 30 s at 55℃, 3 min at 72℃ and a final extension of 10 min at 72℃.

2.3. Transformation of yeast cells

Yeast transformation was performed based on lithium acetate method previously describe (Gietz et al. 1995). Transformed cells were spread on SC agar medium without leucine (SC-Leu) or withour histidine (SC-His) or without uracil (SC-Ura), for epitope switching or plasmid transformation, respectively.

Table III-1. Strains used in this study

Strain	Genotype	Reference
BY4741	*MAT***a** *his3Δ1 leu2Δ0 met15Δ0 ura3Δ0*	Research genetics
BY4742	*MATα his3Δ1 leu2Δ0 lys2Δ0 ura3Δ0*	Research genetics
VN strains	*MAT***a** *his3Δ1 leu2Δ0 met15Δ0 ura3Δ0 GENE-VN::KlURA3*	(Sung et al., 2013)
VC strains *MAT*a	*MAT***a** *his3Δ1 leu2Δ0 met15Δ0 ura3Δ0 GENE-VC::LEU2*	This study
VC strains MATa	*MATα his3Δ1 leu2Δ0 met15Δ0 ura3Δ0 GENE-VC::LEU2*	This study
HY1777	*MAT***a** *his3Δ1 leu2Δ0 met15Δ0 ura3Δ0 His3MX6::*P_{RPL7B}*-VN-RAD52*	This study
HY1778	*MATα his3Δ1 leu2Δ0 lys2Δ0 ura3Δ0 His3MX6::*P_{RPL7B}*-VC-RAD52*	This study
HY1779	*MAT***a** *his3Δ1 leu2Δ0 met15Δ0 ura3Δ0 RAD52-VN::KlURA3*	(Sung et al., 2013)
HY1780	*MATα his3Δ1 leu2Δ0 met15Δ0 ura3Δ0 RAD52-VC::LEU2*	this study
HY1782	*MAT***a** *his3Δ1 leu2Δ0 met15Δ0 ura3Δ0* p416ADH-VN	this study
YS001	*MATα his3Δ1 leu2Δ0 met15Δ0 ura3Δ0 MYO2-HA::KlURA3*	This study
YS003	*MATα his3Δ1 leu2Δ0 met15Δ0 ura3Δ0 GLT1-HA::KlURA3*	This study
YS007	*MATα his3Δ1 leu2Δ0 met15Δ0 ura3Δ0 EDE1-HA::KlURA3*	This study
YS009	*MATα his3Δ1 leu2Δ0 met15Δ0 ura3Δ0 GDH2-HA::KlURA3*	This study
YS014	*MATα his3Δ1 leu2Δ0 met15Δ0 ura3Δ0 GCV2-HA::KlURA3*	This study
YS016	*MATα his3Δ1 leu2Δ0 met15Δ0 ura3Δ0 KGD1-HA::KlURA3*	This study
YS020	*MATα his3Δ1 leu2Δ0 met15Δ0 ura3Δ0 YAR044W-HA::KlURA3*	This study
YS021	*MATα his3Δ1 leu2Δ0 met15Δ0 ura3Δ0 APL4-HA::KlURA3*	This study
YS024	*MATα his3Δ1 leu2Δ0 met15Δ0 ura3Δ0 SEY1-HA::KlURA3*	This study
YS025	*MATα his3Δ1 leu2Δ0 met15Δ0 ura3Δ0 RGD2-HA::KlURA3*	This study
YS027	*MATα his3Δ1 leu2Δ0 met15Δ0 ura3Δ0 APL2-HA::KlURA3*	This study
YS031	*MATα his3Δ1 leu2Δ0 met15Δ0 ura3Δ0 UTP8-HA::KlURA3*	This study
YS032	*MATα his3Δ1 leu2Δ0 met15Δ0 ura3Δ0 FAA1-HA::KlURA3*	This study
YS034	*MATα his3Δ1 leu2Δ0 met15Δ0 ura3Δ0 NCL1-HA::KlURA3*	This study
YS037	*MATα his3Δ1 leu2Δ0 met15Δ0 ura3Δ0 NOC3-HA::KlURA3*	This study
YS043	*MATα his3Δ1 leu2Δ0 met15Δ0 ura3Δ0 URA7-HA::KlURA3*	This study
YS044	*MATα his3Δ1 leu2Δ0 met15Δ0 ura3Δ0 GCD1-HA::KlURA3*	This study
YS047	*MATα his3Δ1 leu2Δ0 met15Δ0 ura3Δ0 TRM1-HA::KlURA3*	This study
YS052	*MATα his3Δ1 leu2Δ0 met15Δ0 ura3Δ0 HOM3-HA::KlURA3*	This study
YS054	*MATα his3Δ1 leu2Δ0 met15Δ0 ura3Δ0 CYS4-HA::KlURA3*	This study
YS055	*MATα his3Δ1 leu2Δ0 met15Δ0 ura3Δ0 ALD6-HA::KlURA3*	This study
YS056	*MATα his3Δ1 leu2Δ0 met15Δ0 ura3Δ0 GLK1-HA::KlURA3*	This study
YS057	*MATα his3Δ1 leu2Δ0 met15Δ0 ura3Δ0 LPD1-HA::KlURA3*	This study
YS061	*MATα his3Δ1 leu2Δ0 met15Δ0 ura3Δ0 SHM2-HA::KlURA3*	This study

YS066	*MATα his3Δ1 leu2Δ0 met15Δ0 ura3Δ0 WTM1-HA::KlURA3*	This study
YS067	*MATα his3Δ1 leu2Δ0 met15Δ0 ura3Δ0 MDH2-HA::KlURA3*	This study
YS068	*MATα his3Δ1 leu2Δ0 met15Δ0 ura3Δ0 ENT5-HA::KlURA3*	This study
YS074	*MATα his3Δ1 leu2Δ0 met15Δ0 ura3Δ0 MAP1-HA::KlURA3*	This study
YS075	*MATα his3Δ1 leu2Δ0 met15Δ0 ura3Δ0 GLY1-HA::KlURA3*	This study
YS077	*MATα his3Δ1 leu2Δ0 met15Δ0 ura3Δ0 HSP42-HA::KlURA3*	This study
YS081	*MATα his3Δ1 leu2Δ0 met15Δ0 ura3Δ0 GVP36-HA::KlURA3*	This study
YS087	*MATα his3Δ1 leu2Δ0 met15Δ0 ura3Δ0 PRO3-HA::KlURA3*	This study
YS101	*MATα his3Δ1 leu2Δ0 met15Δ0 ura3Δ0 SSP120-HA::KlURA3*	This study
YS111	*MATα his3Δ1 leu2Δ0 met15Δ0 ura3Δ0 AIM13-HA::KlURA3*	This study
YS121	*MATα his3Δ1 leu2Δ0 met15Δ0 ura3Δ0 RDL1-HA::KlURA3*	This study
YS131	*MATα his3Δ1 leu2Δ0 met15Δ0 ura3Δ0 PIM1-HA::KlURA3*	This study
YS143	*MATα his3Δ1 leu2Δ0 met15Δ0 ura3Δ0 OLE1-HA::KlURA3*	This study
YS153	*MATα his3Δ1 leu2Δ0 met15Δ0 ura3Δ0 VPS5-HA::KlURA3*	This study
YS154	*MATα his3Δ1 leu2Δ0 met15Δ0 ura3Δ0 SLC1-HA::KlURA3*	This study
YS155	*MATα his3Δ1 leu2Δ0 met15Δ0 ura3Δ0 ATP3-HA::KlURA3*	This study
YS160	*MATα his3Δ1 leu2Δ0 met15Δ0 ura3Δ0 DPM1-HA::KlURA3*	This study
YS163	*MATα his3Δ1 leu2Δ0 met15Δ0 ura3Δ0 DPP1-HA::KlURA3*	This study
YS176	*MAT**a** his3Δ1 leu2Δ0 met15Δ0 ura3Δ0 MYO2-GFP::His3MX6*	Huh et al., 2003
YS178	*MAT**a** his3Δ1 leu2Δ0 met15Δ0 ura3Δ0 GLT1-GFP::His3MX6*	Huh et al., 2003
YS182	*MAT**a** his3Δ1 leu2Δ0 met15Δ0 ura3Δ0 EDE1-GFP::His3MX6*	Huh et al., 2003
YS184	*MAT**a** his3Δ1 leu2Δ0 met15Δ0 ura3Δ0 GDH2-GFP::His3MX6*	Huh et al., 2003
YS189	*MAT**a** his3Δ1 leu2Δ0 met15Δ0 ura3Δ0 GCV2-GFP::His3MX6*	Huh et al., 2003
YS191	*MAT**a** his3Δ1 leu2Δ0 met15Δ0 ura3Δ0 KGD1-GFP::His3MX6*	Huh et al., 2003
YS195	*MAT**a** his3Δ1 leu2Δ0 met15Δ0 ura3Δ0 YAR044W-GFP::His3MX6*	Huh et al., 2003
YS196	*MAT**a** his3Δ1 leu2Δ0 met15Δ0 ura3Δ0 APL4-GFP::His3MX6*	Huh et al., 2003
YS199	*MAT**a** his3Δ1 leu2Δ0 met15Δ0 ura3Δ0 SEY1-GFP::His3MX6*	Huh et al., 2003
YS200	*MAT**a** his3Δ1 leu2Δ0 met15Δ0 ura3Δ0 RGD2-GFP::His3MX6*	Huh et al., 2003
YS202	*MAT**a** his3Δ1 leu2Δ0 met15Δ0 ura3Δ0 APL2-GFP::His3MX6*	Huh et al., 2003
YS206	*MAT**a** his3Δ1 leu2Δ0 met15Δ0 ura3Δ0 UTP8-GFP::His3MX6*	Huh et al., 2003
YS207	*MAT**a** his3Δ1 leu2Δ0 met15Δ0 ura3Δ0 FAA1-GFP::His3MX6*	Huh et al., 2003
YS209	*MAT**a** his3Δ1 leu2Δ0 met15Δ0 ura3Δ0 NCL1-GFP::His3MX6*	Huh et al., 2003
YS212	*MAT**a** his3Δ1 leu2Δ0 met15Δ0 ura3Δ0 NOC3-GFP::His3MX6*	Huh et al., 2003
YS218	*MAT**a** his3Δ1 leu2Δ0 met15Δ0 ura3Δ0 URA7-GFP::His3MX6*	Huh et al., 2003
YS219	*MAT**a** his3Δ1 leu2Δ0 met15Δ0 ura3Δ0 GCD1-GFP::His3MX6*	Huh et al., 2003
YS222	*MAT**a** his3Δ1 leu2Δ0 met15Δ0 ura3Δ0 TRM1-GFP::His3MX6*	Huh et al., 2003
YS227	*MAT**a** his3Δ1 leu2Δ0 met15Δ0 ura3Δ0 HOM3-GFP::His3MX6*	Huh et al., 2003
YS229	*MAT**a** his3Δ1 leu2Δ0 met15Δ0 ura3Δ0 CYS4-GFP::His3MX6*	Huh et al., 2003

YS230	*MAT***a** *his3Δ1 leu2Δ0 met15Δ0 ura3Δ0 ALD6-GFP::His3MX6*	Huh et al., 2003
YS231	*MAT***a** *his3Δ1 leu2Δ0 met15Δ0 ura3Δ0 GLK1-GFP::His3MX6*	Huh et al., 2003
YS232	*MAT***a** *his3Δ1 leu2Δ0 met15Δ0 ura3Δ0 LPD1-GFP::His3MX6*	Huh et al., 2003
YS236	*MAT***a** *his3Δ1 leu2Δ0 met15Δ0 ura3Δ0 SHM2-GFP::His3MX6*	Huh et al., 2003
YS241	*MAT***a** *his3Δ1 leu2Δ0 met15Δ0 ura3Δ0 WTM1-GFP::His3MX6*	Huh et al., 2003
YS242	*MAT***a** *his3Δ1 leu2Δ0 met15Δ0 ura3Δ0 MDH2-GFP::His3MX6*	Huh et al., 2003
YS243	*MAT***a** *his3Δ1 leu2Δ0 met15Δ0 ura3Δ0 ENT5-GFP::His3MX6*	Huh et al., 2003
YS249	*MAT***a** *his3Δ1 leu2Δ0 met15Δ0 ura3Δ0 MAP1-GFP::His3MX6*	Huh et al., 2003
YS250	*MAT***a** *his3Δ1 leu2Δ0 met15Δ0 ura3Δ0 GLY1-GFP::His3MX6*	Huh et al., 2003
YS252	*MAT***a** *his3Δ1 leu2Δ0 met15Δ0 ura3Δ0 HSP42-GFP::His3MX6*	Huh et al., 2003
YS256	*MAT***a** *his3Δ1 leu2Δ0 met15Δ0 ura3Δ0 GVP36-GFP::His3MX6*	Huh et al., 2003
YS262	*MAT***a** *his3Δ1 leu2Δ0 met15Δ0 ura3Δ0 PRO3-GFP::His3MX6*	Huh et al., 2003
YS276	*MAT***a** *his3Δ1 leu2Δ0 met15Δ0 ura3Δ0 SSP120-GFP::His3MX6*	Huh et al., 2003
YS286	*MAT***a** *his3Δ1 leu2Δ0 met15Δ0 ura3Δ0 AIM13-GFP::His3MX6*	Huh et al., 2003
YS296	*MAT***a** *his3Δ1 leu2Δ0 met15Δ0 ura3Δ0 RDL1-GFP::His3MX6*	Huh et al., 2003
YS306	*MAT***a** *his3Δ1 leu2Δ0 met15Δ0 ura3Δ0 PIM1-GFP::His3MX6*	Huh et al., 2003
YS318	*MAT***a** *his3Δ1 leu2Δ0 met15Δ0 ura3Δ0 OLE1-GFP::His3MX6*	Huh et al., 2003
YS328	*MAT***a** *his3Δ1 leu2Δ0 met15Δ0 ura3Δ0 VPS5-GFP::His3MX6*	Huh et al., 2003
YS329	*MAT***a** *his3Δ1 leu2Δ0 met15Δ0 ura3Δ0 SLC1-GFP::His3MX6*	Huh et al., 2003
YS330	*MAT***a** *his3Δ1 leu2Δ0 met15Δ0 ura3Δ0 ATP3-GFP::His3MX6*	Huh et al., 2003
YS335	*MAT***a** *his3Δ1 leu2Δ0 met15Δ0 ura3Δ0 DPM1-GFP::His3MX6*	Huh et al., 2003
YS338	*MAT***a** *his3Δ1 leu2Δ0 met15Δ0 ura3Δ0 DPP1-GFP::His3MX6*	Huh et al., 2003
YS355	*MATα his3Δ1 leu2Δ0 lys2Δ0 ura3Δ0 AAT2-HA::KlURA3*	This study
YS359	*MATα his3Δ1 leu2Δ0 lys2Δ0 ura3Δ0 PHO84-HA::KlURA3*	This study
YS366	*MAT***a** *his3Δ1 leu2Δ0 met15Δ0 ura3Δ0 AAT2-GFP::His3MX6*	This study
YS370	*MAT***a** *his3Δ1 leu2Δ0 met15Δ0 ura3Δ0 PHO84-GFP::His3MX6*	This study

Table III-2. Oligonucleotide primers used in this study

Primer	Sequence (5' to 3')
F2CORE	GGTCGACGGATCCCCGGGTT
R1CORE	TCGATGAATTCGAGCTCGTT
VC+20R	TTTCTGTTTCAGGTCGTTCG
F2 CHK	AACCCGGGGATCCGTCGACC
RAD52-F4	ATGCAAACAAGGAGGTTGCCAAGAACTGCTGAAGGTTCTGGAATTCGAGCTCGTTTAAAC
RAD52-R5-VN	AAACGGGCTTCTTCTCATCCATATCCATAATTTCATTCATACCACCAGAACCCTCGATGTTGTGGCGGATC
RAD52-R5-VC	AAACGGGCTTCTTCTCATCCATATCCATAATTTCATTCATACCACCAGAACCCTTGTACAGCTCGTCCATG
R5-BiFC-CHK	CAAGATCCGCCACAACATCG
VN-6 (BamHI)	CAGA**GGATCC**CTATGAGTTTAATTAACAGATC
VN+519R (XhoI)	GTCA**CTCGAG**GCCCTACTCGATGTTGTGGC
ERG6-F2	CGCCGAAACCCCCTCCCAAACTTCCCAAGAAGCAACTCAAGGTCGACGGATCCCCGGGTT
ERG6-R1	ATATCGTGCGCTTTATTTGAATCTTATTGATCTAGTGAATTCGATGAATTCGAGCTCGTT
ERG6-CHK	TGAACTAGGTGATGGTATCC
VMA2-F2	CGGTAAGAAGAAGGACGCCAGCCAAGAAGAATCTCTAATCGGTCGACGGATCCCCGGGTT
VMA2-R1	GACAAAATAAAAAAAGCCTTTTTCTTCAGCAACCGTCCTCTCGATGAATTCGAGCTCGTTT
VMA2-CHK	TACCGAGGGTCAAATCTTCG
COP1-F2	TAA GAT CGG TGC ACC TGC ATC CGG ATT AAGAAT ACG TGT AGG TCG ACG GAT CCC CGG GTT
COP1-R1	CAGAATACAATCCCGAGAAAATCAATAGGCAAAATAGCATTCGATGAATTCGAGCTCGTT
COP1-CHK	TACTGTACGCATGCTTGAGC

ATG8-R5-VC	TTTTTTCAAATGGATATTCAGACTTAAATGTAGACTTCAT ACCACCAGAACCCTTGTACAGCTCGTCCATG
ATG8-R3	TTTTTTCAAATGGATATTCAGACTTAAATGTAGACTTCATACCACCAGAACCGCACTGAGCAGCGTAATCTG
ATG8-F4	TAAAGTTGAGAAAATCATAATAAAAATAATTACTAGAGACGAATTCGAGCTCGTTTAAAC
YLL067C-F2	CGTTGAAGTTCTCGCTGCAGATAACACGAGGGTACCATGCGGTCGACGGATCCCCGGGTT
YLL067C-R1	GAACATCATTCGCTATCCAGCTCTTTGTGAACCGCTACCATCGATGAATTCGAGCTCGTT
YLL067C-CHK	ATCGAAGACAGAGGTGCTGC
PPS1-F2	CATCTGTAGGGGTATCGCTGAGGTTAATATGAAGTACACAGGTCGACGGATCCCCGGGTT
PPS1-R1	TACGTATTATACAGTTGTACGTATACTTATATAACAAAGTTCGATGAATTCGAGCTCGTT
PPS1-CHK	AGAGCTGATACTGTGGTCAG
GEM1-F2	TACGTTAATGAAATTATTCAAATCATCAAAATTCTCAAAAGGTCGACGGATCCCCGGGTT
GEM1-R1	GAAATGCAACACTTCCCTAATATAGAAATTTGGGCATTAATCGATGAATTCGAGCTCGTT
GEM1-CHK	CTACCGTTGGTATTTGTAGC
ALT1-F2	GGAAAGTTTCCATAAAGAATTTTTTGACCAATACCGTGACGGTCGACGGATCCCCGGGTT
ALT1-R1	TATTTAAATGTTTATTGAAGACTGTTCTGCCCCCTTTTATTCGATGAATTCGAGCTCGTT
ALT1-CHK	TGATGGTTCGTCCACCAGTG
AAT2-F2	TGATGAAGTGGTGCGCTTCTATACTATTGAAGCTAAATTGGGTCGACGGATCCCCGGGTT
AAT2-R1	ATGAAGAGTGTAATAGGTAAGTATAAGTATTATTTAATCATCGATGAATTCGAGCTCGTT
AAT2-CHK	ATGTACGGTGAGCGTGTAGG
FBP1-F2	TGAAATTGACAAATTTTTAGACCATATTGGCAAGTCACAGGGTCGACGGATCCCCGGGTT
FPB1-R1	TACAGAACAAAGAAAATAAGAAAAGAAGGCGATCATTGAATCGATGAATTCGAGCTCGTT
FBP1-CHK	ACCCTCTACTGGAACGAGAC
MST27-F2	GCGGCATCCCAATATCGATGCGCTTCTTAAAAAGACGGAAGGTCGACGGATCCCCGGGTT
MST27-R1	TCTAGTTTATGTTCGCTTTACGTATGGCAGTGTCTCTAAGTCGATGAATTCGAGCTCGTT

MST27-CHK	TTAGTGGATGTCATCACACG
YML010C-B-F2	GCCCCGCCGTAGGCTGACCTATCACCGGTACCACCCCAAGGGTCGACGGATCCCCGGGTT
YML010C-B-R1	TCCACTTGGGCGTCGGGTGGTGAATCTAATGGTGCCATGTTCGATGAATTCGAGCTCGTT
YML010C-B-CHK	TCGAATACGCAGACGTTACG
PHO84-F2	CATTGAATCTTCCAGCCCATCTCAACTTCAACATGAAGCAGGTCGACGGATCCCCGGGTT
PHO84-R1	TTTGTTCTAGTTTACAAGTTTTAGTGCATCTTTGAGGCTTTCGATGAATTCGAGCTCGTT
PHO84-CHK	TGGTGACCATGGTCTGTTGG
SCO2-F2	GGAGCGTAGGTCAAAAAAATGGTACTCTTTTATCTTCAATGGTCGACGGATCCCCGGGTT
SCO2-R1	GTTCGGTATCCTAGCTGTGTCTTTTTCTTTTTTTTTTTGCTCGATGAATTCGAGCTCGTT
SCO2-CHK	TGTCCAGAAGAGCTTGACAG

Restriction enzyme sites are indicated in bold.

2.4. Microscopic analysis and fluorescence quantification

For a genome-wide screening of protein homomers, each strain of the VC-tagged *MAT*α strain collection was grown to mid-logarithmic phase at 30℃ in YPD medium and mated with its cognate strain of the VN-tagged *MAT***a** strain collection. Diploid cells were selected on SC-LU medium. Then diploid cells were grown to mid-logarithmic phase at 30°C in SC medium and were microscopically analyzed in 96-well glass-bottomed microplates (MGP096, Matrical Bioscience). Microscopy was performed on a Nikon Eclipse E1 microscope with a Plan Fluor 100×/1.30 NA oil immersion objective. Fluorescence images were taken using a PhotoFluor LM-75 light source (89 North Inc.) with appropriate filters. Quantification of fluorescent images (BiFC and GFP) was performed using the NIS-Elements imaging software (Nikon). Cell boundary was defined manually and the sum fluorescence intensity of single cell was obtained. Background fluorescence intensity of non-cell area of the analyzed image was also quantified and subtracted from the sum fluorescence intensity of single cell, resulting in the net fluorescence intensity of single cell. For each experiment, at least 50 cells were analyzed and the mean intensity±SD values were calculated.

2.5. Spot assay

Yeast cells were grown to OD600 = 1.0 in YPD medium. 2 ml from 10-fold serial dilutions was spotted on SC agar medium. Plates were than incubated at 23℃, 30℃, 37℃ for 3 days.

2.6 Western blot analysis

For western blot analysis, yeast cells grown to logarithmic phase in YPD medium were harvested and washed twice with phosphate-buffered saline. Cells then were disrupted by

bead beating in lysis buffer (50 mM tris-Cl, pH 7.5, 150 mM NaCl, 0.15% NP-40, 1 mM EDTA) with protease inhibitors (10 mM phenylmethylsulfonyl fluoride, 1 mM benzamidine, 1 mM leupeptin, 1 mM pepstatin). Cell debris was eliminated by centrifugation at 13,000 rpm for 10 min at 4℃, and the extracts in the supernatant were collected and mixed with 6X SDS (sodium dodecyl sulfate) sample buffer. SDS-PAGE and Western blot analysis were performed using standard methods with a HRP-conjugated anti-mouse IgG antibody (A9044, Sigma), a HRP-conjugated anti-rabbit IgG antibody (A6154, Sigma), a HRP-conjugated anti-GFP antibody (SC-9996 HRP, Santa Cruz), a HRP-conjugated anti-myc antibody (SC-40 HRP, Santa Cruz), a HRP-conjugated anti-HA antibody (SC-7392 HRP, Santa Cruz), a HRP-conjugated anti-GFP antibody (600-103-215, Rockland) and an anti-hexokinase antibody (H2035-02, United States Biological).

2.7. Co-Immunoprecipitation assay

Diploid cells expressing GFP and HA or myc tagged target proteins were used for Co-IP assay. Cell extracts were prepared as previously described (Sung et al. 2008). An anti-myc antibody (SC-40, Santa Cruz) or anti-HA antibody (SC-7932, Santa Cruz) was added to cell extracts and incubated with gentle rocking for 4 h at 4°C. Protein A-Sepharose (17-5138-01, GE healthcare) was then added to the immunoprecipitation reaction and incubated with gentle rocking for 4 h at 4°C. For control, only protein A-sepharose was treated without antibody for the same cell extracts. Beads were washed four times with 25 mM Tris, pH 7.5, 150 mM NaCl, and 0.2% NP40. After the final wash, beads were resuspended in SDS sample buffer, boiled, and then loaded on SDS-PAGE gels. Proteins were detected with a HRP-conjugated anti-GFP antibody (SC-9996 HRP, Santa Cruz), a HRP-conjugated anti-myc antibody (SC-40 HRP, Santa Cruz), or a HRP-conjugated anti-

HA antibody (SC-7392 HRP, Santa Cruz).

2.8. Flow cytometry

Flow cytometry of cells were performed based on description in the previous study (Murozuka et al. 2013) using BD FACS canto II (BD Biosciences) equipped with BD FACSDiva 8.0.1 software. The yeast cells were incubated in SC to OD600 = 1.0 and washed twice and suspended in phosphate buffered saline (PBS) to make 1 ml suspension. For starvation condition, cells grown in SC media were washed twice and incubated in SD-N media for 90 min at 30°C. 100,000 cells were analyzed at each condition and intensities of fluorescence of cells were plotted on a histogram using FITC (525 nm) and the geometric mean of fluorescence intensity was obtained using BD FACSDiva software. For negative control, cells expressing VN and VC-tagged Mds3 were used to normalize fluorescence intensity of the candidates. At least 3 independent experiments were performed for each condition, and the results were presented as mean±SD with *P*-value calculated using Student's t-tests.

3. Results

3.1. Genome-wide screening of protein homomers by BiFC using the VC and VN fusion libraries

It is common for proteins to form homomers and defining proteins that form homomers is critical for understanding biological functions of proteins. To address this issue, we identified protein homomers by a genome-wide BiFC assay using VN and VC fusion libraries. To do this, we mated each strain of the *MAT*α VC fusion library with its cognate strain of the *MAT*a VN fusion library and analyzed fluorescence of the resulting diploid strains by fluorescence microscopy, as depicted in Fig. III-1. Of 5,597 strains examined, 630 showed the BiFC signals above background level. To find out whether or not the detected fluorescence is generated by false-positive self-assembly of VN and VC fragments, we mated a *MAT*a strain (HY1782) expressing VN alone, without any fusion partner, with 630 VC-tagged strains and confirmed fluorescence of the cells by BiFC assay. Of 630 strains, 444 showed fluorescence above background level and were regarded as false-positives. Representative images of self-assembly signal are represented in Figure III-2. Interestingly, among the 444, 16 showed self-assembly signal localized to different cellular sites than those observed in the homomer screening (Figure III-2B), while the rest are presented at the same cellular localization in both screenings (Figure III-2A). As a result, we could finally obtain 186 protein homomer candidates. Representative images of BiFC images of protein homomer candidates in diverse subcellular organelles are shown in Figure III-3. All protein homomer candidates are listed in Table III-3 with information about BiFC intensities and subcellular localization.

To validate the homomer candidates identified above, we performed a co-immunoprecipitation (Co-IP) assay using HA- and GFP-tagged strains. Of 186 homomer

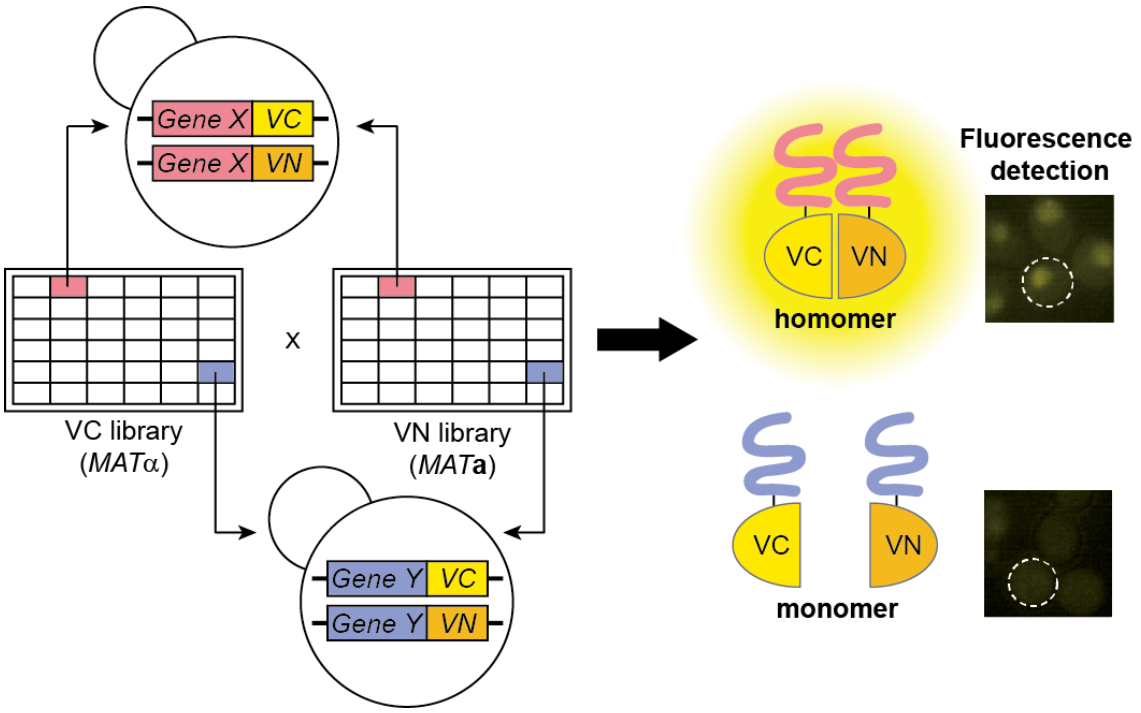

Figure III-1. Scheme of genome-wide BiFC analysis of protein homomers.

Each strain of the *MAT*α VC fusion library was mated with its cognate strain of the *MAT***a** VN fusion library. The resulting diploid cells expressing both the VC and VN fusion proteins were analyzed by fluorescence microscopy to detect homomierzation signal.

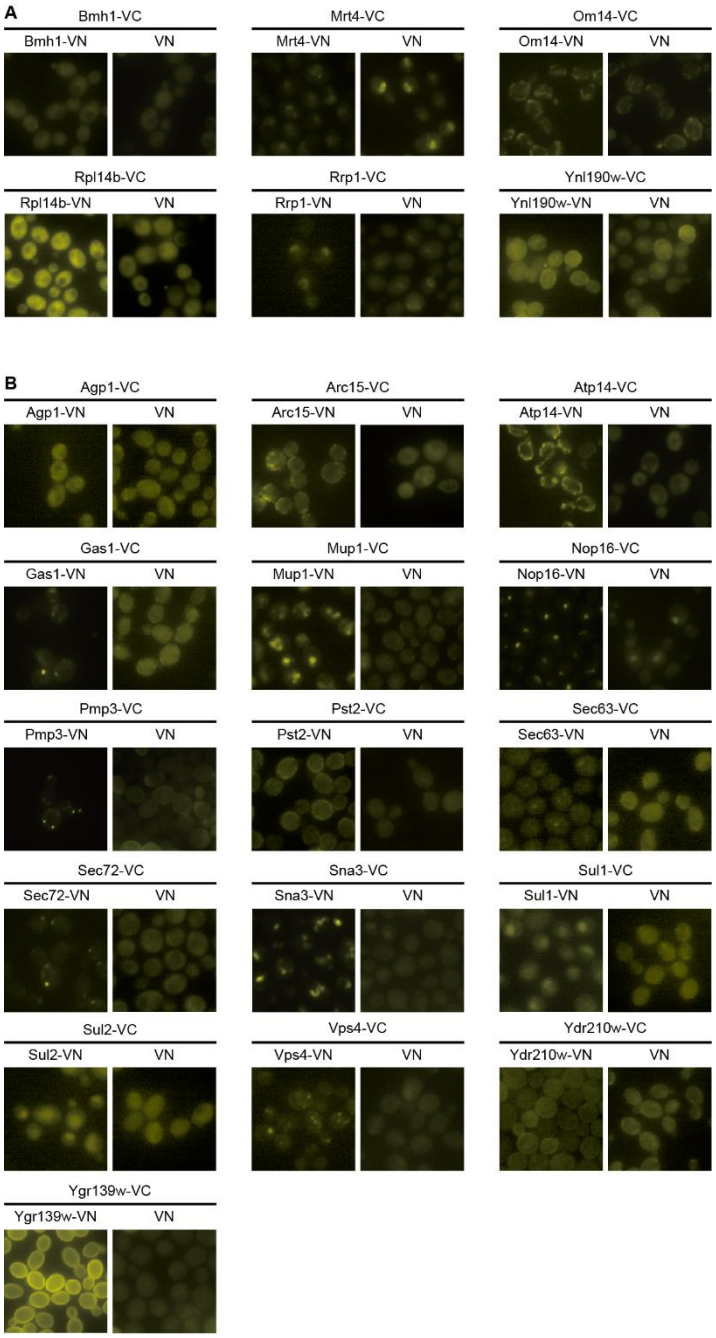

Figure III-2. Examples of self-assembly signals.

Self-assembly signals located at the same (A) or at different (B) subcellular localization to the signals detected in cells expressing both VN- and VC-tagged proteins. *Left* panels show BiFC images of cells expressing both VN- and VC-tagged target proteins. *Right* panels show BiFC images of cells expressing VC-tagged target proteins and free VN. The names of proteins tagged with VN or VC is indicated at the *top* of images.

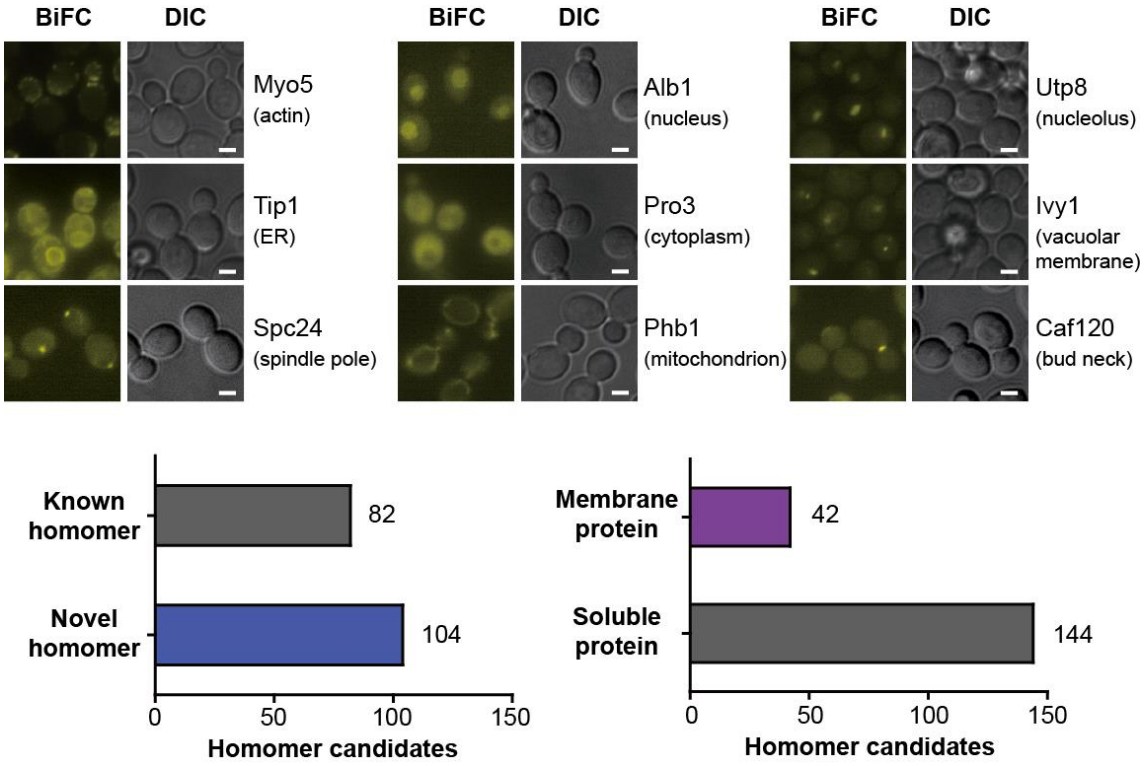

Figure III-3. BiFC images of homomer candidates with diverse subcellular localizations and composition of homomer candidates.

Representative images of BiFC signals in diverse subcellular localization are shown above. Proteins located at actin, bud neck, cytoplasm, ER, mitochondrion, nucleolus, nucleus, spindle pole, and vacuolar membrane are depicted. The names of proteins and their localizations are designated on the right side of the images. Scale bars, 2 μm. For detailed information, see also Table III-3.

Table III-3. Protein homomer candidates identified in this study

Standard name	*Systematic name*	*Known*	*Novel*	*GFP localization*[a]	*BiFC localization*	*BiFC intensity*
AAT2	YLR027C	v		cytoplasm	same	1027526
ABP140	YOR239W	v		actin*	same	2296166
ACO2	YJL200C	v		mitochondrion	same	1793338
ACS1	YAL054C	v		cytoplasm, nucleus	same	2278109
ALD6	YPL061W	v		cytoplasm, nucleus	same	20621325
APL4	YPR029C	v		punctate	same	1911197
APL6	YGR261C	v		punctate, Golgi, early Golgi	same	1746203
ATP10	YLR393W	v		mitochondrion	same	1621670
BCP1	YDR361C	v		cytoplasm, nucleus	same	1296963
CPR1	YDR155C	v		cytoplasm, nucleus	same	8679628
CYS4	YGR155W	v		cytoplasm	partial	10206117
DAD3	YBR233W-A	v		spindle pole	same	1663404
DCP2	YNL118C	v		punctate	same	2001703
DID2	YKR035W-A	v		endosome	same	897249
DPP1	YDR284C	v		vacuolar membrane	same	1949846
EDE1	YBL047C	v		punctate	same	3628596
EMP24	YGL200C	v		punctate	same	1700918
ERP1	YAR002C-A	v		vacuolar membrane	same	1317516
ERV25	YML012W	v		ER	same	1950817
FBP1	YLR377C	v		NA[b]	punctate foci	2290528
GCD1	YOR260W	v		cytoplasm	partial	1525074
GCD11	YER025W	v		cytoplasm	same	2165329
GCD6	YDR211W	v		cytoplasm	partial	1963410
GIN4	YDR507C	v		bud neck, cytoplasm, bud	same	1484951
GLE1	YDL207W	v		nuclear periphery	same	1944388
GLK1	YCL040W	v		cytoplasm, punctate	same	1894332
GLT1	YDL171C	v		ambiguous	same	3073160
HOM3	YER052C	v		cytoplasm	same	2266853
HSP42	YDR171W	v		cytoplasm	same	1531958
ILV1	YER086W	v		mitochondrion	same	1891207
KES1	YPL145C	v		cytoplasm	partial	1688042
KGD1	YIL125W	v		mitochondrion	same	2581085
LOC1	YFR001W	v		nucleolus, nucleus	same	1532780
LSB3	YFR024C-A	v		bud neck, cytoplasm, mitochondrion, cell periphery	same	1868230
LSM1	YJL124C	v		cytoplasm	partial	683210
MCM1	YMR043W	v		nucleus	same	2213965

MDH2	YOL126C	v	peroxisome	same	1003452
MDJ1	YFL016C	v	mitochondrion	same	1058018
MDV1	YJL112W	v	mitochondrion	same	1809308
MEH1	YKR007W	v	vacuolar membrane	same	742044
MST27	YGL051W	v	NA	ambiguous	1785263
MYO2	YOR326W	v	bud neck, cytoplasm, cell periphery, bud	same	2207040
MYO4	YAL029C	v	bud neck, cytoplasm, cell periphery, bud	same	1409354
MYO5	YMR109W	v	actin	same	2177699
NAB2	YGL122C	v	nucleus	partial	1983494
NHP10	YDL002C	v	nucleus	same	1645573
NOC3	YLR002C	v	nucleolus, nucleus	same	1747119
NOP15	YNL110C	v	nucleolus, nucleus	same	2090763
OLE1	YGL055W	v	ER	same	2112716
PEX6	YNL329C	v	peroxisome	same	1427470
PIM1	YBL022C	v	mitochondrion	same	1910524
POM33	YLL023C	v	ER	same	740012
PRO3	YER023W	v	cytoplasm	same	3456978
RAD51	YER095W	v	cytoplasm, nucleus	same	4489774
RBD2	YPL246C	v	Golgi, early Golgi	same	2046156
RGD2	YFL047W	v	bud neck, cytoplasm, cell periphery	same	2118413
RRP42	YDL111C	v	cytoplasm, nucleolus, nucleus	same	1670322
RTN2	YDL204W	v	ER	same	2595707
RVS167	YDR388W	v	actin	same	1268702
SCO2	YBR024W	v	NA	ambiguous	1626924
SEC3	YER008C	v	bud neck, cell periphery, bud	same	1895407
SEY1	YOR165W	v	punctate	same	2367047
SGF29	YCL010C	v	nucleus	same	1677009
SLM4	YBR077C	v	vacuolar membrane	same	865243
SNF7	YLR025W	v	endosome	same	2104653
SPC24	YMR117C	v	spindle pole	same	1657706
SRP1	YNL189W	v	cytoplasm, nuclear periphery	partial	2404673
TGL3	YMR313C	v	punctate, lipid particle	same	1940653
TIM11	YDR322C-A	v	mitochondrion	same	2270796
TRM1	YDR120C	v	nuclear periphery, nucleus	same	2251588
TRS33	YOR115C	v	punctate	same	2040507
TSA1	YML028W	v	cytoplasm, punctate	same	9461788
TVP15	YDR100W	v	early Golgi	same	1509598
URA7	YBL039C	v	cytoplasm	partial	3255155
UTP8	YGR128C	v	nucleolus	same	2165005

VMA21	YGR105W	v		vacuole	same	1686192
VPS35	YJL154C	v		vacuolar membrane, endosome	same	1430959
VPS5	YOR069W	v		endosome	same	1764528
VPS60	YDR486C	v		vacuolar membrane	same	2105548
WTM1	YOR230W	v		nucleus, anti-nucleolar nucleus	same	3071872
XRN1	YGL173C	v		cytoplasm	partial	3362175
YMR010W	YMR010W	v		punctate, early Golgi	same	2854989
ADK2	YER170W		v	mitochondrion	same	1796657
AIM13	YFR011C		v	cytoplasm, mitochondrion	same	1793051
AIM17	YHL021C		v	mitochondrion	same	631011
AIM24	YJR080C		v	mitochondrion	same	2537457
AIP1	YMR092C		v	actin	same	630661
ALB1	YJL122W		v	nucleus	same	1293149
ALT1	YLR089C		v	NA	mitochondrion	1559191
ANT1	YPR128C		v	peroxisome	same	1850982
APL2	YKL135C		v	late Golgi	same	1654257
APL5	YPL195W		v	early Golgi	same	1805319
ARC35	YNR035C		v	actin	same	1816870
ARO4	YBR249C		v	cytoplasm, nucleus	partial	1290798
ATG8	YBL078C		v	NA	punctate foci	336084
ATP19	YOL077W-A		v	mitochondrion	same	2067765
ATP3	YBR039W		v	mitochondrion	same	1928097
BSC2	YDR275W		v	lipid particle	same	1887016
BUR6	YER159C		v	nucleus	same	1991056
BXI1	YNL305C		v	vacuole	same	1844098
CAF120	YNL278W		v	bud neck, cytoplasm, bud	same	1294282
CBP3	YPL215W		v	mitochondrion	same	1787924
COQ3	YOL096C		v	mitochondria	same	1804712
COX7	YMR256C		v	mitochondrion	same	2095145
CYT1	YOR065W		v	mitochondrion	same	1796591
DDR2	YOL052C-A		v	cytoplasm, vacuole	same	1674657
DPM1	YPR183W		v	ER	same	2178291
ELF1	YKL160W		v	nucleus	same	1701835
ELO2	YCR034W		v	ER	same	1787854
ENT5	YDR153C		v	late Golgi	same	2116847
FAA1	YOR317W		v	ER	same	3396713
FCY2	YER056C		v	vacuole	same	1818077
FSF1	YOR271C		v	mitochondrion	same	1503810
GCV2	YMR189W		v	mitochondrion	same	2428776

GDH2	YDL215C	v	cytoplasm	same	2898555
GEA1	YJR031C	v	Golgi	same	831203
GEM1	YAL048C	v	NA	ambiguous	1599355
GLY1	YEL046C	v	cytoplasm, nucleus	same	8155149
GVP36	YIL041W	v	Golgi**	same	4743695
ILV6	YCL009C	v	mitochondrion	same	3003939
INP53	YOR109W	v	punctate	same	1636176
IVY1	YDR229W	v	vacuolar membrane	same	1022127
JIP5	YPR169W	v	nucleolus, nucleus	same	1408779
KAP123	YER110C	v	cytoplasm, nucleus	partial	2789939
LAM6	YLR072W	v	mitochondrion, punctate	same	1646567
LPD1	YFL018C	v	mitochondrion	same	3304539
MAP1	YLR244C	v	cytoplasm, nucleus	partial	582213
MCX1	YBR227C	v	mitochondrion	partial	1681900
MDH1	YKL085W	v	mitochondrion	same	8101062
MDM12	YOL009C	v	mitochondrion	same	1314100
MET10	YFR030W	v	cytoplasm	same	1543586
MET14	YKL001C	v	cytoplasm	same	671142
MRPL19	YNL185C	v	mitochondrion	same	1614745
MSB3	YNL293W	v	ambiguous	same	1596779
MSS116	YDR194C	v	mitochondrion	same	2421457
NCL1	YBL024W	v	nucleus	same	1610624
NUP60	YAR002W	v	nuclear periphery	same	3094987
PET10	YKR046C	v	lipid particle	same	1968393
PFD1	YJL179W	v	cytoplasm	same	1654813
PGA3	YML125C	v	ER	same	1735280
PHB1	YGR132C	v	mitochondrion	same	1558693
PHO84	YML123C	v	ER	same	1847551
PMC1	YGL006W	v	vacuolar membrane	same	1935685
PPS1	YBR276C	v	NA	ambiguous	1650313
PSE1	YMR308C	v	cytoplasm, nucleus	partial	1366222
QCR10	YHR001W-A	v	mitochondrion	same	1616425
RAI1	YGL246C	v	nucleus	same	1666970
RDL1	YOR285W	v	ER	same	718186
RGD1	YBR260C	v	bud neck, cytoplasm, bud	same	1525989
RHO5	YNL180C	v	endomembrane system***	same	1931498
ROM2	YLR371W	v	bud neck, cytoplasm, bud	same	1601616
RPL7A	YGL076C	v	cytoplasm	same	15169517
RPS18B	YML026C	v	cytoplasm	same	2221056

RPS24B	YIL069C	v	cytoplasm	same	2195984
RRP17	YDR412W	v	nucleolus, nucleus	same	1951178
RRT8	YOL048C	v	lipid particle	same	1187125
RVS161	YCR009C	v	cytoplasm, actin	same	1907368
SDH4	YDR178W	v	mitochondrion	same	1745969
SET2	YJL168C	v	nucleus	same	2548343
SHM2	YLR058C	v	cytoplasm, nucleus	same	12905422
SLC1	YDL052C	v	ER	partial	2117340
SMX2	YFL017W-A	v	nucleus	same	1604259
SNC2	YOR327C	v	vacuole	same	1876343
SOL2	YCR073W-A	v	cytoplasm	partial	3293119
SSP120	YLR250W	v	punctate, Golgi, early Golgi	same	1692938
TIP1	YBR067C	v	ER	same	1627459
TRX2	YGR209C	v	cytoplasm, nucleus	same	3727572
UTP30	YKR060W	v	nucleolus, nucleus	partial	1715056
UTP5	YDR398W	v	nucleolus	same	1723762
UTR2	YEL040W	v	ER	same	3647821
VID27	YNL212W	v	cytoplasm	partial	1863347
VPS16	YPL045W	v	vacuolar membrane	same	2059389
YAH1	YPL252C	v	mitochondrion	same	1618816
YAR044W	YAR044W	v	punctate	same	502587
YER156C	YER156C	v	cytoplasm, nucleus	same	3033241
YHR127W	YHR127W	v	nucleus	same	1913395
YKL077W	YKL077W	v	vacuole	same	2330867
YLL067C	YLL067C	v	NA	ambiguous	1263120
YLR257W	YLR257W	v	cytoplasm	partial	3097750
YML010C-B	YML010C-B	v	NA	ambiguous	1604097
YMR122W-A	YMR122W-A	v	ER, cytoplasm	partial	1949357
YOL092W	YOL092W	v	vacuolar membrane	same	1482482
YPL162C	YPL162C	v	vacuolar membrane	same	1717985
YPR090W	YPR090W	v	late Golgi	same	1650711
YPR097W	YPR097W	v	ambiguous	partial	1619596
ZPR1	YGR211W	v	cytoplasm, nucleus	same	1326059
MDS3[c]	YGL197W				140997

[a]Huh et al. (2003) [b]NA: not available [c]negative control

* (Asakura et al. 1998; Yang and Pon 2001) ** (Inadome et al. 2005) *** (Singh et al. 2008)

candidates tested, we could detect Co-IP bands with 44 proteins, of which 19 were novel homomer candidates (Figure III-4). However, we could not see Co-IP bands with the rest 142 proteins, presumably because homomeric forms of these proteins are present at too low levels to be detected by Western blotting or are severely lost during the immunoprecipitation procedure due to weak and transient interaction between subunits. To make it clearer, we compared expression levels of BiFC-signal detected candidates to Co-IP band detected candidates. Notably, 44 proteins with positive Co-IP results showed a tendency of high expression level as we expected, while 186 BiFC-positive homomer candidates exhibited a more even distribution of expression level (Figure III-5). This result suggests that our approach of using the VC and VN fusion libraries is reliable for identifying protein homomers regardless of their expression levels or interaction strengths.

We found that some known homomers were not identified in our screening process. There are several possible explanations we can think of. First, because we regarded any VC fusion proteins showing fluorescence with free VN fragment as false-positives during self-assembly analysis, there is a high possibility that true homomers may have been eliminated by this step. Indeed, among 444 homomer candidates designated as false-positives, 171 are known homomers reported in previous studies. Second, some homomers may have difficulties in the BiFC complex formation because of topological constraints. It is estimated that BiFC occur when VN and VC are separated by a distance no greater than approximately 10 nm (Hu et al. 2002), and it was recommended that 8 combinations of two complementary fragments tagged at different locus of proteins should be tested for BiFC signal appearance (Kerppola 2009). So we chose Rad52 to check a possibility that the topological constraints prevent the BiFC complex formation. Rad52, a recombinase involved in the repair of DNA double-strand breaks, has been reported to form a homomer, but it was not detected in our screen. We tagged VN and VC

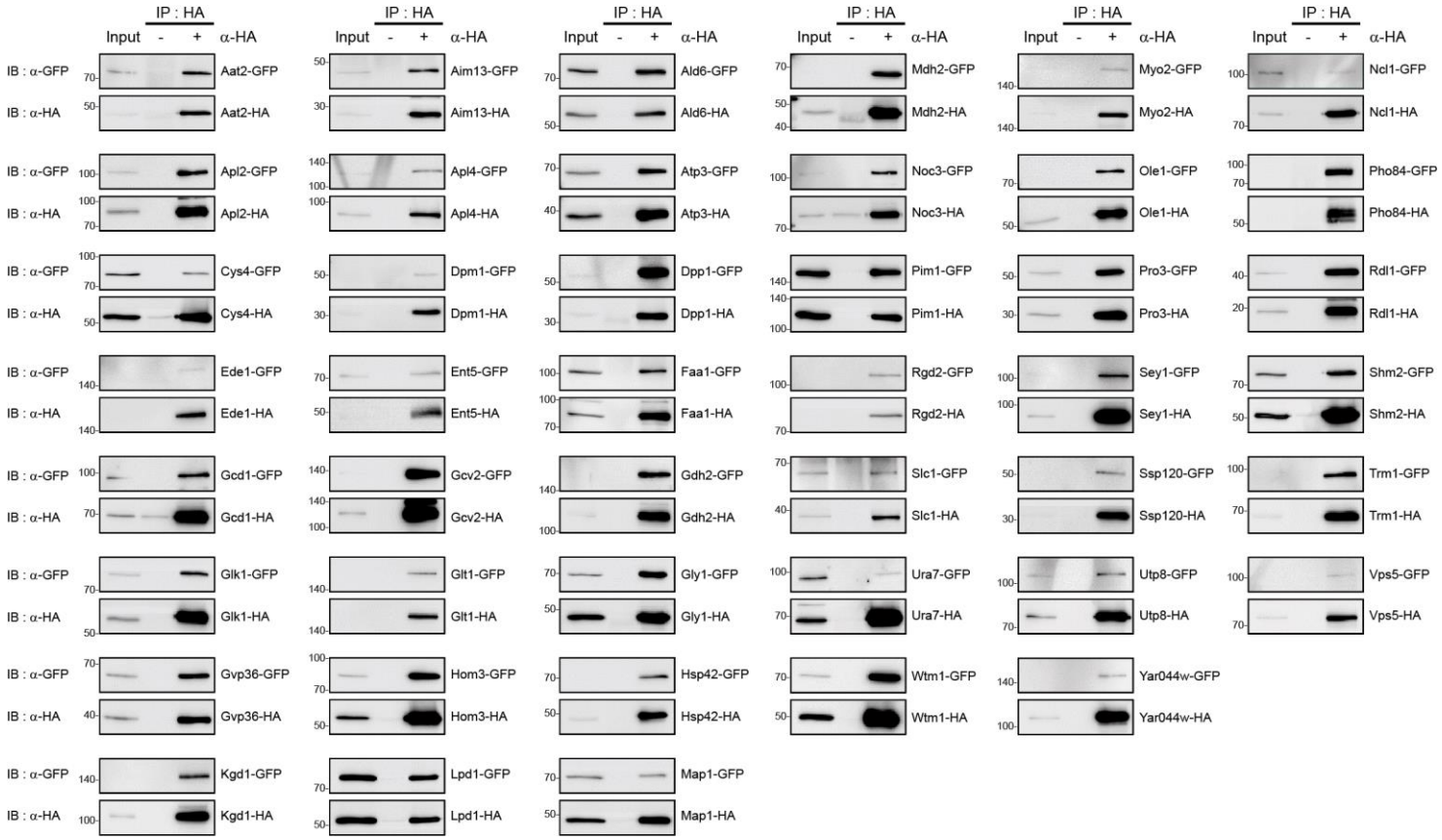

Figure III-4. Co-IP assay of homomer candidates.

GFP-tagged haploids and HA-tagged haploids were mated and the resulting diploid cells were subjected to Co-IP assay. The names of proteins tagged with GFP or HA are designated at the *right* of each panel. The positions of molecular weight markers (in kDa) are indicated on the *left* of each blot.

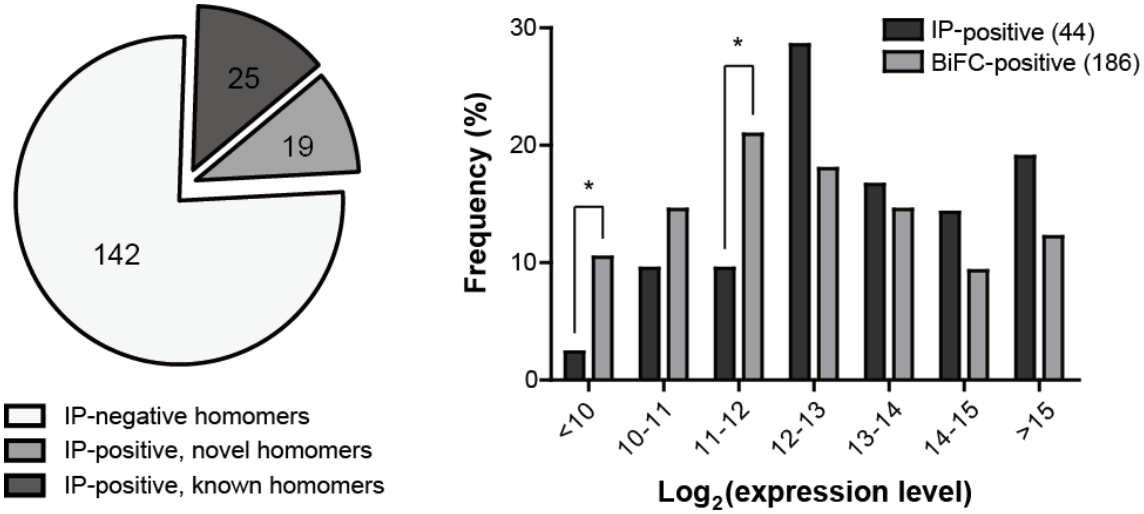

Figure III-5. Results of Co-IP verification and comparison of expression level.

(Left panel) Venn diagram depicting the numbers of homomer candidates detected by Co-IP and BiFC assay. For detail information about Co-IP assay, see Figure III-4. (Right panel) Bar graph depicting the comparison of expression levels of homomer candidates detected by Co-IP (black bars) and BiFC assay (gray bars). The expression level of each protein was obtained from the Yeast GFP Fusion Localization Database (https://yeastgfp.yeastgenome.org). Asterisks indicate significant enrichment in BiFC compared with Co-IP ($P < 0.05$; Hypergeometric p-value).

at the N-terminus of Rad52 and performed BiFC assay using four kinds of combinations. And as shown Figure III-6, Rad52 exhibited a clear nuclear signal only when both VN and VC were tagged N-terminally, suggesting that C-terminally tagged Rad52 has the topological constraints in the BiFC complex formation. Given that we used C-terminally VN- or VC-tagged strains in our screen, it is reasonable to assume that several true homomers did not show positive BiFC signals due to the topological constraints. Third, although all tested proteins in Fig. II-3 showed sufficient expression at the expected protein sizes, C-terminal tagging of VC to some genes may disturb proper expression or folding of fusion gene products as discussed in the previous chapter.

As explained at the introduction chapter, one of the pitfalls when applying BiFC assay is its irreversible characteristics (Shyu and Hu 2008). This feature may make two fused proteins hard to be separated as needed, which can result in imparied phenotypes. So we generated diploids in which both alleles of selected homomer gene are tagged with VC gene and compared their growth phenotypes to those of diploids with VN and VC tagged to each allele. Proteins reported to be inviable or decreased in growth in null mutant were selected for this assay to more easily observe the effect of irreversible complex formation: Aco2 (Yjl200c), Acs1 (Yal054c), Gin4 (Ydr507c), Kap123 (Yer110c), Myo2 (Yor326w), Pse1 (Ymr308c), Utp8 (Ygr128c), and Xrn1 (Ygl173c) (Giaever et al. 2002; Asano et al. 2006; Yoshikawa et al. 2011; Chen et al. 2012; Orij et al. 2012; Sinturel et al. 2012). As depicted in Figure III-7, we could detect no significant difference in growth phenotypes at every tested temperature between two types of diploids, which is implying that there are mild or little perturbation caused by irreversibility in the tested candidates.

3.2. Characterization of protein homomers

Among the 186 protein homomers identified in this study, 144 (77%) were soluble and

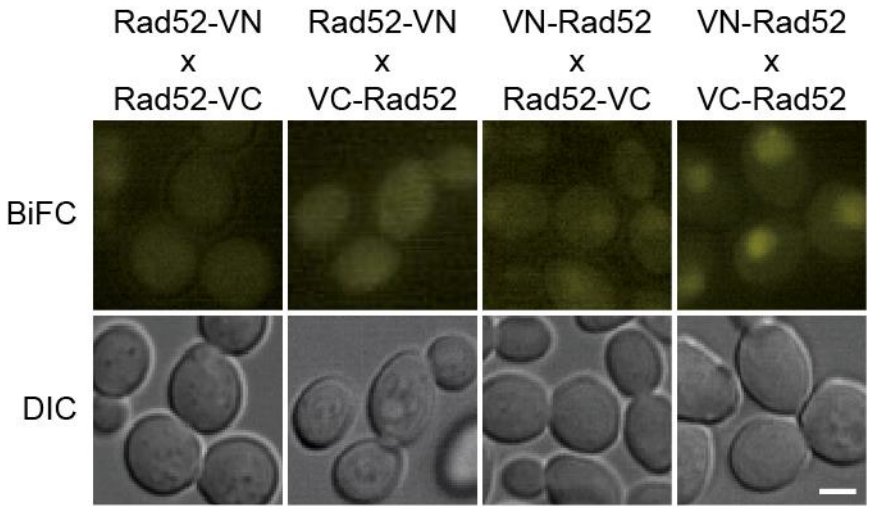

Figure III-6. BiFC analysis of Rad52 homomer.

Cells expressing N-terminally VN- or VC-tagged Rad52 were constructed and mated with cells expressing C-terminally VC- or VN-tagged Rad52. The resulting diploid cells expressing four kinds of combinations of VN- and VC-tagged Rad52 (Rad52-VN × Rad52-VC, Rad52-VN × VC-Rad52, VN-Rad52 × Rad52-VC, and VN-Rad52 × VC-Rad52) were subjected to BiFC assay. Scale bars, 2 μm.

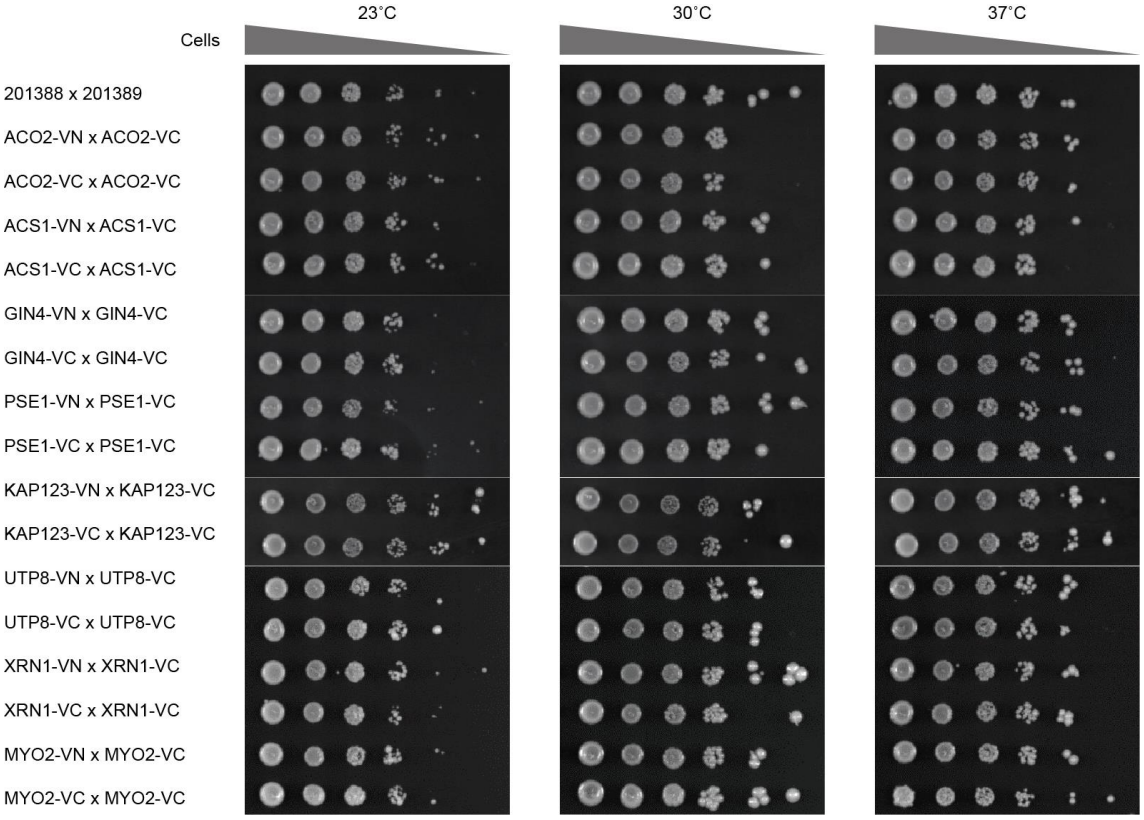

Figure III-7. Spot assay for growth phenotypes of VN/VC-tagged and VC/VC-tagged diploids.

10-fold serial dilution of each strain were spotted on SC agar media and incubated either at 23°C, 30°C, or 37°C for three days. Names of genes and tagged epitopes are indicated at the left of the panels.

the remaining 42 (23%) were membrane proteins. And 82 out of 186 are known to form homomers according to the *Saccharomyces* Genome Database (https://www.yeastgenome.org, as of June 14th, 2017) while the rest 104 are novel homomers (Table III-3). 519 homomer candidates have been reported in previous studies that tried to define protein interactome in *S. cerevisiae* (Krogan et al. 2006; Tarassov et al. 2008; Yu et al. 2008). We compared our dataset to theirs and investigated how many candidates overlapped between different studies. Only 47 out of 186 candidates identified here also appeared in 519 homomer candidates of previous data sets, and the rest 139 were defined only in this study (Figure III-8A). In addition, our data set showed a modest concordance with previous reports from Krogan et al. (2006) (4%), Tarassov et al. (2008) (9%), and Yu et al. (2008) (3%) (Figure III-8B). And this small percentage of overlap was similarly observed in comparison between other studies. Studies of Krogan et al. (2006) and Yu et al. (2008) were performed with TAP-MS and the yeast two-hybrid method, respectively, which do not measure PPI in the natural cellular context. Tarassov et al. (2008) employed a protein-fragment complementation assay utilizing the murine dihydrofolate reductase. The identification of 104 new protein homomers in this study reflects the difference in the employed experimental methods of each research and, thus, our data set appears to be highly complementary to the existing data sets. We also believe that the relatively low overlap between previous data sets and our data set is partly due to the topological constraints in the BiFC complex formation as described above.

One of the advantages of the BiFC assay is, as emphasized in the introduction chapter, that the subcellular localization where the PPI occurs can be directly visualized. So the subcellular region in which the BiFC signal is observed in this study represents the localization of the protein homomer. Based on the Yeast GFP Fusion Localization Database (Huh et al. 2003), protein homomers identified in this study were found to be

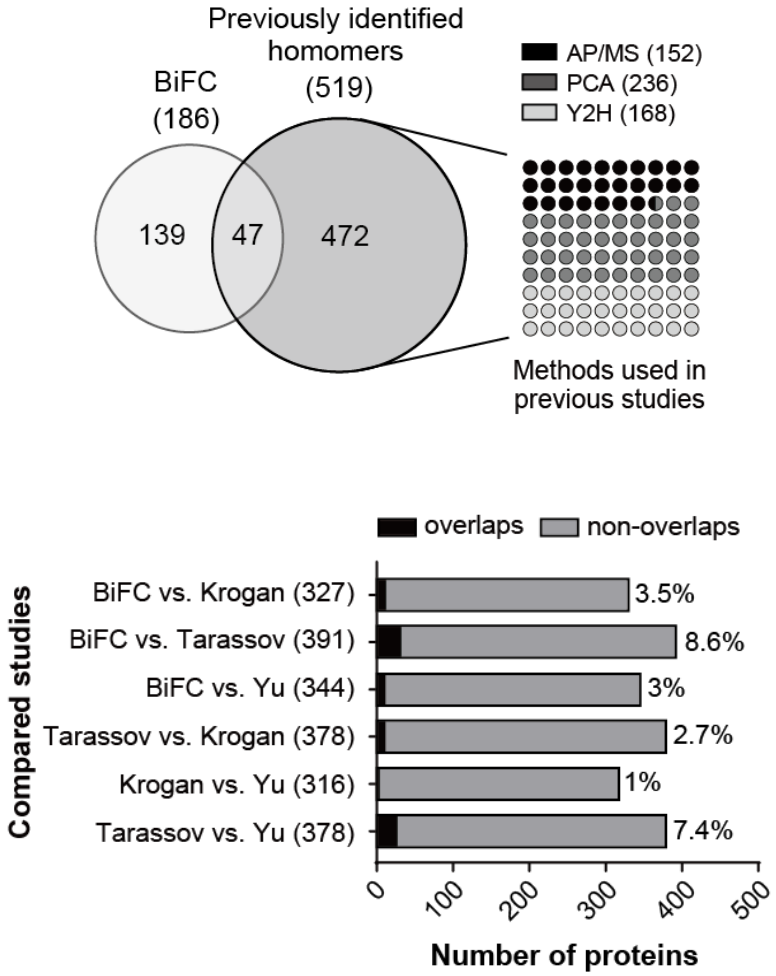

Figure III-8. Comparisons of protein homomer datasets

(Upper graph) (Left) Venn diagram depicting the comparison of homomer candidates identified in this study and those identified in three previous analyses. (Right) Analysis methods used in previous studies and the number of homomer candidates detected by each method. AP/MS, PCA, Y2H represent affinity purification-mass spectrometry, protein complementation assay, and yeast two-hybrid assay, respectively. (Lower) Bar graph depicting the comparison between the data set in this study and each of the three previous data sets. Black and gray bars indicate the number of homomer candidates that overlap and do not overlap, respectively, with the data set in this study. The percentage of concordance between data sets is indicated on the right side of the bars. Numbers in parentheses indicate the total number of homomer candidates identified in two studies.

present at various subcellular regions (Figure III-9A). Notably, protein homomers were significantly enriched in the bud neck (P=0.0399), the mitochondrion (P=0.0444), the vacuolar membrane (P=0.0001), the actin (P=0.0122), the lipid droplet (P=0.017), and the bud (P=0.0363). And we could also see that known and novel homomers were distributed evenly across various organelles except the mitochondrion, where novel homomers were highly enriched (P=0.0138) (Figure III-9B). To give a reliability to this localization analysis, we further analyzed an exact site of homomers which were categorized in organelles with dot-shaped patterns - early Golgi, endosome, late Golgi, lipid droplet, peroxisome, and vacuolar membrane - with corresponding RFP markers, and it turned out that all tested homomers co-localized with RFP marker proteins of their reported localization. BiFC and RFP images of them can be found on Figure III-10.

Results of gene ontology (GO) analysis of protein homomers are listed in Table III-4. Protein homomers identified in this study can be categorized into a variety of biological processes including transport, cellular component organization or biogenesis, metabolic process, DNA and RNA metabolism, translation, protein modification, and cell cycle. Interestingly, we found that protein homomers were significantly overrepresented in the biological processes of transport and cellular component organization. This is not surprising given that many proteins functioning in transport, such as vesicle proteins or channel proteins, are reported to form homomers to provide cavity and specificity for their cargos. Recent studies have provided many examples of these cases. For example, aquaporins, an integral membrane proteins that selectively transport water, but not ions, are homotetrameric to form a central pore across cell membranes (Agre and Kozono 2003). The crystallographically determined structures of several K^+ channels in bacteria, archaea, and eukaryotes have also been revealed to form homotetramers (MacKinnon 2003). Among the homomer candidates detected in this screening, various proteins which

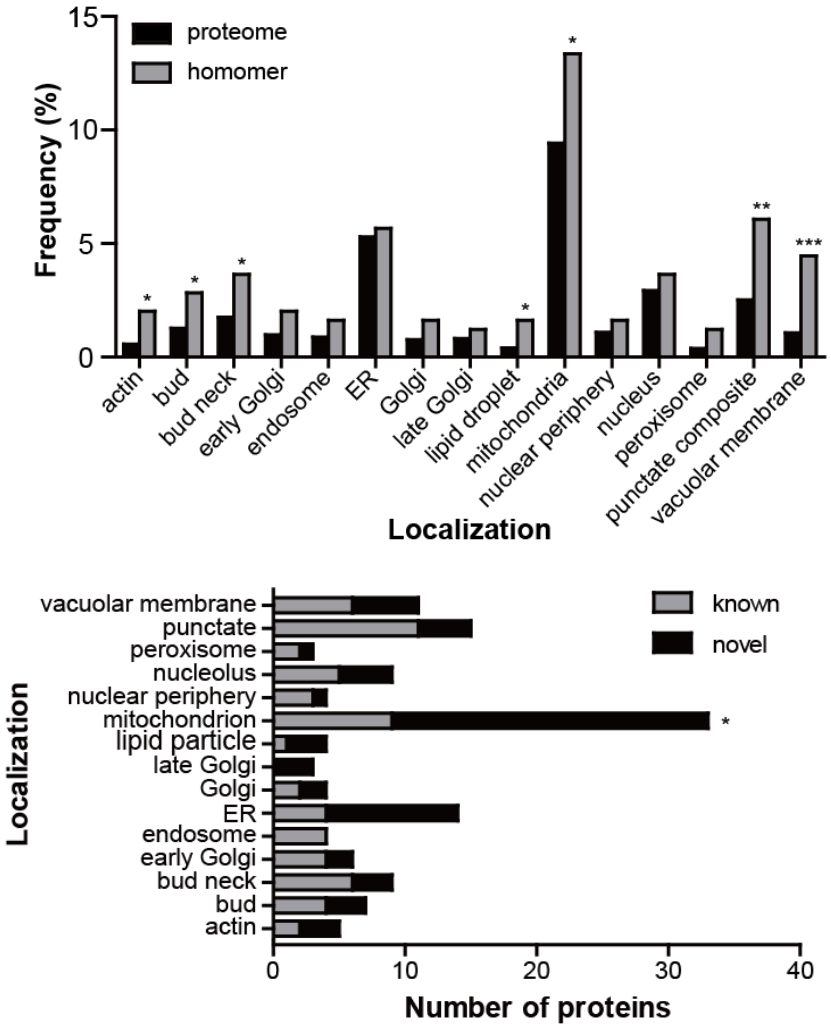

Figure III-9. Enrichments of subcellular localization with protein homomers.

(Upper graph) Subcellular localization of homomer candidates identified in this study. Black bars indicate whole proteins for which subcellular localization has been annotated in the Yeast GFP Fusion Localization Database, and gray bars represent homomer candidates identified in this study. Asterisks indicate significant differences compared with proteome (*$P < 0.05$, **$P < 0.01$, ***$P < 0.001$; Fisher's exact test). (Lower graph) Localization distribution of known and novel homomers. Gray and black bars indicate percentage of known and novel homomers, respectively. Asterisks indicate significant differences compared with known homomers (*$P < 0.05$; Fisher's exact test).

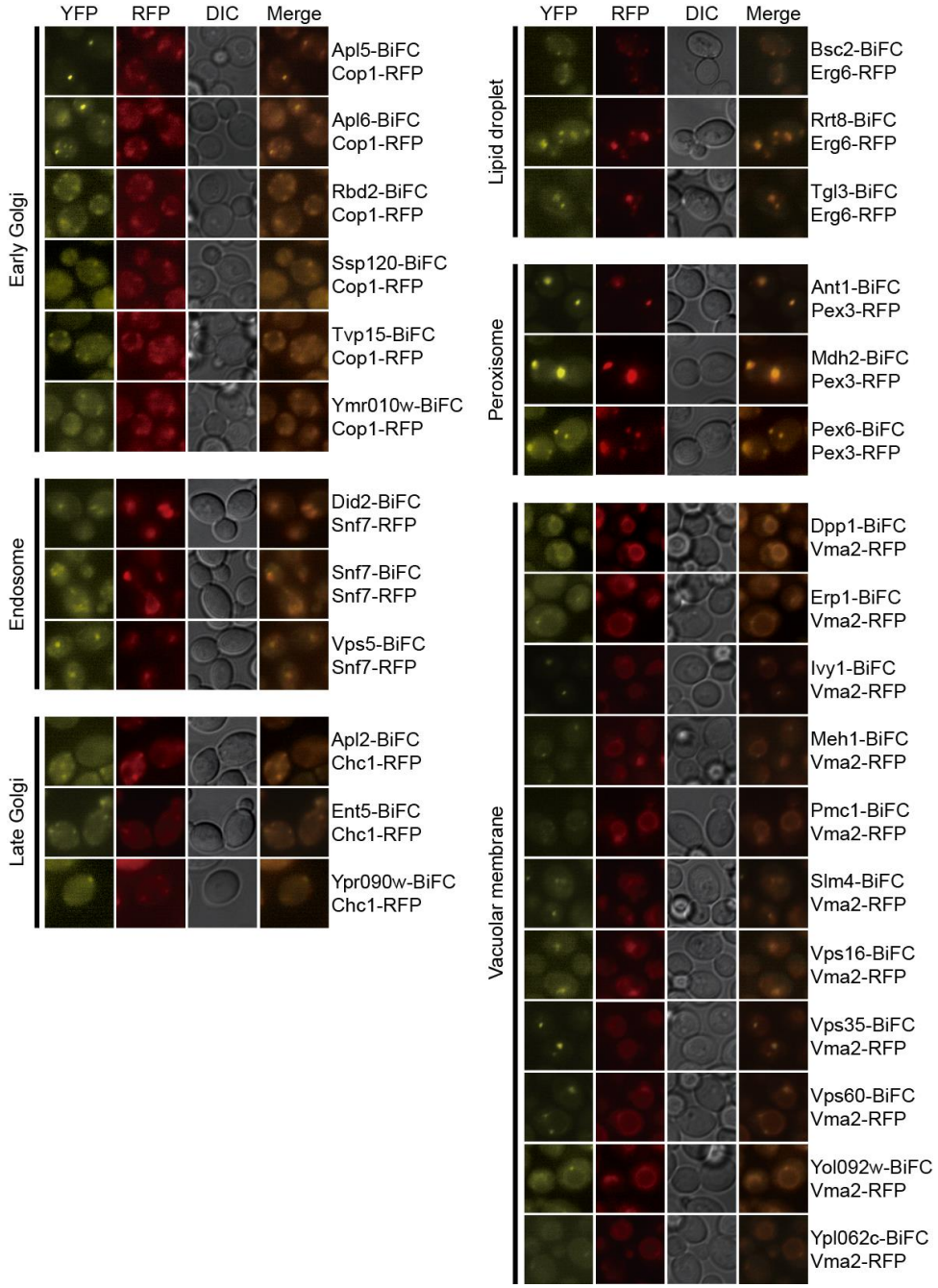

Figure III-10. BiFC and RFP images of homomer candidates and marker proteins.

Homomers known to localize at endosome, early and late Golgi, lipid droplet, peroxisome, and vacuolar membrane were checked by RFP-tagged marker proteins – Cop1, Snf7, Chc1, Pex3, Erg6 (Huh et al. 2003), and Vma2 (Makrantoni et al. 2007), respectively. Names of homomers and marker proteins are indicated at the right of merged images. Subcellular organelles expected by marker proteins are at the left of each panel.

Table III-4. Gene ontology analysis of protein homomers

Biological Process	GO ID	GO category description	Frequency in homomer population (total 186)	*P*-value
transport	**48193**	**Golgi vesicle transport**	**16**	**0.000116665**
	51169	**nuclear transport**	**11**	**0.015468138**
	6811	ion transport	11	0.139209593
	55085	transmembrane transport	10	0.139479466
	16197	**endosomal transport**	**8**	**0.009086389**
	6869	lipid transport	4	0.133088545
	8643	carbohydrate transport	1	0.621167231
	15931	**nucleobase-containing compound transport**	**10**	**0.008225172**
	6897	**endocytosis**	**10**	**0.000454607**
	6605	protein targeting	13	0.106865701
	6887	exocytosis	6	**0.002679747**
cellular component organization or biogenesis	**70271**	**protein complex biogenesis**	**17**	**0.004610225**
	7005	**mitochondrion organization**	**16**	**0.004049322**
	7010	**cytoskeleton organization**	**15**	**0.00358111**
	48308	**organelle inheritance**	**11**	**8.75213E-07**
	7033	**vacuole organization**	**7**	**0.01334185**
	7031	**peroxisome organization**	**6**	**0.002973437**

	71554	cell wall organization or biogenesis	5	0.487193395
	70925	organelle assembly	4	0.551952211
	16050	vesicle organization	5	0.084515152
	42274	ribosomal small subunit biogenesis	6	0.195624163
	42273	ribosomal large subunit biogenesis	6	0.080007965
	48284	organelle fusion	5	0.114475985
	61025	**membrane fusion**	**6**	**0.022112408**
metabolic process	**6520**	**cellular amino acid metabolic process**	**13**	**0.004867284**
	55086	**nucleobase-containing small molecule metabolic process**	**11**	**0.028010544**
	6629	lipid metabolic process	10	0.352254338
	51186	cofactor metabolic process	6	0.26153279
	32787	**monocarboxylic acid metabolic process**	**8**	**0.049416376**
	6091	**generation of precursor metabolites and energy**	**9**	**0.033960724**
RNA metabolism	6364	rRNA processing	12	0.18837999
	6401	RNA catabolic process	6	0.182404401
	43144	snoRNA processing	2	0.37546641
	6360	transcription from RNA polymerase I promoter	2	0.590036772
	6354	DNA-templated transcription, elongation	5	0.148816733
	6352	DNA-templated transcription, initiation	3	0.353800041
	6353	DNA-templated transcription, termination	2	0.354483876
response to stimulus	6970	response to osmotic stress	5	0.126868101
	42594	response to starvation	4	0.0777646
	9408	response to heat	4	0.159867504

DNA metabolic process	6310	DNA recombination	3	0.21112246
	6260	DNA replication	4	0.625120163
translation	6417	regulation of translation	5	0.186965956
	6413	translational initiation	4	0.099142222
protein modification process	31399	regulation of protein modification process	5	0.217668178
	18193	peptidyl-amino acid modification	5	0.444078043
	16570	histone modification	4	0.420292202
	43543	protein acylation	3	0.297957367
	6457	protein folding	5	0.139849834
cell cycle	**51726**	**regulation of cell cycle**	**11**	**0.074132695**
	910	cytokinesis	5	0.095207269
single-organism cellular process	7114	cell budding	4	0.086011204
	902	cell morphogenesis	1	0.573752213
	45333	**cellular respiration**	**7**	**0.009838538**
	23052	signaling	9	0.277615077

Gene ontology over-enriched in homomer population are listed. Hypergeometric p-value was calculated and those with P<0.05 are presented in bold.

are components of ion channels or transport vesicles were included. Pmc1(Ygl006w), a vacuolar Ca2+ transporter (Cunningham and Fink 1994) and Pho84 (Yml123c), a high affinity inorganic phosphate transporter (Bun-Ya et al. 1991), showed BiFC signal in their previously reported subcellular localization. Tim11(Ydr322c-a), a subunit of F1F0 ATPase (Arnold et al. 1998), was also detected by BiFC screening. Snf7 (Ylr024w), another homomer candidates detected in this study, was reported to form oligomer to make vesicles in MDV (multivesicular body) pathway, mediating cargo transports from late endosome to vacuole (Saksena et al. 2009). Several members of AP-complex (Apl2, Apl4, Apl5, Apl6) (Hirst et al. 2011; Pastor-Cantizano et al. 2016) and yeast p24 family (Erp1, Emp24, Erv1) (Pastor-Cantizano et al. 2016) are also included in our dataset and these examples partially explain high enrichment of protein homomers in transport activity.

We also analyzed GO enrichment of homomer candidates detected in previous studies (the same studies analyzed in the Figure III-8B) and found that different biological processes are enriched in homomer populations detected by different PPI analyzing tools. 152 homomer candidates obtained by Krogan et al (2006) were extremely concentrated in biological processes related to DNA and RNA metabolic pathways while 168 candidates detected by Yu et al (2008) showed no noticeable connectivity between highly enriched groups. These different GO enrichments between the two studies and dataset of this study might have partly caused by different sensitivity and preference of analyzing tools exploited in each study. Since AP/MS and yeast-two-hybrid were used in the researches of Krogan et al (2006) and Yu et al (2008), both dataset are highly concentrated on abundant, soluble protein. GO analysis of 236 homomer candidates found by Tarassov et al (2008), on the other hand, revealed the similar results to those of dataset of this study, showing highly enrichment in biological processes related to transport activity and

organelle organization. These candidates were detected by using DHFR survival assay, which is an another common method based on protein fragments complementation, so we assumed that the similarities of GO enrichment found in two datasets, Tarassov et al (2008) and this study, are results of exploiting similar PPI analyzing tools.

Next we compared the subcellular localization between the BiFC and GFP signals of protein homomers. As presented in Figure III-11, most protein homomers, 156 out of 186, showed identical localization patterns between the BiFC and GFP signals. However, the BiFC signals of 21 proteins appeared in foci or partial localization within a region where the corresponding GFP fusion protein was detected. This results can be interpreted that only a small fraction of these proteins form homomers whereas the rest of them stay as monomers. It also likely means that for some proteins, the subcellular localizations of homomers and monomers are differentially regulated. Information about partial or same localization of protein homomers can be found in Table III-3.

3.3. Changes of homomerization signal upon nitrogen deprivation

Nitrogen is an essential element in every living organism, and global readjusting of gene expression and signaling pathways in yeast cells are caused in nitrogen-deprived environment (Gasch et al. 2000; Gasch and Werner-Washburne 2002; Kamada et al. 2004; Conway et al. 2012; Song and Kumar 2012), leading to various biological phenomena such as autophagy, filamentous growth, and accumulation of specific macromolecules (Gimeno et al. 1992; Schulze et al. 1996; Lorenz and Heitman 1997; Parrou et al. 1999; Onodera and Ohsumi 2005). To examine how protein homomerization is rearranged in response to nitrogen deprivation, we investigated changes in the BiFC signal pattern of protein homomers with yeast cells treated with nitrogen-deprived medium. Strikingly, we found that 21 protein homomers showed significantly increased BiFC signals under

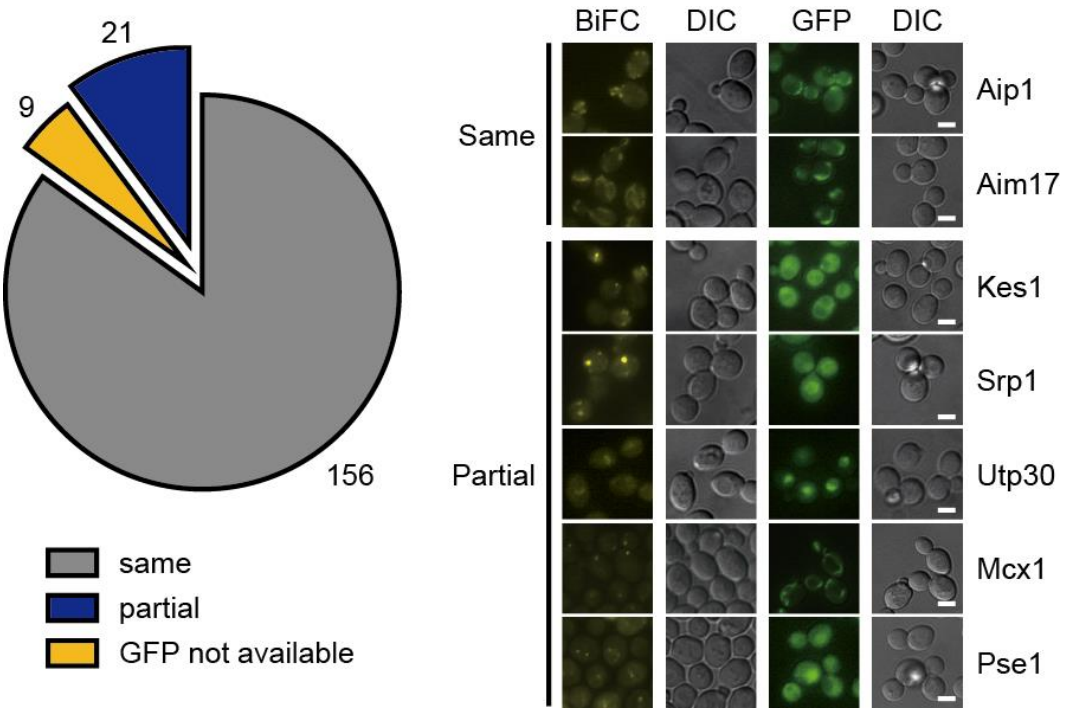

Figure III-11. Comparison of localization between BiFC and GFP signals

(Left panel) Venn diagram is depicting the comparison between the BiFC signal and GFP signal of each protein homomer. Proteins with identical BiFC and GFP signal patterns are shown as a gray pie. Proteins showing the BiFC signal partially localized within the GFP signal are indicated as a green pie. Proteins for which subcellular localization has not been annotated in the Yeast GFP Fusion Localization Database are shown as a yellow pie. (Right panel) Representative fluorescence images of proteins showing the same or partial localization between the BiFC and GFP signals. Scale bars, 2 μm.

nitrogen starvation (Figure III-12 and 13), while other15 proteins presented clearly decreased signals (Figure III-14 and 15). To confirm whether these changes of the BiFC signals are due to changes in expression or homomerization itself, we also examined changes of the GFP signals in the same culture condition. As a result, 4 out of 21 showed increased GFP signal (Aim17, Met14, Rdl1, and Rvs167) and 7 out of 15 proteins showed decreased GFP signal (Apl2, Bcp1, Caf120, Gly1, Mdh2, Myo2, and Myo4), suggesting that changes in the BiFC signal intensity of the above 11 proteins under nitrogen starvation are due to their altered expression levels rather than altered homomerization. In contrary, the other 25 proteins, which showed changes in the BiFC signal intensity but steady GFP signal intensity under nitrogen starvation, are likely subjected to alteration in their homomeric states by nitrogen deprivation.

To verify that the results from BiFC signal quantification accurately reflect actual increase or decrease of homomerization, several selected protein homomers were analyzed for their homomerization changes with two independent. First, 8 homomer candidates that showed increased or decreased homomeric signal were randomly selected measured by flow cytometry for their fluorescence intensity after incubation in nutrient-rich or nitrogen-deprived media. As depicted in Figure III-16, the tested homomers all showed consistent fluorescence changes detected by fluorescence microscope, regardless of their subcellular localization. Secondly, 3 homomer candidates – Glk1, Mdh2, Myo2- were checked for their changes of homomeric states by Co-IP assay. Ratios of GFP co-precipitated with HA in each condition were quantified and compared as depicted in Figure III-17, and again, the results correlated with the previous data – Glk1 increased and Mdh2 and Myo2 decreased in homomerization in nitrogen-deprived condition. Interestingly, decrease of BiFC signals of Mdh2 and Myo2 was considered as results of decreased expression levels at first, but this co-IP data suggests these proteins are changed

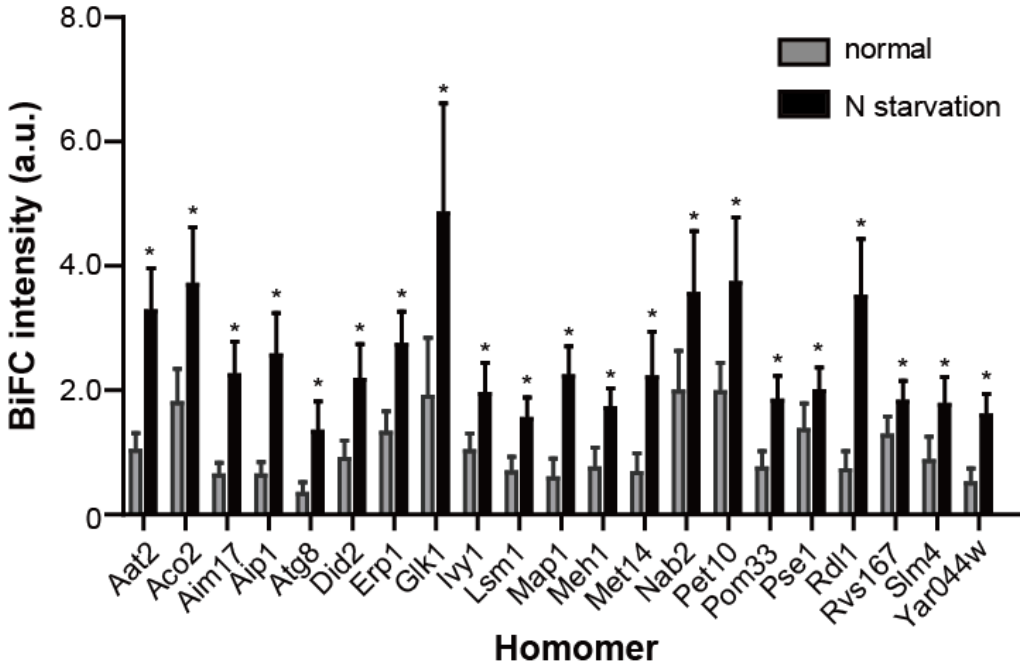

Figure III-12. Protein homomers showing increased BiFC signals upon nitrogen starvation.

Gray and black bars indicate the mean BiFC signal intensity of protein homomers under normal condition and nitrogen starvation, respectively. At least 50 cells were quantified under each condition. Error bars represent standard deviation. Asterisks indicate significant differences compared with normal condition (*$P < 0.0001$; Student's t test). For detailed information, see also Table III-5.

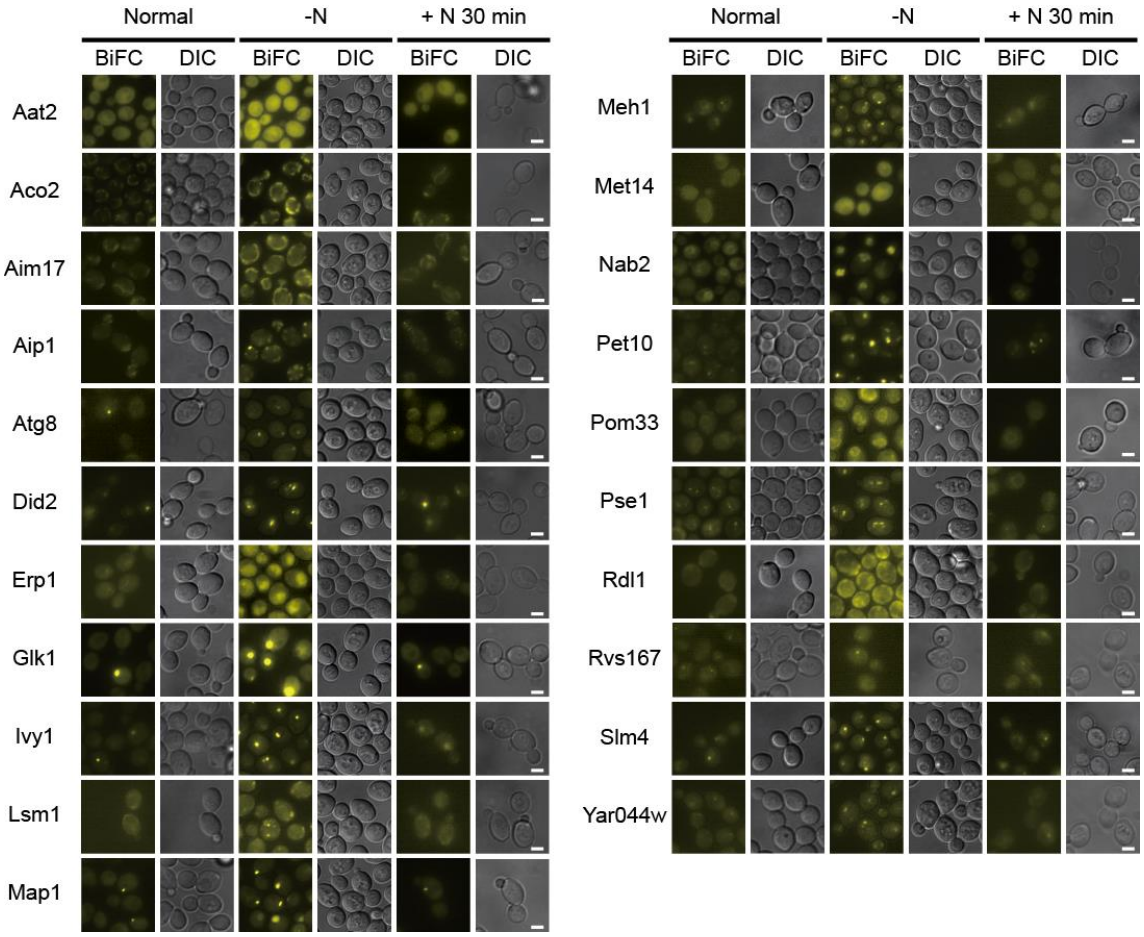

Figure III-13. Increased of homomerization upon nitrogen starvation.

Representative BiFC images of protein homomers showing increased BiFC signals upon nitrogen starvation and recovered BiFC signals after transfer to nitrogen containing media are depicted. Name of protein homomers are indicated at the left of each image. Culture conditions in which cells were analyzed are indicated at the top of images. Scale bars, 2 μm.

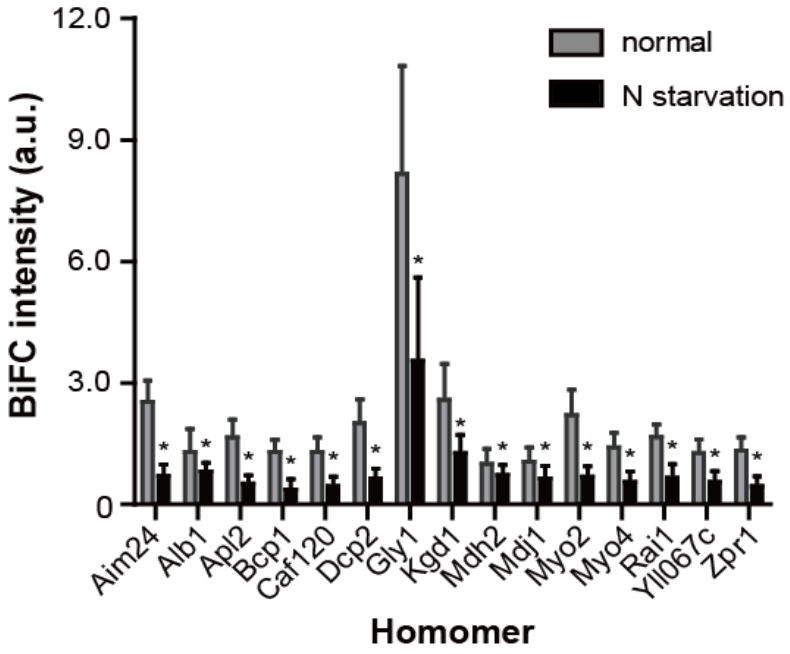

Figure III-14. Protein homomers showing decreased BiFC signals upon nitrogen starvation.

Gray and black bars indicate the mean BiFC signal intensity of protein homomers under normal condition and nitrogen starvation, respectively. At least 50 cells were quantified under each condition. Error bars represent standard deviation. Asterisks indicate significant differences compared with normal condition (*P < 0. 0001; Student's t test). For detailed information, see also Table III-5.

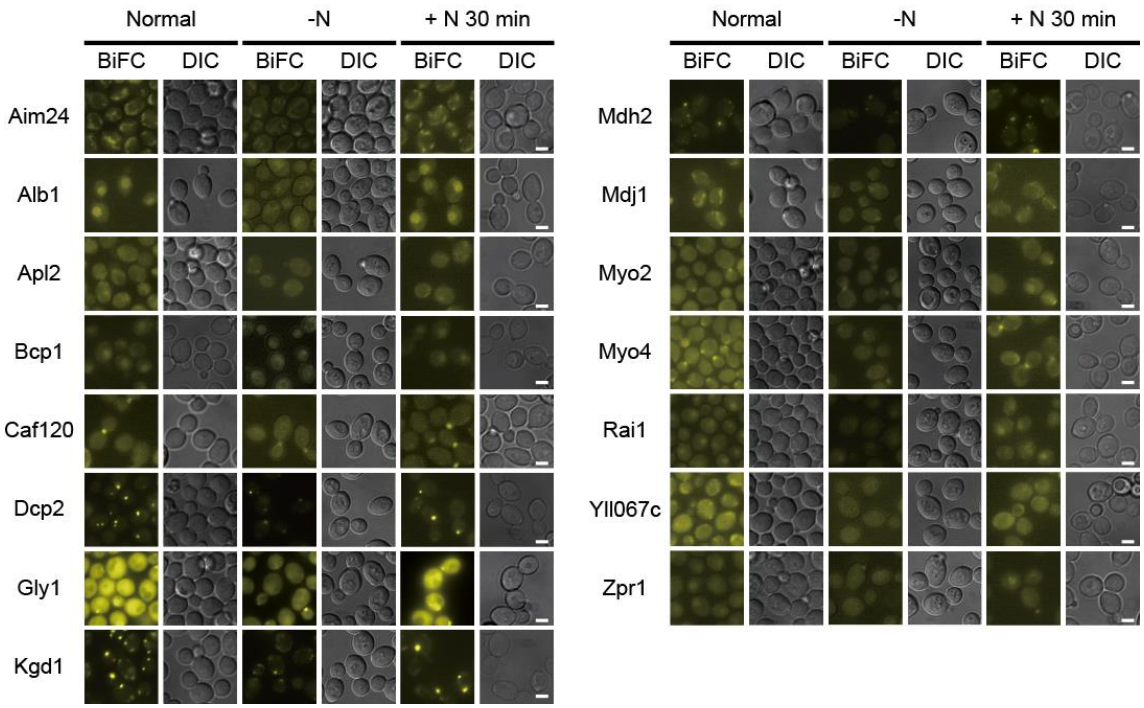

Figure III-15. Decreased of homomerization upon nitrogen starvation.

Representative BiFC images of protein homomers showing decreased BiFC signals upon nitrogen starvation and recovered BiFC signals after transfer to nitrogen containing media are depicted. Name of protein homomers are indicated at the left of each image. Culture conditions in which cells were analyzed are indicated at the top of images. Scale bars, 2 μm.

in both homomerization and expression upon starvation. Together, these results give a reliability for the observed changes of homomeric states and potentials that the same strategy can be exploited under various other stress conditions.

Apart from the above, 12 protein homomers were found to be changed in their BiFC localization under nitrogen starvation. As shown in Figure iii-18, 9 of them (Arc35, Atp19, Ilv6, Kap123, Noc3, Nop15, Rad51, Wtm1, and Yhr127w) localized to punctate foci under nitrogen starvation. GFP strains were also tested at the same condition, and localization of GFP of 12 proteins showed similar changes by nitrogen deprivation, demonstrating that changes of the BiFC localization of these proteins are results from translocation of the proteins, not from alteration in their homomeric states. The GFP images are presented in Figure III-19. Finally, we examined BiFC signals of all 48 homomer candidates after re-incubation in nitrogen-containing media. Signal intensities were all recovered to the similar levels as shown before starvation (Figure III-12~15) and candidates that showed changed localization under starvation also all re-localized to their original subcellular sites as observed in normal condition (Figure III-18) proposing that BiFC complex formation has little effect on protein dynamics in response to environmental changes. Protein homomers that showed changes in BiFC signal under nitrogen starvation are listed in Table III-5 and Table III-6.

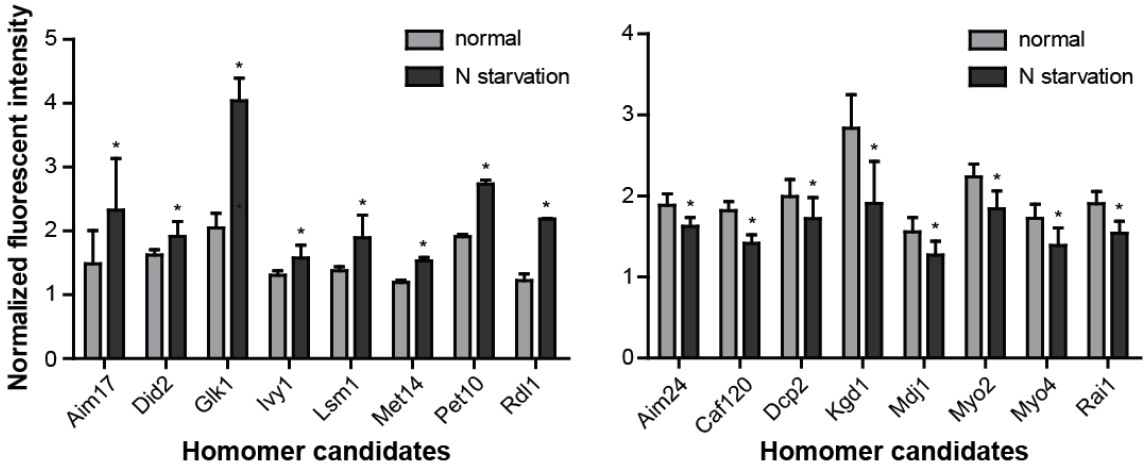

Figure III-16. Flow cytometry to detect fluorescence changes of homomer candidates.

(Left graph) Fluorescence increase of 8 candidates under nitrogen starvation. Grey and black bars indicate relative fluorescence intensity under normal and nitrogen-deprived condition, respectively. At least 100,000 cells were counted at each condition and average intensity was calculated from 3 independent experiments. Cells expressing VN and VC-tagged Mds3 were used as negative control to normalize fluorescent intensity of candidates. Error bars represent standard deviation. Asterisks indicate significant differences compared with normal condition. (*$P < 0.05$; Student's *t* test) (Right graph) Fluorescence decrease of 8 candidates under nitrogen starvation. Grey and black bars indicate relative fluorescence intensity under normal and nitrogen-deprived condition, respectively. At least 100,000 cells were counted at each condition and average intensity was calculated from 3 independent experiments. Cells expressing VN and VC-tagged Mds3 were used as negative control to normalize fluorescent intensity of candidates. Error bars represent standard deviation. Asterisks indicate significant differences compared with normal condition. (*$P < 0.05$; Student's *t* test)

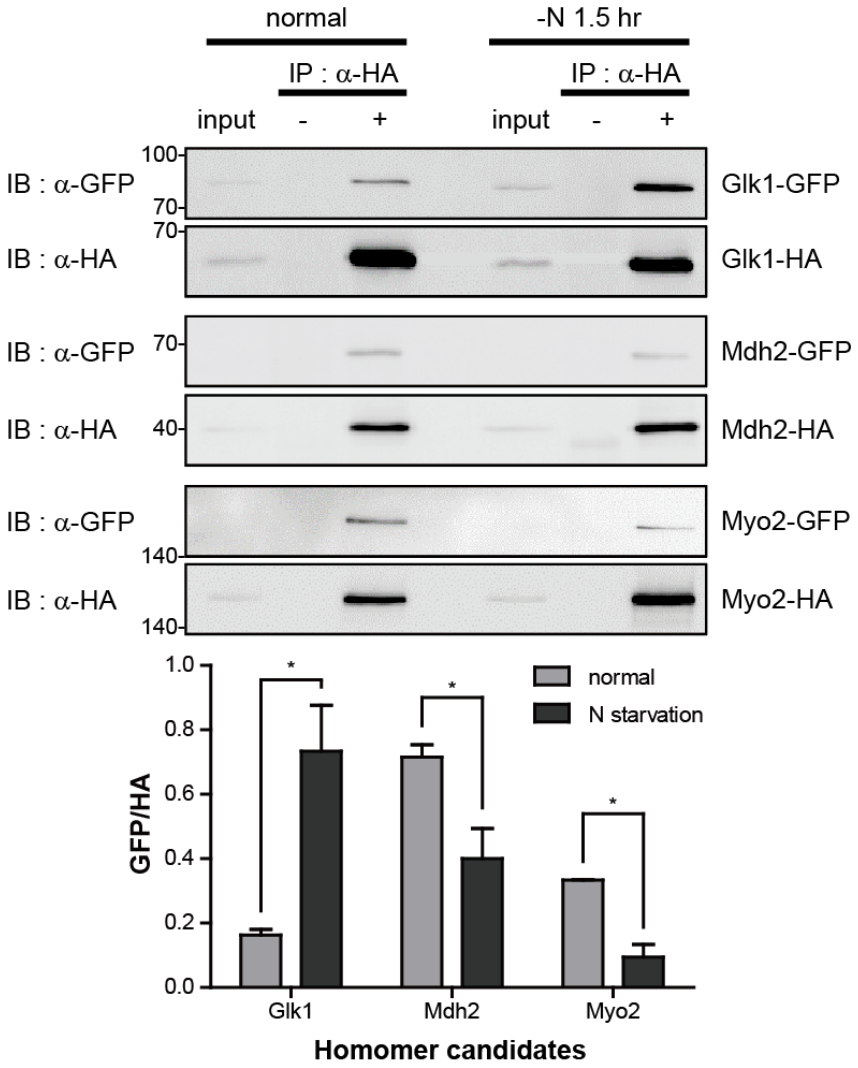

Figure III-17. Co-IP assays to determine homomeric states under two conditions.

(Upper) Images of Co-IP results under normal and nitrogen-deprived condition are shown. The names of proteins tagged with GFP or HA are marked at the right of each panel. The positions of molecular weight markers (in kDa) are indicated on the left of each blot. (Lower) Ratios of GFP-tagged proteins co-precipitated with HA-tagged proteins were calculated by using ImageJ (Schneider et al. 2012) and depicted as graph. Average of 2 independent experiments were presented by bar graphs with error bars representing standard deviation. Asterisks indicate significant differences compared with normal condition (*$P < 0.05$; Student's *t* test).

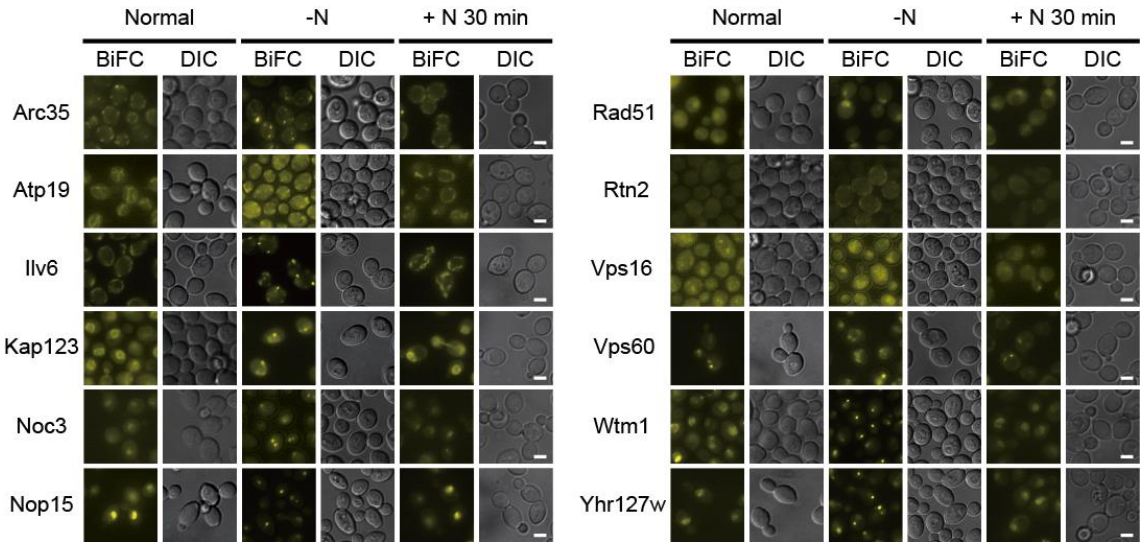

Figure III-18. Localization changes of homomers upon nitrogen starvation.

Representative BiFC images of protein homomers showing changed BiFC signals in their subcellular localization upon nitrogen starvation and recovered BiFC signals after transfer to nitrogen containing media are depicted. Name of protein homomers are indicated at the left of each image. Culture conditions in which cells were analyzed are indicated at the top of images. Scale bars, 2 μm.

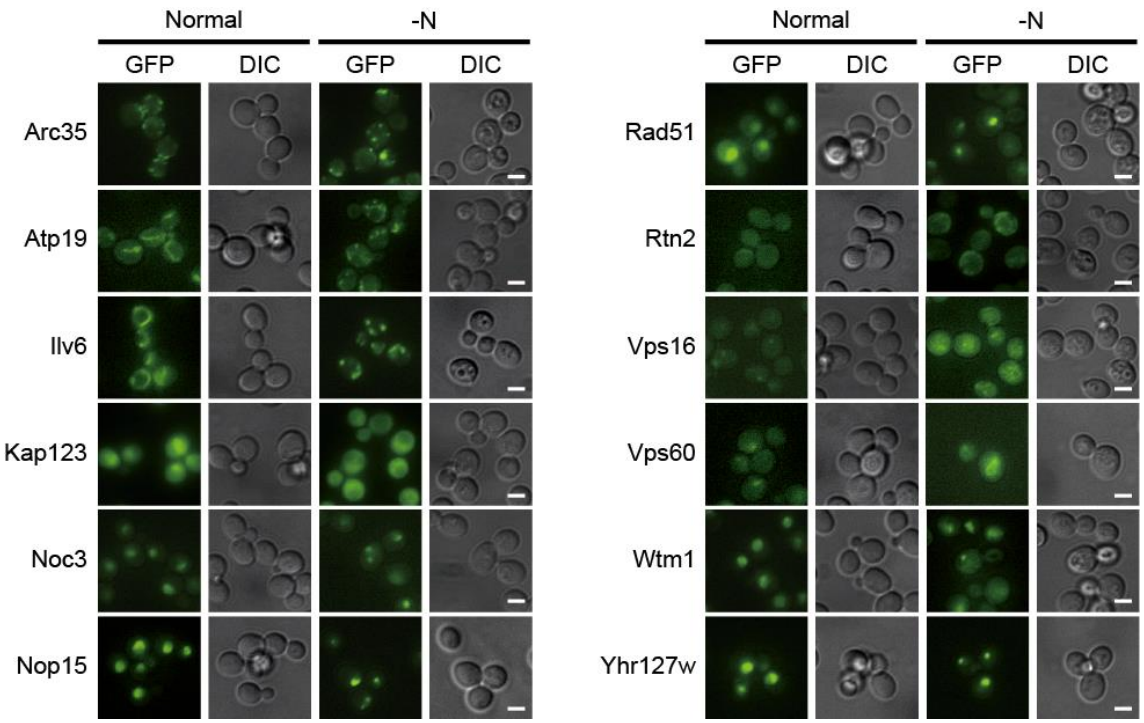

Figure III-19. Localization changes of GFP signals upon nitrogen starvation.

Representative GFP images of protein homomers showing changed in their subcellular localization of BiFC signals upon nitrogen starvation are depicted. Name of protein homomers are indicated at the left of each image. Culture conditions in which cells were analyzed are indicated at the top of images. Scale bars, 2 μm.

Table III-5. Protein homomers showing changes in the BiFC signal intensity upon N starvation

Gene name	Signal change	BiFC intensity				*P*-value	GFP intensity				*P*-value	BiFC intensity	
		Normal condition		N starvation			Normal condition		N starvation			Media transfer to SC after starvation	
		Mean	SD	Mean	SD		Mean	SD	Mean	SD		Mean	SD
AAT2	increased	1027526	284376	3267393	694128	3.7396E-30	NA[a]	NA	NA	NA	NA	1108550	439961
ACO2	increased	1793338	552359	3695635	925076	1.51057E-31	645174	189211	626574	171313	NS[b]	1792256	512603
AIM17	increased	631011	206713	2240128	542831	9.92144E-33	499457	127909	607727	111235	3.34203E-29	687626	301165
AIP1	increased	630661	215981	2564543	679329	1.64682E-24	718575	153048	701529	152945	NS	634219	240076
ATG8	increased	336084	186983	1334661	487203	1.17856E-22	NA	NA	NA	NA	NS	375859	126767
DID2	increased	897249	291359	2172651	572455	3.51593E-33	505961	86216	507292	102930	NS	879400	296147
ERP1	increased	1317516	346521	2727993	533566	1.05831E-41	740583	174622	746194	200849	NS	1350160	253736
GLK1	increased	1894332	948904	4841434	1772968	3.90326E-28	730495	295006	708647	313826	NS	2023013	1556487
IVY1	increased	1022127	279742	1945671	494838	4.23879E-32	462220	94459	464526	121968	NS	1022620	288151
LSM1	increased	683210	246316	1539428	345669	1.05502E-28	562840	96880	557797	112278	NS	778739	363016
MAP1	increased	582213	322730	2222202	487910	2.17712E-38	707016	163922	708851	177854	NS	705521	291795
MEH1	increased	742044	332086	1715386	312549	4.43808E-37	543663	113733	548660	124754	NS	705521	291795
MET14	increased	671142	317533	2212701	732883	2.50858E-30	396236	102627	565903	110659	4.13882E-49	664887	285105
NAB2	increased	1983494	651200	3549036	1012280	2.95415E-26	755636	192387	745787	184451	NS	1922907	586407
PET10	increased	1968393	474356	3724972	1057533	3.09247E-21	388906	97996	381218	107236	NS	1875303	379521
POM33	increased	740012	283586	1833334	399176	5.24651E-47	777560	145280	763322	164933	NS	719698	216705
PSE1	increased	1366222	422360	1990892	380247	1.11984E-15	825006	163233	823485	171620	NS	1214963	238441
RDL1	increased	718186	303336	3503421	936027	4.98813E-34	678822	192957	832256	234369	4.57758E-26	715492	291184

RVS167	increased	1268702	305230	1814506	338791	7.61435E-42	450061	130037	648876	109004	5.22893E-39	1247080	270435
SLM4	increased	865243	394250	1763449	453708	3.43497E-54	619949	125573	621270	139854	NS	801722	196772
YAR044W	increased	502587	238508	1595366	348880	4.70233E-49	599213	155071	597198	170936	NS	506470	209050
AIM24	decreased	2537457	518699	701905	284351	1.57035E-45	575363	120935	576080	140805	NS	2469201	274083
ALB1	decreased	1293149	571085	815717	213194	7.92916E-11	673414	153601	675090	139643	NS	1267444	203627
APL2	decreased	1654257	443263	514540	198854	7.95002E-33	799235	118744	231722	79187	1.29692E-56	1555102	289205
BCP1	decreased	1296963	297050	368464	257345	1.93919E-38	677596	142673	304528	80487	5.89085E-39	1242036	323254
CAF120	decreased	1294282	359856	450332	229948	3.86863E-40	699086	162955	233476	81374	2.58069E-38	1260769	196169
DCP2	decreased	2001703	598164	641186	243662	1.01451E-30	628672	149515	621444	132867	NS	1870623	217774
GLY1	decreased	8155149	2668036	3542082	2054111	1.03627E-30	2963637	591944	2006516	380446	6.7859E-33	8256921	1983719
KGD1	decreased	2581085	880616	1261206	450903	9.78149E-22	1169415	315979	1144677	374498	NS	2353482	392357
MDH2	decreased	1003452	376448	722164	256512	2.84682E-18	1200365	261792	458286	113133	4.55315E-36	1038207	298835
MDJ1	decreased	1058018	343087	648683	304163	1.0622E-42	817354	141557	785585	191013	NS	1039526	222982
MYO2	decreased	2207040	628357	689573	255867	2.07679E-32	612945	153564	300787	77482	1.34037E-31	2364030	205985
MYO4	decreased	1409354	357217	559248	256104	1.91444E-43	491736	113805	297733	77600	1.62017E-31	1379795	296395
RAI1	decreased	1666970	311378	658950	335540	1.27331E-41	658133	139239	649702	131837	NS	1652780	262618
YLL067C	decreased	1263120	343697	558140	264092	2.35259E-42	NA	NA	NA	NA	NS	1257482	320724
ZPR1	decreased	1326059	332876	458635	235708	4.40009E-46	957186	204334	939027	134037	NS	1363628	262645

[a]NA: not available
[b]NS: not significant

Table III-6. Protein homomers showing changes in the BiFC signal localization upon N starvation

Gene name	Subcellular localization of the BiFC signal		Subcellular localization of the GFP signal	
	Normal condition	N starvation	Normal condition	N starvation
ARC35	actin	punctate foci	actin	punctate foci
ATP19	mitochondrion	punctate foci	mitochondrion	punctate foci
ILV6	mitochondrion	punctate foci	mitochondrion	punctate foci
KAP123	nuclear membrane	punctate foci	cytoplasm, nucleus	cytoplasm
NOC3	nucleolus, nucleus	punctate foci	nucleolus, nucleus	punctate foci
NOP15	nucleolus, nucleus	punctate foci	nucleolus, nucleus	punctate foci
RAD51	cytoplasm, nucleus	nuclear foci	cytoplasm, nucleus	nuclear foci
RTN2	ER	plasma membrane	ER	plasma membrane
VPS16	vacuolar membrane	vacuole	vacuolar membrane	vacuole
VPS60	vacuolar membrane	vacuole	vacuolar membrane	vacuole
WTM1	nucleus	punctate foci	nucleus	punctate foci
YHR127W	nucleus	punctate foci	nucleus	punctate foci

4. Discussion

In this study, we identified protein homomers at a genome-wide scale to demonstrate the validity of the VC fusion library constructed in the previous chapter by using it with VN fusion library. Through this genome-wide BiFC analysis, 186 protein homomer candidates in yeast were detected. Remarkably, our data set includes 104 protein homomers that have never been identified in previous studies, probably due to various technical limitations. Given that protein homomerization is one of the simplest and efficient ways cells can use to regulate function, concentration, and structure of proteins, we are expecting that our data set will be a valuable resource for understanding of physiological effects protein homomerization is having.

Despite of discovery of 104 novel homomer candidates, 171 known homomers were screened out during self-assembly analysis, revealing critical downsides of this system. The second criterion should be applied to minimize missing of true positives. Firstly, localization difference observed between the self-assembly signal and candidate-tagged BiFC signal can be considered. Indeed, among 16 candidates satisfying this criterion, 8 candidates are known homomers. But this was valid only for proteins localized to restricted area of subcellular organelle, and every cytoplasmic or nuclear candidates with sufficient intracellular abundance failed to be selected, including well-known homomers including Hsp104 (Wendler et al. 2007), Fas1 (Babu et al. 2012), Fas2 (Johansson et al. 2008), Hsp82 (Marsh et al. 1998) and ribosomal proteins (Qiu et al. 2006). Further approaches, e.g., Co-IP, mass spectrometry, and FCS, only for those whose expression level exceeds a certain cut-off may help to minimize loss of true PPIs in genome-wide BiFC screens with fewer efforts.

While many proteins with transport activity are scored in the BiFC screening, relatively small number of transcription factors were detected. As described in the introduction section, many DNA-binding proteins use homomerization to obtain increased affinity in their binding interfaces. Among the 150 transcription factors of S. cerevisiae, 47 were reported to form homomeric interaction based on the PPIs in the *Saccharomyces* Genome Database (https://www.yeastgenome.org, as of June 19th, 2018), however, only 2 were included in the homomer candidates detected in this study. We found that 4 were eliminated by self-assembly screening, 3 were not available in VC-tagged strains, and 23 had relatively low expression levels to be visualized by BiFC assay. But for the remaining 15 transcription factors, we assume that for at least some of these candidates, BiFC complex formation are hampered by topological constraints. Investigation of BiFC signal appearance with N-terminal VN/VC-tagged strains of these candidates will help to estimate false-negative rate of homomer screening using C-terminally tagged VN and VC libraries.

We obtained subcellular localization of homomer candidates and found that 21 candidates showed partial signals when compared to GFP signals of the same proteins. One of interesting candidates is Pse1 (Ymr308c), a yeast importin, which showed BiFC signal as dots on nuclear envelope while its GFP-tagged form in our data as well as previous studies (Seedorf and Silver 1997) both are localized to cytoplasm and nucleus. It was reported that C-terminally epitope tagged Pse1 behaved like non-tagged wild type Pse1 and *pse1* mutant not interacting with Ran-GTP was observed to be accumulated on nuclear envelope (Seedorf et al. 1999), similar to BiFC signal we detected. This suggests a possibility that localization of this protein may be dependent of its interacting partner. Several cases of importins: Pse1, Srp1 (Solsbacher et al. 1998), Kap123 (Seedorf and Silver 1997) are included in 21 candidates and showed similar signal patterns.

Adenovirus-based β-arrestin BiFC assay was successfully used to monitor activation of G protein-coupled receptors, a typical membrane protein family (Song et al. 2014), and the aquaporin complexes were screened and purified by using BiFC assay (Sjohamn et al. 2016), revealing suitability of this methods for analyzing interactions of membrane proteins as well as soluble proteins (Sjohamn and Hedfalk 2014). In this study as well, we identified 42 membrane protein homomers, which represents 23% of 186 homomers. This percentage is slightly higher than that of membrane proteins in the yeast proteome, suggesting that BiFC assay is well suited to membrane proteins.

BiFC is particularly advantageous for observing weak or transient PPIs with low protein level that are not easily detected by other biochemical methods as appeared in our data. This sensitivity of the BiFC assay to capture weak interaction is obtained because the two fragments meet and form a stable complex. This feature, conversely, may lock the interacting fused proteins and thus induce unnatural consequences. However, our results consistently imply that irreversibility is not a major problem in our experimental conditions, as revealed in spot assays or signal rescues detected upon media change. These are presumably because in our system, complementary fragments are tagged under endogenous promoter, resulting in overall moderate intracellular abundance. Similar cases against irreversibility of BiFC have been reported in previous studies using budding yeast as a model organelle (Cole et al. 2007a; Sung and Huh 2007; Kang et al. 2010). These reversible characteristics of BiFC complex formation was also found in vitro and human cell system (Guo et al. 2005; Demidov et al. 2006). Under the assumption that irreversibility is negligible, this system can provide a suitable tool for studying the changes of protein interactome dynamics in response to various stresses.

Investigation of signal changes under nitrogen starvation filtered out a various interesting candidates. GO analysis revealed that 48 candidates are highly enriched in

RNA catabolism process (GOID 6401, *P*=0.0394), protein transport (GOID 6605, *P*= 0.0419), vacuole organization (GOID 7033, *P*= 0.0743) when compared to 186 homomer population. Under nitrogen starvation conditions, cells undergo autophagy to enhance cell viability and vacuolar degradation of cellular components including mRNA occurs (Onodera and Ohsumi 2005; Huang et al. 2015) and based on our enriched candidates, we can assume that active changes of homomeric state are accompanied in the processes. It is noteworthy that two components of the EGO complex, Meh1 and Slm4 (Binda et al. 2009), showed increased BiFC signals. Given that the homomeric state of Slm4 has been reported to be important for the regulation of TORC1 signaling (Zhang et al. 2012), it will be interesting to examine whether Meh1 homomerization also influences TORC1 signaling and how the increase in homomerization of Meh1 and Slm4 is related to the regulation of TORC1 signaling. Several proteins involved in the multivesicular body (MVB) pathway, such as Did2 and Vps60 (Rue et al. 2008), are also included in candidates showing the BiFC signal changes. The MVB pathway is required for starvation-induced degradation of plasma membrane proteins (Jones et al. 2012) and its proper activation is related to autophagy (Lee et al. 2007). Homomerization of these proteins may be an indication of the MVB pathway activation. As such, the analysis of dynamics of protein homomerization under stress conditions raises many research issues and challenges, which need to be addressed. Also, our analysis did not include possible homomer candidates that do not exist as homomers in nutrient-rich condition but homomerize upon starvation so screening genome-wide homomer candidates in starvation condition from the beginning has the potential to give a different population than we obtained from this study.

Chapter IV. Homomerization of Pet10 and its physiological effects

1. Introduction

Lipid droplets have been considered for decades as simple, inert storage sites for energy just as glycogen granules. They are surrounded by phospholipid monolayer with neutral lipids in their core, mainly triacylglycerol and steryl esters (Tauchi-Sato et al. 2002). And they varied in diameters which are waxing and waning in response to metabolic status cells encounter. Recently, however, many reports rearranged lipid droplet as much more dynamic organelle that moves around on cytoskeleton, actively interact with other organelles. Lipid droplet can be found in all eukaryotic cells, although most early studies are focused on their role of storage in adipose tissue (Packter and Olukoshi 1995). At the beginning of the lipid droplet formation, it buds from specific regions of ER outer membrane with helps from several proteins that act in neutral lipids biosynthesis or ER-lipid droplet membrane junctions. After certain amounts of neutral lipids are concentrated in the lumen of ER, then matured lipid droplet falls off from ER to cytoplasm (Murphy and Vance 1999). Even though they originated from ER membranes, they usually have different composition in their membranes compared to those of ER, most cases many lipid droplet specific proteins are bound to on the surface either peripherally or integrally - hairpin structures are needed for this case (Capuano et al. 2007).

Lipid droplet proteins have various purposes. For example, sufficient surface proteins help lipid droplets to maintain structural stability and prevent their coalescing. Oleosins in plants and perilipin in mammalian adipose tissue are reported to act in this context (Greenberg et al. 1991; Hsieh and Huang 2005). Proteins related to lipid biosynthesis are also associated with lipid droplets. In S. cerevisiae, high-throughput screening with a combination of mass spectrometry and NMR spectroscopy revealed that several sterol and acylglycerol biosynthetic enzymes are localized to this organelle (Bartz et al. 2007;

Rajakumari et al. 2008). And more surprisingly, proteins regulating trafficking pathways or vesicle docking in the exocytic and endocytic pathways are also highly enriched in the lipid droplet (Cohen et al. 2004; Pol et al. 2004; Le Lay et al. 2006). Many ER, mitochondria, and peroxisome-resident proteins were found to exist in droplet preparation, suggesting their involvement in organelle communication (Chapman and Trelease 1991; Blanchette-Mackie et al. 1995; Habeler et al. 2002; Binns et al. 2006). Because of growing evidence indicating significant roles lipid droplet has as not only storage spot for important metabolic molecules but also a hub that associates with various organelles to enable smooth regulation of metabolic processes, functional studies of lipid droplet proteins are getting more important. In this study, we revealed homomerization of Pet10 protein, a lipid droplet-resident protein with no functional study done previously, and found some experimental results indicating its role in lipid accumulation required in nitrogen starvation. Our results support the recent finding that Pet10 has a PAT domain, a lipid droplet binding domain found in Perilipin protein family in mammalian cells (Gao et al. 2017).

2. Materials and Methods

2.1. Yeast strains and culture conditions

Yeast strains used in this study are listed in Table IV-1. Yeast cells were grown at 30°C in YPD (1% yeast extract, 2% peptone, and 2% glucose) or synthetic complete (SC) medium lacking appropriate amino acids for selection (Sherman 2002). For solid media, 2% agar was added. For nitrogen starvation, cells grown to mid-logarithmic phase in SC medium were washed twice with and incubated in SD-N medium (0.17% yeast nitrogen base without amino acids and ammonium sulfate, 2% glucose) for 90 min at 30°C. For media change after starvation, cells incubated in SD-N medium were washed twice with and incubated in SC medium for 30 min at 30°C.

2.2. Amplification of PCR fragments

Oligonucleotide primers used in this study are listed in Table IV-2. PCR amplification was performed in a 50 μl reaction mixture that contained 5 μl 10x Taq buffer, 5 μl of 2 mM each dNTP, 5 μl of 5 μM each oligonucleotide primer, 10 ng template plasmid DNA and 2.5 U Taq polymerase. The PCR cycle was initiated by denaturing at 95℃ for 5 min, followed by 40 cycles of 30 s at 95℃, 30 s at 55℃, 3 min at 72℃ and a final extension of 10 min at 72℃.

2.3. Construction of plasmids

To construct p416ADH-PET10-GFP vector, the ~3,000 bp PCR product of PET10-GFP region was obtained using genomic DNA of cells expressing C-terminally GFP-tagged Pet10 as a template, forward primer PET10_F (SLIC) and reverse primer GFP+1000R (KpnI). The PCR product was digested with XbaI and KpnI and ligated into XbaI-KpnI-

Table IV-1. Yeast strains used in this study

Number	Genotype	Reference
BY4741	*MAT***a** *his3Δ1 leu2Δ0 met15Δ0 ura3Δ0*	Research genetics
BY4742	*MATα his3Δ1 leu2Δ0 lys2Δ0 ura3Δ0*	Research genetics
VN strains	*MAT***a** *his3Δ1 leu2Δ0 met15Δ0 ura3Δ0 GENE-VN::KlURA3*	(Sung et al., 2013)
VC strains MATα	*MATα his3Δ1 leu2Δ0 met15Δ0 ura3Δ0 GENE-VC::LEU2*	this study
HY1752	*MAT***a** *his3Δ1 leu2Δ0 met15Δ0 ura3Δ0 pet10 ::LEU2*	this study
HY1753	*MAT***a** *his3Δ1 leu2Δ0 met15Δ0 ura3Δ0 dga1 ::LEU2*	this study
HY1754	*MAT***a** *his3Δ1 leu2Δ0 met15Δ0 ura3Δ0 rad50 ::KanMX*	(Giaever et al., 2002)
HY1755	*MAT***a** *his3Δ1 leu2Δ0 met15Δ0 ura3Δ0 PET10-GFP::His3MX6*	(Huh et al., 2003)
HY1756	*MAT***a** *his3Δ1 leu2Δ0 met15Δ0 ura3Δ00 FAS1-GFP::His3MX6*	(Huh et al., 2003)
HY1757	*MAT***a** *his3Δ1 leu2Δ0 met15Δ0 ura3Δ0 FAS2-GFP::His3MX6*	(Huh et al., 2003)
HY1758	*MAT***a** *his3Δ1 leu2Δ0 met15Δ0 ura3Δ0 SLC1-GFP::His3MX6*	(Huh et al., 2003)
HY1759	*MATα his3Δ1 leu2Δ0 lys2Δ0 ura3Δ0* pADH-Pet10-Myc	this study
HY1760	*MAT***a**/α *his3Δ1/his3Δ1 leu2Δ0/ leu2Δ0 met15Δ0/MET15 LYS2/lys2Δ0 ura3Δ0/ura3Δ0 FAS1-GFP::His3MX6* p416ADH-PET10-Myc	this study
HY1761	*MAT***a**/α *his3Δ1/his3Δ1 leu2Δ0/ leu2Δ0 met15Δ0/MET15 LYS2/lys2Δ0 ura3Δ0/ura3Δ0 FAS2-GFP::His3MX6* p416ADH-PET10-Myc	this study
HY1762	*MAT***a**/α *his3Δ1/his3Δ1 leu2Δ0/ leu2Δ0 met15Δ0/MET15 LYS2/lys2Δ0 ura3Δ0/ura3Δ0 SLC1-GFP::His3MX6* p416ADH-PET10-Myc	this study
HY1115	*MAT***a** *his3Δ1 leu2Δ0 met15Δ0 ura3Δ0 atg8Δ::KanMX KlURA3::*P_{ATG8}*-GFP-ATG8*	(Shin et al., 2011)
HY1772	*MAT***a** *his3Δ1 leu2Δ0 met15Δ0 ura3Δ0 PET10-VN::KlURA3*	(Sung et al., 2013)
HY1773	*MATα his3Δ1 leu2Δ0 met15Δ0 ura3Δ0 PET10-VC::LEU2*	this study

HY1774	*MATα his3Δ1 leu2Δ0 met15Δ0 ura3Δ0 FAS1-VC::LEU2*	this study
HY1775	*MATα his3Δ1 leu2Δ0 met15Δ0 ura3Δ0 FAS2-VC::LEU2*	this study
HY1776	*MATα his3Δ1 leu2Δ0 met15Δ0 ura3Δ0 SLC1-VC::LEU2*	this study
HY1781	*MAT***a** *his3Δ1 leu2Δ0 met15Δ0 ura3Δ0* p413ADH-GFP	this study
HY1875	*MAT***a** *his3Δ1 leu2Δ0 met15Δ0 ura3Δ0 His3MX6::*P_{CET1}*-LZ-PET10*	this study
HY1876	*MAT***a** *his3Δ1 leu2Δ0 met15Δ0 ura3Δ0 KlURA3::*P_{CET1}*-LZ-PET10-GFP::His3MX6*	this study
HY1877	*MAT***a** *his3Δ1 leu2Δ0 met15Δ0 ura3Δ0 His3MX6::*P_{CET1}*-LZ-PET10-VN::KlURA3*	this study
HY1878	*MATα his3Δ1 leu2Δ0 met15Δ0 ura3Δ0 His3MX6::*P_{CET1}*-LZ-PET10-VC::LEU2*	this study
HY1879	*MATα his3Δ1 leu2Δ0 met15Δ0 ura3Δ0 HSP104-RFP::His3MX6*	this study

Table IV-2. Oligonucleotide primers used in this study

Primer	Sequence (5' to 3')
F2CORE	GGTCGACGGATCCCCGGGTT
R1CORE	TCGATGAATTCGAGCTCGTT
CgLEU2-600 (BamHI)	GTCA**GGATCC**AAGGCTTCAAGTCATATAGC
CgLEU2+1320R (TEF)	CGTCATTGGTAGTCATTATGCGGATTTACG
T(TEF)-F3-L	CGTAAATCCGCATAATGACTACCAATGACGTTCCCTCAAC
T(TEF)-R	CATCGATGAATTCGAGCTCG
VC+20R	TTTCTGTTTCAGGTCGTTCG
F2 CHK	AACCCGGGGATCCGTCGACC
CgCHK	GGTCATAGCTGTTTCCTGTG
PET10-CHK	CTCTTGGTGTTCAAGGAGGG
PET10-F	CCATCTGTGGAATTGCCACAAGCAACCTGGTCGCATCTGCCACAGGAAACAGCTATGACC
PET10-R	GCCTTTAGCTTCTCAATGGTGGCATTGCCCAAGTCCAACCGTTGTAAAACGACGGCCAGT
PET10-400	AGAAGAAGATGATGATCACG
RAD52-F4	ATGCAAACAAGGAGGTTGCCAAGAACTGCTGAAGGTTCTGGAATTCGAGCTCGTTTAAAC
RAD52-R5-VN	AAACGGGCTTCTTCTCATCCATATCCATAATTTCATTCATACCACCAGAACCCTCGATGTTGTGGCGGATC
RAD52-R5-VC	AAACGGGCTTCTTCTCATCCATATCCATAATTTCATTCATACCACCAGAACCCTTGTACAGCTCGTCCATG
R5-BiFC-CHK	CAAGATCCGCCACAACATCG
GFP_F, XbaI	AC**TCTAGA**ATGAGTAAAGGAGAAGAACTTTTC
GFP_R, BamHI	AT**GGATCC**TTTGTATAGTTCATCCATGCC
DGA1-F	TAAGGAAACGCAGAGGCATACAGTTTGAACAGTCACATAACACAGGAAACAGCTATGACC
DGA1-R	AATGAATTCATTATTACCCAACTATCTTCAATTCTGCATCGTTGTAAAACGACGGCCAGT
DGA1-400	CTGGTAATCAGAGCAAGAAG
VN-6 (BamHI)	CAGA**GGATCC**CTATGAGTTTAATTAACAGATC
VN+519R (XhoI)	GTCA**CTCGAG**GCCCTACTCGATGTTGTGGC
bZIP_F (PacI)	GC**TTAATTAA**CGAATCCAGTGATCCTGCTGC

bZIP_R (AscI)	AT**GGCGCGCC**TTCGCCAACTAATTTCTTTAATC
PET10_F4	GTATCGGTAATCATTAACCATCACTCACTCTCCAGAACCGGAATTCGAGCTCGTTTAAAC
N-bZIP-to-PET10	CCACAGATGGTTTAGAAGAAGAAATAGATGATTCAGACATACCACCAGAACCTTCGCCAACTAATTTCTTTAATC
PET10+300R	GAACCACACCAGCCAGATCC
HSP104_F2	CGATAATGAGGACAGTATGGAAATTGATGATGACCTAGATGGTCGACGGATCCCCGGGTT
HSP104_R1	ATTCTTGTTCGAAAGTTTTTAAAAATCACACTATATTAAATCGATGAATTCGAGCTCGTT
HSP104-CHK	CAAAGATCCAAGAATCTACC
ERG6-F2	CGCCGAAACCCCCTCCCAAACTTCCCAAGAAGCAACTCAAGGTCGACGGATCCCCGGGTT
ERG6-R1	ATATCGTGCGCTTTATTTGAATCTTATTGATCTAGTGAATTCGATGAATTCGAGCTCGTT
ERG6-CHK	TGAACTAGGTGATGGTATCC

Restriction enzyme sites are indicated in bold.

digested pRS416ADH. To construct p416ADH-PET10-Myc, pFA6a-Myc-KlURA3 was digested with PacI and AscI and ligated into the PacI-AscI-digested p416ADH-PET10-GFP. For pFA6a-His3MX6-pCET1-LZ construction, the ~200 bp PCR product of bZIP domain was obtained using BY4741 genomic DNA as a template, with forward primer bZIP_F (PacI) and reverse primer bZIP_R (AscI). The PCR product was digested with PacI and AscI and ligated into PacI-AscI-digested pFA6a-His3MX6-pCET1-VN (Sung and Huh 2007)

2.4. Transformation of yeast cells

Yeast transformation was performed based on lithium acetate method previously describe (Gietz et al. 1995). Transformed cells were spread on SC agar medium without leucine (SC-Leu) or without histidine (SC-His) or without uracil (SC-Ura), for epitope switching or plasmid transformation, respectively

2.5. Microscopic analysis and fluorescence quantification

For fluorescence detection, yeast cells carrying GFP, RFP, or VN-VC tagged proteins of interest were grown to mid-logarithmic phase at 30°C in YPD medium. Then cells were grown to mid-logarithmic phase at 30°C in SC medium and were microscopically analyzed in 96-well glass-bottomed microplates (MGP096, Matrical Bioscience). Microscopy was performed on a Nikon Eclipse E1 microscope with a Plan Fluor 100×/1.30 NA oil immersion objective. Fluorescence images were taken using a PhotoFluor LM-75 light source (89 North Inc.) with appropriate filters. Quantification of fluorescent images (BiFC and GFP) was performed using the NIS-Elements imaging software (Nikon). Cell boundary was defined manually and the sum fluorescence intensity of single cell was obtained. Background fluorescence intensity of non-cell area

of the analyzed image was also quantified and subtracted from the sum fluorescence intensity of single cell, resulting in the net fluorescence intensity of single cell. For each experiment, at least 50 cells were analyzed and the mean intensity±SD values were calculated.

2.6 Western blot analysis

For western blot analysis, yeast cells grown to logarithmic phase in YPD medium were harvested and washed twice with phosphate-buffered saline. Cells then were disrupted by bead beating in lysis buffer (50 mM tris-Cl, pH 7.5, 150 mM NaCl, 0.15% NP-40, 1 mM EDTA) with protease inhibitors (10 mM phenylmethylsulfonyl fluoride, 1 mM benzamidine, 1 mM leupeptin, 1 mM pepstatin). Cell debris was eliminated by centrifugation at 13,000 rpm for 10 min at 4℃, and the extracts in the supernatant were collected and mixed with 6X SDS (sodium dodecyl sulfate) sample buffer. SDS-PAGE and Western blot analysis were performed using standard methods with a HRP-conjugated a HRP-conjugated anti-rabbit IgG antibody (A6154, Sigma), a HRP-conjugated anti-GFP antibody (SC-9996 HRP, Santa Cruz), a HRP-conjugated anti-myc antibody (SC-40 HRP, Santa Cruz), and an anti-hexokinase antibody (H2035-02, United States Biological).

2.7. Co-Immunoprecipitation assay

Diploid cells expressing GFP and myc tagged target proteins were used for Co-IP assay. Cell extracts were prepared as previously described (Sung et al. 2008). An anti-myc antibody (SC-40, Santa Cruz) was added to cell extracts and incubated with gentle rocking for 4 h at 4°C. Protein A-Sepharose (17-5138-01, GE healthcare) was then added to the immunoprecipitation reaction and incubated with gentle rocking for 4 h at 4°C. For

control, only protein A-sepharose was treated without antibody for the same cell extracts. Beads were washed four times with 25 mM Tris, pH 7.5, 150 mM NaCl, and 0.2% NP40. After the final wash, beads were resuspended in SDS sample buffer, boiled, and then loaded on SDS-PAGE gels. Proteins were detected with a HRP-conjugated anti-GFP antibody (SC-9996 HRP, Santa Cruz) or a HRP-conjugated anti-myc antibody (SC-40 HRP, Santa Cruz).

2.8. FCS and PCH

FCS and PCH measurements were all performed at 25°C with a LSM 780 confocal microscope (Carl Zeiss) equipped with GaAsP multichannel spectral detectors as previously described (Herrick-Davis et al. 2013; Kim et al. 2017). Confocal pinhole diameter was adjusted to 35 μm for the 488 nm laser. Emission signal was detected at 500-550 nm for GFP. Cells grown to OD_{600} = 1.0 at 30°C in YPD medium were diluted to OD_{600} = 0.1 in SC medium. After 4 h of incubation, FCS and PCH measurements on yeast cells were recorded sequentially 10 times with duration of 5 s. Laser power was adjusted to minimize photobleaching of the GFP probe while maintaining a good signal to noise ratio, because rapid and gradual photobleaching by cellular depletion of GFP affected diffusion analysis of fluorescence correlation functions and PCH analysis. 140 cells were measured for each experiment. Autocorrelation analyses were performed using the ZEN 2012 software package (Carl Zeiss) and FCS data were fit to a three-dimensional model with one or two-components as previously described (Kawai-Noma et al. 2009; Pack et al. 2014). PCHs were constructed using the PCH module in the ZEN software (Herrick-Davis et al. 2013). The structure parameter in FCS analysis and the first-order correction were determined with the standard Rhodamine 6G solution and then fixed for live cell experiment (Huang et al. 2004; Kawai-Noma et al. 2009).

2.9. TAG quantification assay

Cells grown to mid-logarithmic phase were washed with cold phosphate-buffered saline and homogenized in two volumes of 5% NP-40 solution. Cells were disrupted by bead beating and then heated for 5 min at 80°C. Cell lysates were cooled down to room temperature and heated again. All insoluble materials were removed by centrifugation at 13,000 rpm for 3 min. TAG was quantified by using the Triglyceride Quantification Assay kit (ab65336, Abcam) according to the manufacturer's instructions. Detection was performed using the FlexStation 3 microplate reader (Molecular Devices) and the absorbance at 570 nm was measured. The net absorbance was obtained by subtracting the absorbance of the blank and then normalized by the number of cells

3. Results

3.1. Increased homomerization of Pet10 upon nitrogen starvation

Pet10 (Ykr046c) is a protein that localizes to the lipid droplets (Athenstaedt et al. 1999) and its homomerization has not been reported before. In BiFC screen we described in the previous chapter, C-terminally VN- and VC-tagged Pet10 showed a clear BiFC signal. As illustrated in Figure IV-1, we also checked that both BiFC and GFP signal of Pet10 merged with RFP-tagged Erg6, a lipid droplet marker protein (Athenstaedt et al. 1999), so we could assume that subcellular localization of Pet10 is independent of its homomeric state. Notably, the BiFC signal of Pet10 increased significantly upon nitrogen deprivation (Figure III-12 and 13, Figure IV-1), suggesting that homomerization of Pet10 is enhanced in that condition, meanwhile sites of homomerization remained same because the increased BiFC signal still overlapped with RFP signal of Erg6. And the signal intensity of Pet10-GFP did not change under the same condition, so we assumed that the observed increase in the BiFC signal of Pet10 was induced by increased expression of Pet10.

To verify homomeric interaction of Pet10, we tried to perform biochemical assays such as cross-linking and Co-IP, but we failed to see any positive results (data not shown). We inferred that Pet10 homomers are rather weakly or transiently formed so that they cannot be detected by conventional biochemical methods. To verify homomerization of Pet10 and its increase under nitrogen starvation, we performed a fluorescence correlation spectroscopy (FCS) and photon counting histogram (PCH) analysis with C-terminally GFP-tagged Pet10. FCS and PCH simultaneously analyze the same fluorescence fluctuation in different ways and the results are displayed in different parameters, the diffusion rate and the brightness, respectively. Although FCS (Fluorescence correlation

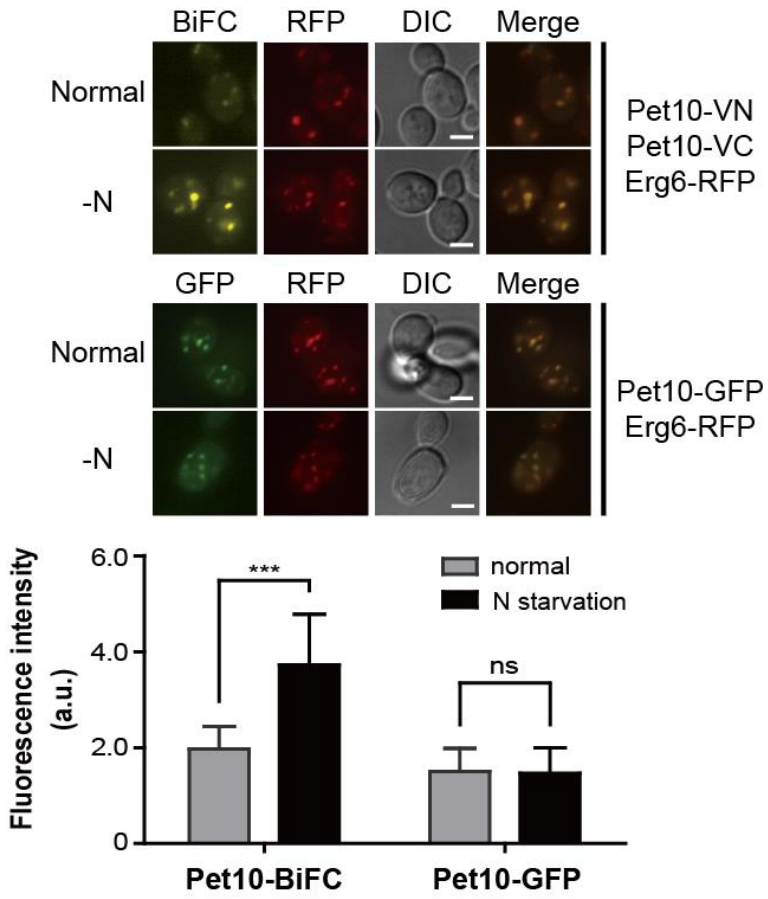

Figure IV-1. Homomerization of Pet10 under normal and nitrogen starvation condition.

(Upper panel) Representative BiFC and GFP images of Pet10 under normal condition and nitrogen starvation. Erg6-RFP was used as lipid droplet marker. Scale bars, 2 μm. (Lower panel) Quantification of fluorescence intensity of cells. Gray and black bars indicate fluorescence intensity of cells under normal condition and nitrogen starvation, respectively. At least 50 cells were quantified under each condition. Error bars represent standard deviation. Asterisks indicate significant differences compared with normal condition (***$P < 0.001$; Student's *t* test).

spectroscopy) can measure the fluctuation of fluorescence intensity and thus can obtain information about molecular dynamics in cells (Berland et al. 1995), changes in molecular mass induced by protein oligomerization is hard to be determined by this assay. PCH (photon counting histogram), in contrast, is more suitable for detecting monomer or oligomeric forms of proteins because it can capture the intensity distribution of the fluctuating signal. In PCH, distribution of photon burst from each fluorescent proteins are described as two parameters – the molecular brightness of the particle and the average number of particles in the analyzed volume (Chen et al. 1999), and molecular brightness can be used as marker for protein association. If fluorescent probe-tagged proteins form homodimer, then the complex will produce twice amounts of photons than those emitted by monomer (Muller et al. 2000). This approach was also found to work properly with membrane-bound protein in detection of it homotypic interaction in previous study. (Rigler et al. 1993; Pack et al. 1999; Chen et al. 2002; Saffarian et al. 2007; Hink et al. 2008; Malengo et al. 2008). As shown in Figure IV-2, Pet10-GFP showed more than one peak while free GFP exhibited a clear, predominant single peak implying that Pet10 exists not only as monomers but also as homomers. And under nitrogen starvation, PCH for Pet10-GFP slightly moved to the right as illustrated in Figure IV-3. This observation is consistent with the increase in the BiFC signal of Pet10 under the same condition and suggests that the population of Pet10 homomers is increased by nitrogen deprivation.

3.2. Finding novel interactors of Pet10

In an attempt to get clues about the function of Pet10, we performed a BiFC screen to identify its interactors. Based on previous studies we first suspected its role in respiration (Brown et al. 2000) or lipid metabolic process (Athenstaedt et al. 1999; Currie et al. 2014), so firstly we selected 44 candidates which are key components of electron transfer chain,

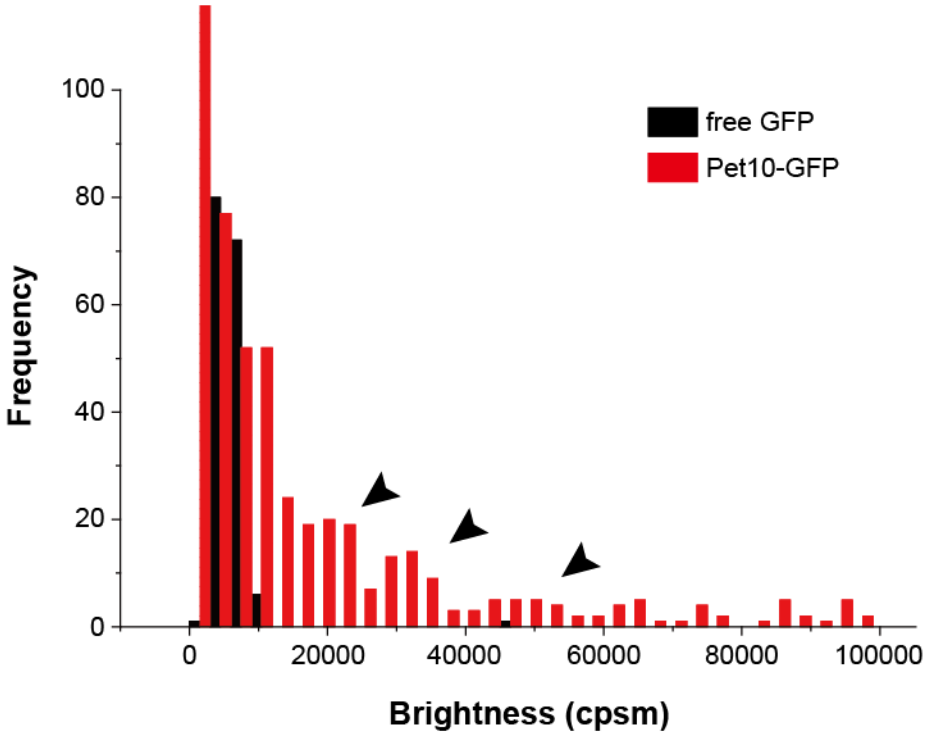

Figure IV-2. PCH analysis of Pet10-GFP and free GFP.

Brightness (counts per second per molecule; cpsm) of Pet10-GFP and free GFP was counted and shown as a histogram. Black and red bars indicate the frequency of free GFP and Pet10-GFP, respectively. Brightness of free GFP was analyzed by using a strain carrying a vector encoding the *GFP* gene under the *ADH1* promoter. Peaks of Pet10-GFP are marked with black arrowheads. A single cell was measured for five times and total 25 cells were analyzed for each strain.

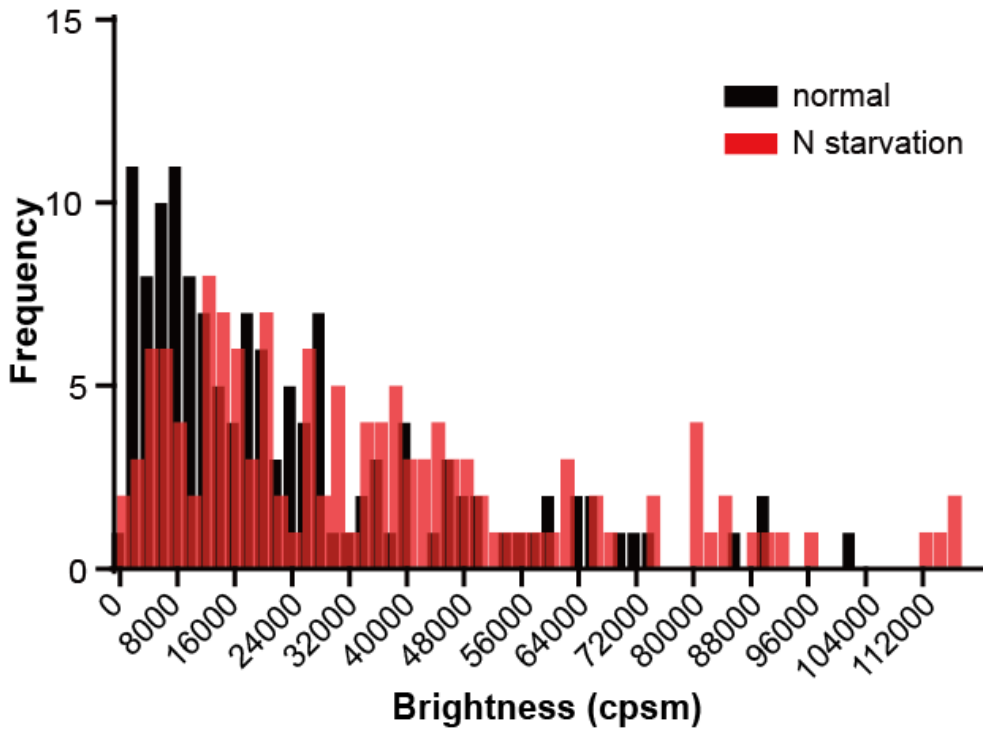

Figure IV-3. PCH analysis of Pet10-GFP under normal and nitrogen starvation condition.

Brightness (counts per second per molecule; cpsm) of Pet10-GFP under normal condition and nitrogen starvation was counted and shown as a histogram. Black and red bars indicate the frequency of Pet10-GFP fluorescence under normal condition and nitrogen starvation, respectively. 140 cells were counted under each condition. Statistical significance was determined by Student's *t* test ($P = 0.0097$).

mitochondrial dynamics, phospholipid or sterol synthesis that are available in VC fusion library. The tested proteins can be found on the Table IV-3. 44 VC-tagged *MAT*α strains from the VC fusion library were mated with a *MAT***a** strain expressing C-terminally VN-tagged Pet10 and the resulting diploid cells were analyzed for fluorescence from the BiFC complex formation. Among the 44 candidates, three proteins (Fas1, Fas2, and Slc1) showed positive BiFC signals with Pet10-VN. Fas1 and Fas2 are β and α subunit of FAS (fatty acid synthase) complex (Stoops and Wakil 1978; Wieland et al. 1978; Mohamed et al. 1988; Nagiec et al. 1993), and Slc1 is an acyltransferase acting in phosphatidic acid synthesis (Nagiec et al. 1993; Athenstaedt and Daum 1999). BiFC signals between Pet10 and Fas2, Fas2 co-localize with RFP-tagged Erg6, indicating that these interactions occur on lipid droplet, as depicted in Figure IV-4, although Fas1 and Fas2 is known to be diffused in cytoplasm (Huh et al. 2003). To confirm their interaction with Pet10, we performed Co-IP assay using GFP-tagged Fas1/Fas2/Slc1 and Myc-tagged Pet10. As shown in Figure IV-5 and Figure IV-6, all three proteins were efficiently co-precipitated with Pet10, indicating that Fas1, Fas2 and Slc1 physically interact with Pet10. Interestingly, ratios of Pet10 physically interacting with Fas1 and Fas2 significantly decreased under nitrogen starvation as indicated by both BiFC assay (Figure IV-4) and Co-IP (Figure IV-5), while interaction between Slc1 and Pet10 remained constant in both conditions (Figure IV-6). This is probably not caused by reduced level of Pet10 because it was revealed to remain constant under nitrogen-deprived condition while homomeric Pet10 even increased (Fig IV-1). From these, we assumed that Pet10 can exist at least two different interacting partners – Pet10 itself and FAS components- and prefers its homomeric state to interacting with FAS components in nitrogen-deprived condition, although it is not yet clear what physiological effect each state has.

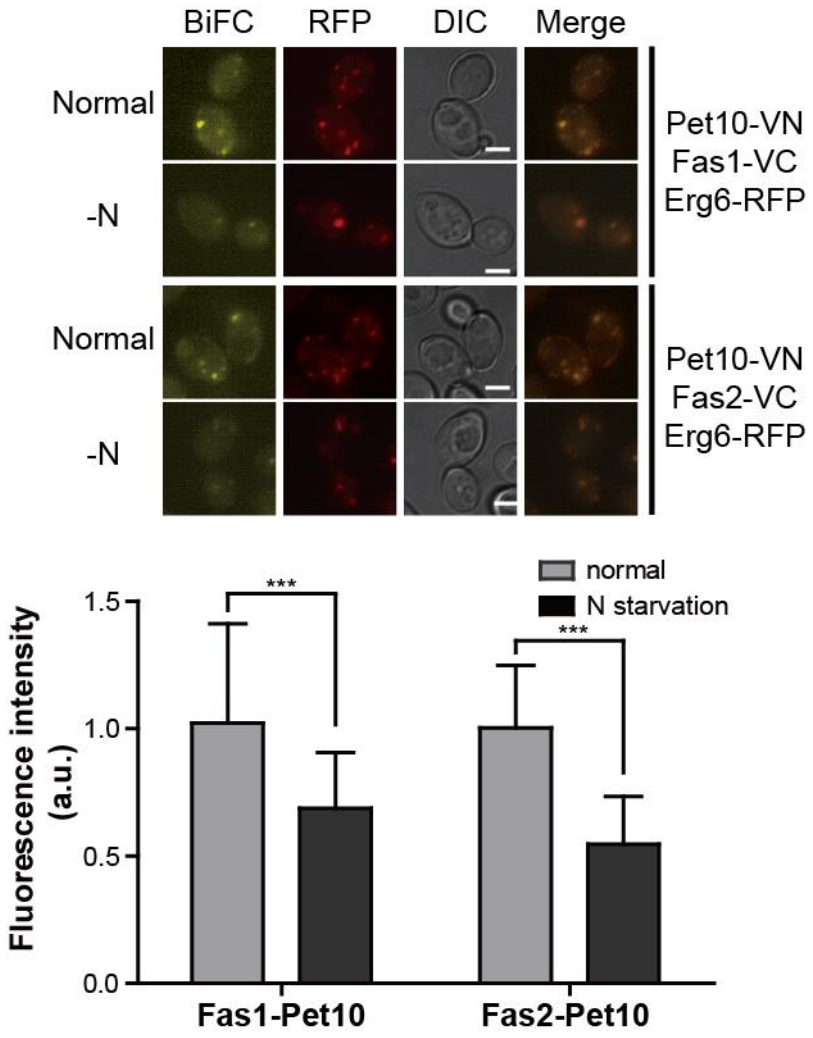

Figure IV-4. Interaction of Pet10 with Fas1, Fas2 in normal and nitrogen-deprived condition detected by BiFC assay.

(Upper panel) BiFC assay for interaction of Pet10 with Fas1, Fas2. Erg6-RFP was used as lipid droplet marker Scale bars, 2 μm. (Lower panel) Quantification of fluorescence intensity of cells. Gray and black bars indicate fluorescence intensity of cells under normal condition and nitrogen starvation, respectively. At least 50 cells were quantified under each condition. Error bars represent standard deviation. Asterisks indicate significant differences compared with normal condition (***$P < 0.001$; Student's t test).

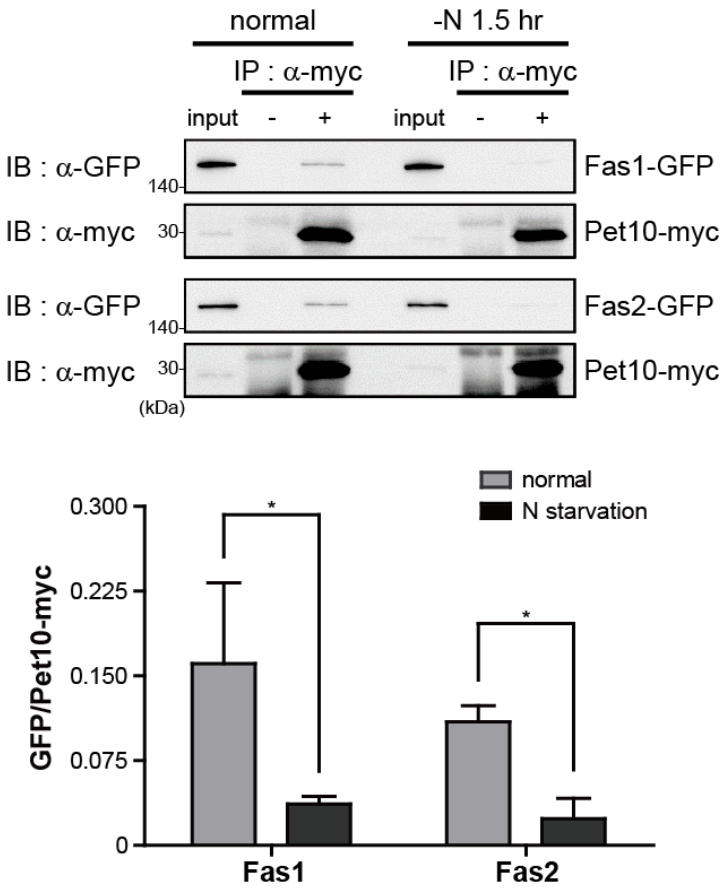

Figure IV-5. Interaction of Pet10 with Fas1, Fas2 in normal and nitrogen-deprived condition detected by Co-IP assay.

(Upper) Co-IP assay to validate interaction of Pet10 with Fas1, Fas2 in normal and nitrogen-deprived condition. Co-IP assay was performed using myc-tagged Pet10 expressed under *ADH1* promoter and GFP-tagged Fas1, Fas2. The positions of molecular weight markers (in kDa) are indicated on the *left* of each blot. (Lower) Quantification of Co-IP. Ratios of GFP-tagged proteins co-precipitated with myc-tagged proteins in each condition were calculated by using ImageJ (Schneider et al. 2012) and average of 3 independent experiments were presented by bar graphs. Error bars represent standard deviation. Asterisks indicate significant differences compared with normal condition (*P < 0.05; Student's t test).

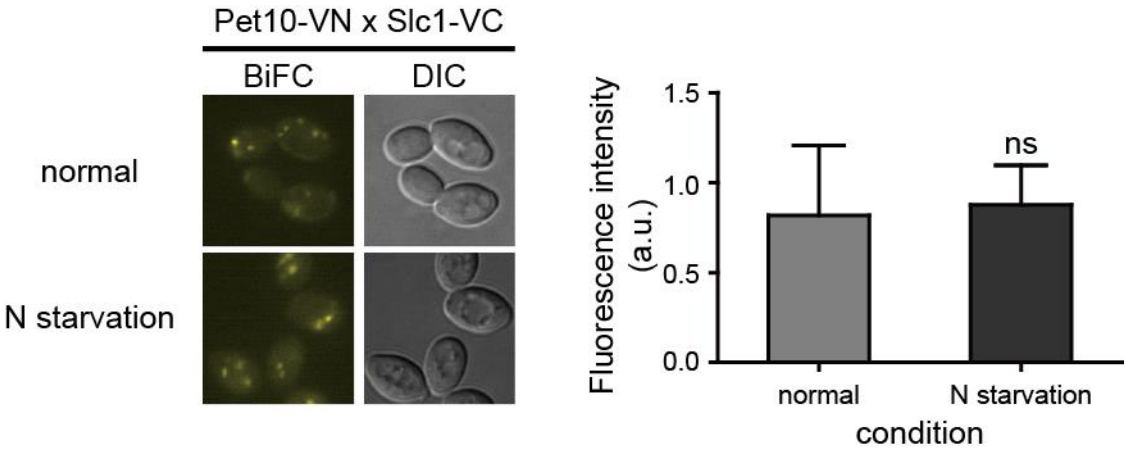

Figure IV-6. Interaction between Pet10 and Slc1 detected by BiFC.

(Left panel) BiFC assay for interaction of Pet10 with Slc1. (Right panel) Quantification of fluorescence intensity of cells. Gray and black bars indicate fluorescence intensity of cells under normal condition and nitrogen starvation, respectively. At least 50 cells were quantified under each condition. Error bars represent standard deviation. Asterisks indicate significant differences compared with normal condition.

Table IV-3. Proteins analyzed for interaction with Pet10 by BiFC assay

Mitochondrial fission and fusion[a]		BiFC signal detected
Fzo1	YBR179C	
Ugo1	YDR470C	
Mgm1	YOR211C	
Fis1	YIL065C	
Dnm1	YLL001W	
Mdv1	YJL112W	
Caf4	YKR036C	
Electron transport chain[b]		
Nde1	YMR145C	
Nde2	YDL085W	
Ndi1	YML120C	
Gut2	YIL155C	
Sdh1	YKL148C	
Sdh2	YLL041C	
Sdh4	YDR178W	
Cyc1	YJR048W	
Cyc7	YEL039C	
phosphoslipid metabolism[c]		
Cds1	YBR029C	
Cho1	YER026C	
Psd1	YNL169C	
Opi3	YJR073C	
Cki1	YLR133W	
Cpt1	YNL130C	
Slc1	YDL052C	O
Lcb1	YMR296C	
Ldh1	YBR204C	
Orm2	YLR350W	
Orm1	YGR038W	
Fas1	YKL182W	O
Fas2	YPL231W	O
Ino1	YJL153C	
Sterol synthesis[d]		
Erg1	YGR175C	
Erg7	YHR072W	

Erg11	YHR007C	
Erg24	YNL280C	
Erg25	YGR060W	
Erg26	YGL001C	
Erg27	YLR100W	
Erg6	YML008C	
Erg2	YMR202W	
Erg3	YLR056W	
Erg5	YMR015C	
Erg4	YGL012W	
Are1	YCR048W	
Are2	YNR019W	

[a]Sharma et al. 2010
[b]Rosenfeld et al. 2003, Murray et al. 2011
[c]Raychaudhuri et al. 2012
[d]Tiedje et al. 2007

3.3. Involvement of Pet10 in lipid metabolism

Given that Fas1, Fas2, and Slc1 are key players in lipid metabolism (Raychaudhuri et al. 2012), we hypothesized that Pet10 may have a function in lipid metabolism. Recent study suggesting the role of Pet10 as a yeast Perilipin, Pet10 is found to be enriched especially in triacylglycerol (TAG) droplets and additional role of this protein in neutral lipid homeostasis is also proposed (Gao et al. 2017). To test physiological effect of Pet10 homomerization, we constructed yeast strains expressing Pet10 tagged with the leucine zipper (LZ) motif at its N-terminus and with VC, VN, or GFP at its C-terminus to give driving force of homomerization to Pet10. LZ motif sequence (MKQLEDKVEELLSKNYHLENEVARLKKLVGE) was derived from Gcn4, a bZIP transcriptional activator that is known to dimerize through this sequence (Ellenberger et al. 1992). Remarkably, LZ-Pet10 showed significantly increased BiFC signal compared to that of Pet10 as shown in Figure IV-7, indicating that LZ-tagged Pet10 has a higher tendency to dimerize as we intended. The GFP signal intensity of LZ-Pet10, in contrast, was similar to that of intact Pet10-GFP, suggesting that LZ tagging does not disturb expression or stability of Pet10 protein. In addition, LZ-Pet10 did not colocalize with a disaggregase Hsp104 (Figure IV-8), which accumulates at the site of protein aggregation when proteins lose their solubility because of misfolding or stress (Vashist et al. 2010; O'Connell et al. 2014). This observation indicates that LZ tagging does not induce misfolding of Pet10. We also checked how LZ-Pet10 interact with Fas1 and Fas2 and we found that LZ-Pet10 showed decreased interacting signal with both Fas1 and Fas2, as shown in Figure IV-9. From this, we demonstrated that this mutant form of Pet10 presents similar interacting status to what wild type Pet10 is showing in nitrogen-deprived condition.

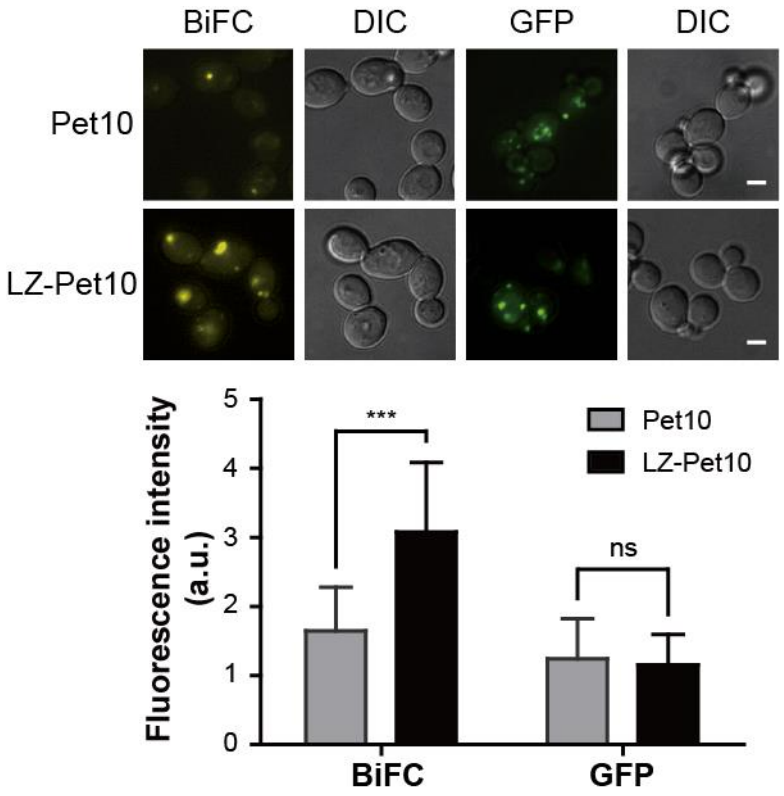

Figure IV-7. Increased homomeric signal of LZ-Pet10.

(Upper panel) Representative BiFC and GFP images of cells expressing Pet10 and LZ-Pet10. Scale bars, 2 μm. (*Middle* panel) Representative BiFC image of cells expressing LZ-Pet10-VN and Fas1- or Fas2-VC. Scale bars, 2 μm. (Lower panel) Quantification of fluorescence intensity of cells. Gray and black bars indicate fluorescence intensity of cells expressing Pet10 and LZ-Pet10, respectively. At least 50 cells were quantified for each strain. Error bars represent standard deviation. Asterisks indicate significant differences compared with Pet10 (***$P < 0.001$; Student's *t* test).

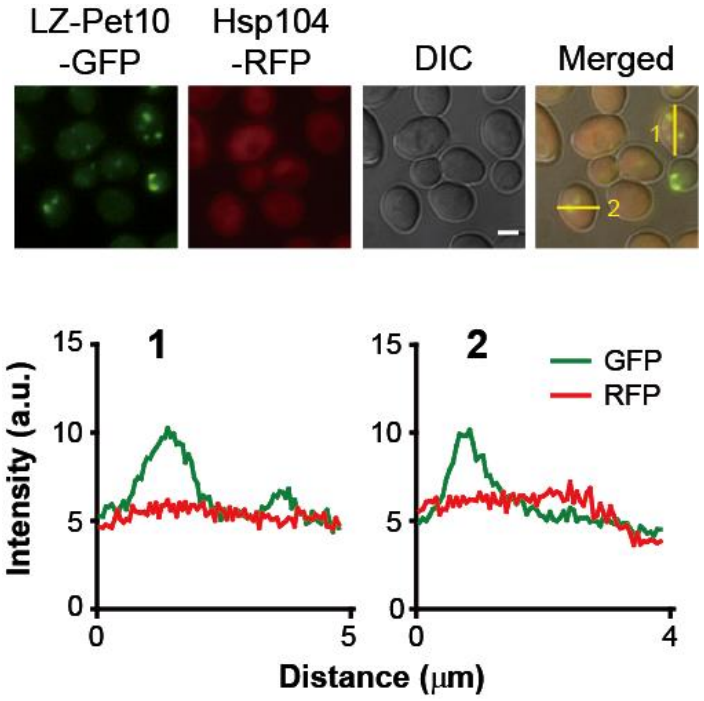

Figure IV-8. Localization of LZ-Pet10 and Hsp104.

Cells with C-terminally GFP-tagged LZ-Pet10 and cells with C-terminally RFP-tagged Hsp104 were mated and the resulting diploid cells were analyzed by fluorescence microscope. (Upper panel) Representative images of LZ-Pet10-GFP and Hsp104-RFP. (Lower panel) Intensities of the GFP and RFP signals along yellow lines indicated as number 1 and 2 were plotted in graphs. Scale bar, 2 μm.

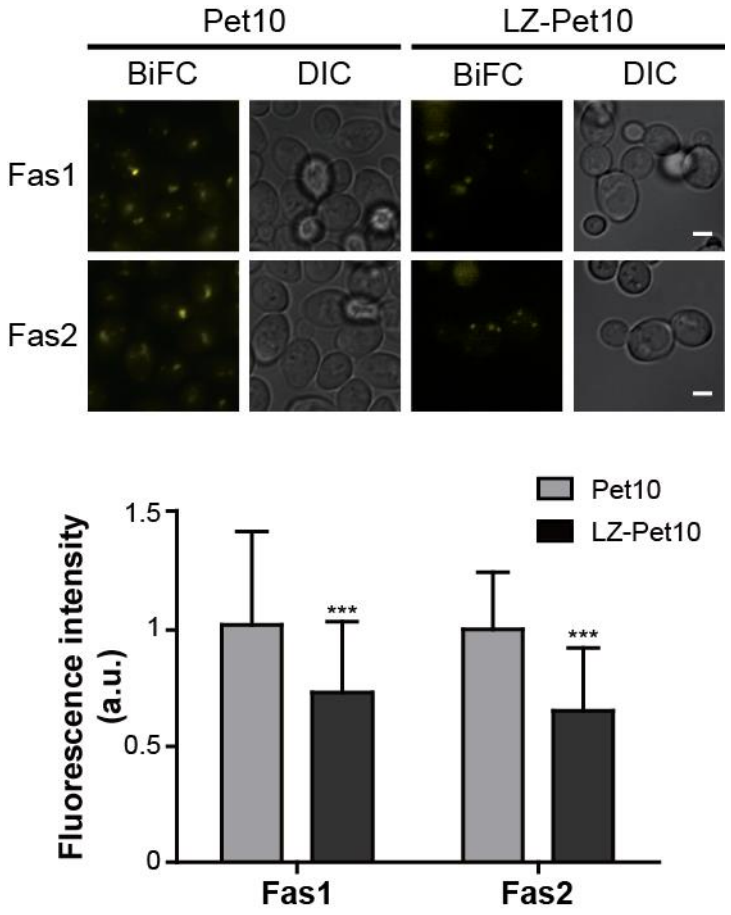

Figure IV-9. Comparison of interacting signal of Pet10-Fas1/Fas2 and LZ-Pet10-Fas1/Fas2.

(Upper panel) Representative BiFC image of cells expressing LZ-Pet10-VN and Fas1- or Fas2-VC. Scale bars, 2 μm. (Lower panel) Quantification of fluorescence intensity of cells. Gray and black bars indicate fluorescence intensity of cells expressing VN-tagged Pet10 and LZ-Pet10, respectively. VC is tagged to Fas1 or Fas2 as indicated at the bottom of the graph. At least 50 cells were quantified for each strain. Error bars represent standard deviation. Asterisks indicate significant differences compared with Pet10 (***$P < 0.001$; Student's *t* test).

Strikingly, cells expressing LZ-Pet10 showed significantly increased TAG level compared to strains expressing wild type Pet10 (Figure IV-10A). Dga1 is a diacylglycerol phosphatase and its deletion affects negatively on intracellular level of TAG in yeast (Sorger and Daum 2002). Rad50 was selected as positive control based on the previous reports about the effects of MRX deletion on TAG levels in yeast (Kanagavijayan et al. 2016). Recently, it has been reported that TAG is accumulated upon nitrogen starvation in various species (Breuer et al. 2012; Lopez Garcia de Lomana et al. 2015; Goncalves et al. 2016). Consistent with these reports, we also observed that TAG level was significantly increased under nitrogen starvation in *S. cerevisiae* (Figure IV-10B). Given the above results that nitrogen starvation enhances Pet10 homomerization while reducing interactions between FAS components, and LZ-Pet10 induces intracellular lipid accumulation even without starvation, and the increase in TAG level by nitrogen deprivation, it is likely that the state of Pet10 homomerization might be regulated to properly manage TAG level in cells in response to nutrient conditions.

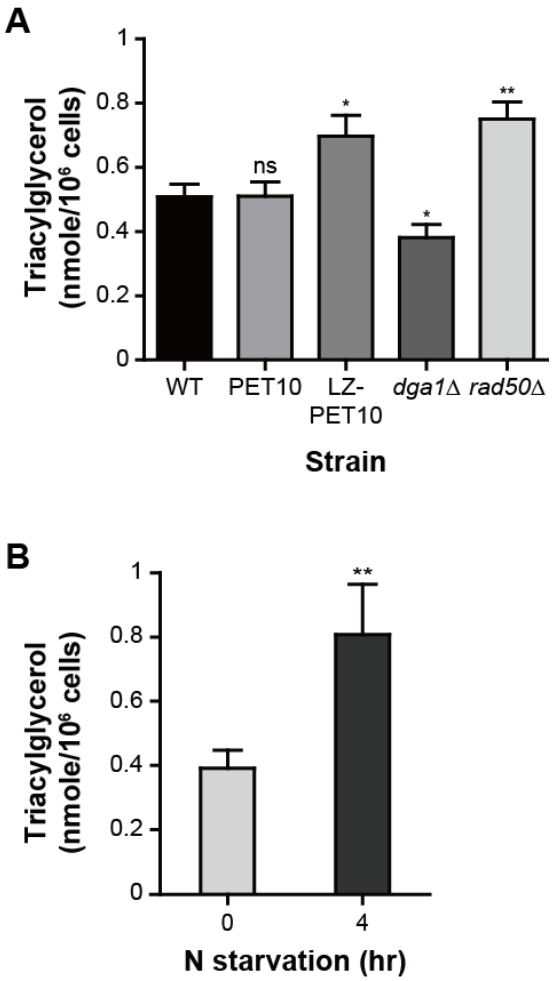

Figure IV-10. Triacylglycerol quantification.

(A) Measurements of TAG contents of various mutants. The graph shows the mean TAG levels measured in eight independent experiments. Error bars represent standard deviation. *dga1*Δ and *rad50*Δ cells were used as negative and positive controls, respectively (Oelkers et al. 2002; Kanagavijayan et al. 2016). LZ represents leucine zipper. Asterisks indicate significant differences compared with wild-type cells (*$P < 0.05$, **$P < 0.01$; Student's *t* test). (B) Measurements of TAG contents of cells under nitrogen starvation. TAG levels in wild-type cells under normal and nitrogen-deprived condition were measured. The graph shows the mean TAG levels measured in three independent experiments. Error bars indicate standard deviation. Asterisks indicate significant differences compared with normal condition (**$P < 0.01$; Student's *t* test).

4. Discussion

The lipid droplet has long been thought of as an inert organelle for lipid storage, but in recent decades, they were newly recognized as a dynamic organelle that affects lipid metabolism and undergoes various changes in number and size (Goodman 2008; Olofsson et al. 2009; Walther and Farese 2012). Studies of the lipid droplets are important because understanding of lipid metabolism has significant implications for metabolic diseases.

In this study, we discovered homomerization of Pet10, a lipid droplet protein, and also revealed 3 novel interactors Fas1, Fas2, and Slc1, all of which function in lipid metabolism (Raychaudhuri et al. 2012) by using BiFC assay. A recent study reported that most of yeast lipid droplet proteins are involved in lipid metabolism (Currie et al. 2014). We suspected that biological role of Pet10 is related to lipid metabolism as many other lipid droplet proteins because increased homomerization of Pet10 promotes TAG accumulation even without nitrogen starvation in our study. Our results indicated Pet10 homomers increased upon starvation while interaction of Pet10 with Fas1 or Fas2 decreased at the same condition. Many lipid droplet proteins were found to be regulated differentially dependent on intracellular metabolic status and homomerization of Pet10 can be one of them. LZ-induced dimeric form of Pet10 led to lipid accumulation without starvation suggesting that increase in the homomeric form of Pet10 may affect accumulation of intracellular lipids upon nitrogen starvation as detected in this study and in many species (Breuer et al. 2012; Lopez Garcia de Lomana et al. 2015; Goncalves et al. 2016). In a recent study, Goodman and colleagues suggested that Pet10 is a yeast perilipin involved in lipid droplet stability (Gao et al. 2017) bus also mentioned possible role of this protein in lipid metabolic process, consistent with our observation. To further convince the role of Pet10 homomers in lipid accumulation, it is necessary to characterize

domain or amino acid residue that is required for homomerization and to check physiological effects of homomer-defect mutants. Experiments with randomly truncated Pet10 mutants indicated that N-terminal region is required for appearance of BiFC signal but we could not conclude this region as homomeric interface because GFP signal of N-terminal truncated Pet10 showed cytoplasmic diffused pattern, indicating mislocalization of mutant form (data not shown). We also constructed mutants in which smaller regions of N-terminus of Pet10 are deleted but it turned out that mutation in any region of PAT domain of this protein (Gao et al. 2017) caused defects in subcellular localization. Domain substitution from PAT region to other LD-targeting domains may be worth trying to make properly localized, monomeric form of Pet10 in the future study.

Strikingly, Pet10 is the only lipid droplet protein found to interact with FAS component Fas1 and Fas2 so far and the fact that only overexpressed Pet10 could be detected by Co-IP assay again emphasized the benefits of BiFC assay in searching novel interactors. But this research left many to be explained in further refined study including how lipid droplet protein Pet10 interacts with cytoplasmic diffused proteins and which factor mediates homomerization of Pet10. Understanding the functional role of Pet10 will also be useful in bioengineering applications, given that increasing lipid production in microorganisms has long been a challenge (Brennan and Owende 2010; Zeng et al. 2011)

In homomer screening described in the chapter III, diploid yeast strains generated by mating strains from VC *MAT***a** library and VN library were analyzed by BiFC, so an important issue we should consider is that whether transcriptional or post-transcriptional regulation of the proteins is the same in haploid and diploid. In the previous research, majority of yeast proteins were revealed to be constant in their quantities in haploid or diploid and noticeable differences were only found in genes related to pheromone signaling and mating pathway (de Godoy et al. 2008). However, another group discovered

that under ethanol stress condition, various genes acting in stress response, electron transport and metal ion metabolism are differently regulated in their transcription levels between haploid and diploid, and even between haploids *MAT***a** and *MAT*α (Li et al. 2010). And these cell-type specific regulations were supposed to be related to different sensitivity of each cell type to ethanol. It is possible that similar variation exists in the way proteins act in response to nitrogen-deprived condition in haploid and diploid, so for the candidates that showed signal changes upon nitrogen starvation, it should be checked whether they present the same effects in haploid cell.

Chapter V. Conclusion

In this study, we constructed two kinds of VC fusion libraries based on different mating types, both of which cover more than 90% of all ORFs in *S. cerevisiae*. Of the two libraries, the *MAT*α VC fusion library can be used together with the *MAT***a** VN fusion library to examine about 33 million of PPIs through BiFC assay. This number represents most of possible interactions in the yeast proteome. In an attempt to demonstrate the validity of the VC and VN fusion libraries, we screened protein homomers at a genome-wide scale. Through this genome-wide BiFC analysis, we identified 186 protein homomer candidates in yeast. Remarkably, our data set includes 104 protein homomers that have been missed in previous studies due to various technical limitations. Given that protein homomerization is one of the simplest and efficient ways cells can use to regulate function, concentration, and structure of proteins, our data set will be a valuable resource for providing significant insights into the physiological roles of protein homomerization.

There are some caveats should be addressed for using the VC fusion library. First, unlike the *MAT***a** VN fusion library, construction of the *MAT*α VC fusion library required an additional mating type switching process after epitope switching, during which several strains were lost due to technical issues. Therefore, the *MAT*α VC fusion library consists of fewer strains than the *MAT***a** VN fusion library (5,911 strains), allowing fewer interactions to be checked. And although *MAT*α VC fusion library contains 5,671 strains chromosomally tagged with VC gene, it is hard to say that this number directly reflect the actual number of proteins that can be successfully assessed for their interactors for some reasons aside from the topological problems mentioned above. Our tagging strategy allows efficient construction and endogenous level of expression, but does not give much consideration for proteins whose properties such as folding or post-translational modification required for proper activity can be disturbed by C-terminal tagging. Also, some proteins are expressed as precursor forms and need to be cleaved for complete

maturation, and fused VC fragments can be eliminated in this process. In both cases, proteins cannot make BiFC signal even though they exist in sufficient amounts and form actual interactions. Glycosylphosphatidylinositol (GPI)-anchored proteins are one of examples we can think of. GPI anchored proteins have conserved GPI anchoring signal at the C-terminal region, and it is recognized and removed by GPI transamidase before attachment to GPI anchors (Pittet and Conzelmann 2007). Tagging at the C-terminus of these proteins usually hampers protein detection and has high possibility of mislocalization, so internal tags are recommended in various studies (De Groot et al. 2003; Du et al. 2012; Zordan et al. 2015). Thus, these genes in our library have high probability of tag-lost or mis-localization. Indeed, 22 putative GPI-anchored proteins suggested in the previous study (De Groot et al. 2003) did not show any fluorescence in either homomerization or self-assembly screening except one, Ddr2. 16 of 22 also failed to be detected in GFP localization study(Huh et al. 2003), raising the possibility that C-terminal tagging is not proper modification for these genes. We also found that extremely low portion of proteins with no localization data analyzed in GFP database were detected in homomer screening (10 out of 1,882). Similarly, it was reported that GFP strains showing signals and TAP strains detected by western blot analysis overlap more than 90% (Huh et al. 2003). This repeated coincidence of negative population of three datasets raised necessity of further investigation to ensure whether signal is not detected because of low expression and absence of interaction or unrevealed obstacles induced in the process of library construction. The future construction of N-terminally VN- and VC-tagged strain collections and their utilization will help to resolve this unanswered question and also alleviate topological problems in genome-wide BiFC screens and greatly reduce false-negative results.

171 known homomers eliminated during self-assembly analysis also revealed critical

downsides of this system. This strategy was taken because it was hard to eliminate each interacting motif for a large number of homomer candidates, as most commonly used to screen out false-positive BiFC signals (Horstman et al. 2014), but a large number of true-positives were removed together in this process. In order to overcome these drawbacks, the second criterion should be applied. Firstly, we considered localization difference observed between the self-assembly signal and candidate-tagged BiFC signal. Among 16 candidates satisfying this criterion 8 candidates are known homomers. But this is only valid for proteins localized to restricted area of subcellular organelle, and every cytoplasmic or nuclear candidates with sufficient intracellular abundance failed to be selected. Indeed, well-known homomers localized to cytoplasm or nucleus with high expression levels including Hsp104 (Wendler et al. 2007), Fas1 (Babu et al. 2012), Fas2 (Johansson et al. 2008), Hsp82 (Marsh et al. 1998) and ribosomal proteins (Qiu et al. 2006) showed strong self-assembly signals at their innate subcellular localization indicating that these are not proper candidates to be applied to criteria we made. We suggest further approaches, e.g., Co-IP, mass spectrometry, and FCS, only for those whose expression level exceeds a certain cut-off will help to minimize loss of true PPIs in genome-wide BiFC screens with fewer efforts.

Even with limitations libraries mentioned above, BiFC assay still has many advantages for the analysis of PPIs (Miller et al. 2015). BiFC assay reveals not only the occurrence but also the subcellular localization of PPIs in vivo, so we obtained subcellular localization of homomer candidates and revealed that most of candidates are localized to their previously reported habitats while 21 candidates showed partial signals. One of interesting candidates is Pse1 (Ymr308c), a yeast importin, which showed BiFC signal as dots on nuclear envelope while its GFP-tagged form in our data as well as previous studies (Seedorf and Silver 1997) both are localized to cytoplasm and nucleus. It was reported

that C-terminally epitope tagged Pse1 behaved like non-tagged wild type Pse1 and *pse1* mutant not interacting with Ran-GTP was observed to be accumulated on nuclear envelope (Seedorf et al. 1999), similar to BiFC signal we detected. This suggests a possibility that localization of this protein may be dependent of its interacting partner. Several cases of importins: Pse1, Srp1 (Solsbacher et al. 1998), Kap123 (Seedorf and Silver 1997) are included in 21 candidates and showed similar signal patterns. However, in BiFC assay, it takes time to form a stable fluorophore from two separate fragments, and there is a possibility that sites of fluorescence are not actually where the interaction takes place (Hu et al. 2002; Ohad et al. 2007). Even though we used fragments of Venus protein, which has a greatly improved maturation rate (Miyawaki et al. 2003), we cannot completely rule out this possibility. For this reason, for candidates showing partial localization including importins listed above, it is necessary to confirm whether homomers exist only in the detected sites, or whether only the homomers present in the sites were able to form a stable fluorophore.

Adenovirus-based β-arrestin BiFC assay was successfully used to monitor activation of G protein-coupled receptors, a typical membrane protein family (Song et al. 2014), and the aquaporin complexes were screened and purified by using BiFC assay (Sjohamn et al. 2016), revealing suitability of this methods for analyzing interactions of membrane proteins as well as soluble proteins (Sjohamn and Hedfalk 2014). In this study as well, we identified 42 membrane protein homomers, which represents 23% of 186 homomers. This percentage is slightly higher than that of membrane proteins in the yeast proteome, suggesting that BiFC assay is well suited to membrane proteins. BiFC is particularly advantageous for observing weak or transient PPIs with low protein level that are not easily detected by other biochemical methods as appeared in our data. This sensitivity of the BiFC assay to capture weak interaction is obtained because the two fragments meet

and form a stable complex. This feature, conversely, may lock the interacting fused proteins and thus induce unnatural consequences. However, our results consistently imply that irreversibility is not a major problem in our experimental conditions, as revealed in spot assays or signal rescues detected upon media change. These are presumably because in our system, complementary fragments are tagged under endogenous promoter, resulting in overall moderate intracellular abundance. Similar cases against irreversibility of BiFC have been reported in previous studies using budding yeast as a model organelle (Cole et al. 2007a; Sung and Huh 2007; Kang et al. 2010). Under the assumption that irreversibility is negligible, this system can provide a suitable tool for studying the changes of protein interactome dynamics in response to various stresses.

Investigation of signal changes under nitrogen starvation filtered out a various interesting candidates. GO analysis revealed that 48 candidates are highly enriched in RNA catabolism process (GOID 6401, P=0.0394), protein transport (GOID 6605, P= 0.0419), vacuole organization (GOID 7033, P= 0.0743) when compared to 186 homomer population. Under nitrogen starvation conditions, cells undergo autophagy to enhance cell viability and vacuolar degradation of cellular components including mRNA occurs (Onodera and Ohsumi 2005; Huang et al. 2015) and based on our enriched candidates, we can assume that active changes of homomeric state are accompanied in the processes. It is noteworthy that two components of the EGO complex, Meh1 and Slm4 (Binda et al. 2009), showed increased BiFC signals. Given that the homomeric state of Slm4 has been reported to be important for the regulation of TORC1 signaling (Zhang et al. 2012), it will be interesting to examine whether Meh1 homomerization also influences TORC1 signaling and how the increase in homomerization of Meh1 and Slm4 is related to the regulation of TORC1 signaling. Several proteins involved in the multivesicular body (MVB) pathway, such as Did2 and Vps60 (Rue et al. 2008), are also included in

candidates showing the BiFC signal changes. The MVB pathway is required for starvation-induced degradation of plasma membrane proteins (Jones et al. 2012) and its proper activation is related to autophagy (Lee et al. 2007). Homomerization of these proteins may be an indication of the MVB pathway activation. As such, the analysis of dynamics of protein homomerization under stress conditions raises many research issues and challenges, which need to be addressed. Also, our analysis did not include possible homomer candidates that do not exist as homomers in nutrient-rich condition but homomerize upon starvation so screening genome-wide homomer candidates in starvation condition from the beginning has the potential to give a different population than we obtained from this study.

Our results about Pet10 homomerization increase and interaction of Pet10 with Fas1 or Fas2 decrease upon starvation gives new insights to possible role of this protein. Many lipid droplet proteins were found to be regulated differentially dependent on intracellular metabolic status (Wolins et al. 2001; Jacquier et al. 2011; Olzmann et al. 2013; Markgraf et al. 2014) and homomerization of Pet10 can be one of them, although many things remain to be declare. Lipid accumulation led by LZ-induced dimeric form of Pet10 without starvation suggests that increase in the homomeric form of Pet10 may affect accumulation of intracellular lipids upon nitrogen starvation as detected in this study and in many species (Breuer et al. 2012; Lopez Garcia de Lomana et al. 2015; Goncalves et al. 2016), but the necessity of Pet10 homomerization is not verified because of our failure in constructing monomeric form of *pet10* mutant. What physiological effect observed when Pet10 homomerization is disturbed and how lipid droplet protein interacts with cytoplasmic diffused proteins remains unclear and requires further refined research. Aside from this, as far as we known, Pet10 is the only lipid droplet protein found to interact with FAS component Fas1 and Fas2 so far and the fact that only overexpressed Pet10 could be

detected by Co-IP assay again emphasized benefits of BiFC assay in searching interactors. Understanding the functional role of Pet10 in lipid accumulation will also be useful in bioengineering applications, given that increasing lipid production in microorganisms has long been a challenge (Brennan and Owende 2010; Zeng et al. 2011).

REFERENCES

Agre P, Kozono D. 2003. Aquaporin water channels: molecular mechanisms for human diseases. *FEBS Lett* **555**: 72-78.

Ando R, Mizuno H, Miyawaki A. 2004. Regulated fast nucleocytoplasmic shuttling observed by reversible protein highlighting. *Science* **306**: 1370-1373.

Arnold I, Pfeiffer K, Neupert W, Stuart RA, Schagger H. 1998. Yeast mitochondrial F1F0-ATP synthase exists as a dimer: identification of three dimer-specific subunits. *EMBO J* **17**: 7170-7178.

Asano S, Park JE, Yu LR, Zhou M, Sakchaisri K, Park CJ, Kang YH, Thorner J, Veenstra TD, Lee KS. 2006. Direct phosphorylation and activation of a Nim1-related kinase Gin4 by Elm1 in budding yeast. *J Biol Chem* **281**: 27090-27098.

Athenstaedt K, Daum G. 1999. Phosphatidic acid, a key intermediate in lipid metabolism. *Eur J Biochem* **266**: 1-16.

Athenstaedt K, Zweytick D, Jandrositz A, Kohlwein SD, Daum G. 1999. Identification and characterization of major lipid particle proteins of the yeast Saccharomyces cerevisiae. *J Bacteriol* **181**: 6441-6448.

Babu M, Vlasblom J, Pu S, Guo X, Graham C, Bean BD, Burston HE, Vizeacoumar FJ, Snider J, Phanse S et al. 2012. Interaction landscape of membrane-protein complexes in Saccharomyces cerevisiae. *Nature* **489**: 585-589.

Baird GS, Zacharias DA, Tsien RY. 2000. Biochemistry, mutagenesis, and oligomerization of DsRed, a red fluorescent protein from coral. *Proc Natl Acad Sci U S A* **97**: 11984-11989.

Bartz R, Li WH, Venables B, Zehmer JK, Roth MR, Welti R, Anderson RG, Liu P, Chapman KD. 2007. Lipidomics reveals that adiposomes store ether lipids and mediate phospholipid traffic. *J Lipid Res* **48**: 837-847.

Berendzen KW, Bohmer M, Wallmeroth N, Peter S, Vesic M, Zhou Y, Tiesler FK, Schleifenbaum F, Harter K. 2012. Screening for in planta protein-protein interactions combining bimolecular fluorescence complementation with flow cytometry. *Plant Methods* **8**: 25.

Berland KM, So PT, Gratton E. 1995. Two-photon fluorescence correlation spectroscopy: method and application to the intracellular environment. *Biophys J* **68**: 694-701.

Betzig E, Patterson GH, Sougrat R, Lindwasser OW, Olenych S, Bonifacino JS, Davidson

MW, Lippincott-Schwartz J, Hess HF. 2006. Imaging intracellular fluorescent proteins at nanometer resolution. *Science* **313**: 1642-1645.

Binda M, Peli-Gulli MP, Bonfils G, Panchaud N, Urban J, Sturgill TW, Loewith R, De Virgilio C. 2009. The Vam6 GEF controls TORC1 by activating the EGO complex. *Mol Cell* **35**: 563-573.

Binns D, Januszewski T, Chen Y, Hill J, Markin VS, Zhao Y, Gilpin C, Chapman KD, Anderson RG, Goodman JM. 2006. An intimate collaboration between peroxisomes and lipid bodies. *J Cell Biol* **173**: 719-731.

Blanchette-Mackie EJ, Dwyer NK, Barber T, Coxey RA, Takeda T, Rondinone CM, Theodorakis JL, Greenberg AS, Londos C. 1995. Perilipin is located on the surface layer of intracellular lipid droplets in adipocytes. *J Lipid Res* **36**: 1211-1226.

Boeke JD, Trueheart J, Natsoulis G, Fink GR. 1987. 5-Fluoroorotic acid as a selective agent in yeast molecular genetics. *Methods Enzymol* **154**: 164-175.

Boruc J, Van den Daele H, Hollunder J, Rombauts S, Mylle E, Hilson P, Inze D, De Veylder L, Russinova E. 2010. Functional modules in the Arabidopsis core cell cycle binary protein-protein interaction network. *Plant Cell* **22**: 1264-1280.

Brennan L, Owende P. 2010. Biofuels from microalgae—A review of technologies for production, processing, and extractions of biofuels and co-products. *Renewable and Sustainable Energy Reviews* **14**: 557-577.

Breuer G, Lamers PP, Martens DE, Draaisma RB, Wijffels RH. 2012. The impact of nitrogen starvation on the dynamics of triacylglycerol accumulation in nine microalgae strains. *Bioresour Technol* **124**: 217-226.

Brown MP, Grundy WN, Lin D, Cristianini N, Sugnet CW, Furey TS, Ares M, Jr., Haussler D. 2000. Knowledge-based analysis of microarray gene expression data by using support vector machines. *Proc Natl Acad Sci U S A* **97**: 262-267.

Bruckner A, Polge C, Lentze N, Auerbach D, Schlattner U. 2009. Yeast two-hybrid, a powerful tool for systems biology. *Int J Mol Sci* **10**: 2763-2788.

Bun-Ya M, Nishimura M, Harashima S, Oshima Y. 1991. The PHO84 gene of Saccharomyces cerevisiae encodes an inorganic phosphate transporter. *Mol Cell Biol* **11**: 3229-3238.

Campbell RE, Tour O, Palmer AE, Steinbach PA, Baird GS, Zacharias DA, Tsien RY. 2002. A monomeric red fluorescent protein. *Proc Natl Acad Sci U S A* **99**: 7877-7882.

Cantu D, Yang B, Ruan R, Li K, Menzo V, Fu D, Chern M, Ronald PC, Dubcovsky J. 2013. Comparative analysis of protein-protein interactions in the defense response of rice and wheat. *BMC Genomics* **14**: 166.

Capuano F, Beaudoin F, Napier JA, Shewry PR. 2007. Properties and exploitation of oleosins. *Biotechnol Adv* **25**: 203-206.

Chapman KD, Trelease RN. 1991. Acquisition of membrane lipids by differentiating glyoxysomes: role of lipid bodies. *J Cell Biol* **115**: 995-1007.

Chen Y, Muller JD, Ruan Q, Gratton E. 2002. Molecular brightness characterization of EGFP in vivo by fluorescence fluctuation spectroscopy. *Biophys J* **82**: 133-144.

Chen Y, Muller JD, So PTC, Gratton E. 1999. The photon counting histogram in fluorescence fluctuation spectroscopy. *Biophysical Journal* **77**: 553-567.

Chen Y, Siewers V, Nielsen J. 2012. Profiling of cytosolic and peroxisomal acetyl-CoA metabolism in Saccharomyces cerevisiae. *PLoS One* **7**: e42475.

Choi EW, Seen DS, Song YB, Son HS, Jung NC, Huh WK, Hahn JS, Kim K, Jeong JY, Lee TG. 2012. AdHTS: a high-throughput system for generating recombinant adenoviruses. *J Biotechnol* **162**: 246-252.

Chu J, Zhang Z, Zheng Y, Yang J, Qin L, Lu J, Huang ZL, Zeng S, Luo Q. 2009. A novel far-red bimolecular fluorescence complementation system that allows for efficient visualization of protein interactions under physiological conditions. *Biosens Bioelectron* **25**: 234-239.

Citovsky V, Lee LY, Vyas S, Glick E, Chen MH, Vainstein A, Gafni Y, Gelvin SB, Tzfira T. 2006. Subcellular localization of interacting proteins by bimolecular fluorescence complementation in planta. *J Mol Biol* **362**: 1120-1131.

Clegg RM. 1995. Fluorescence resonance energy transfer. *Curr Opin Biotechnol* **6**: 103-110.

Cohen AW, Razani B, Schubert W, Williams TM, Wang XB, Iyengar P, Brasaemle DL, Scherer PE, Lisanti MP. 2004. Role of caveolin-1 in the modulation of lipolysis and lipid droplet formation. *Diabetes* **53**: 1261-1270.

Cole KC, McLaughlin HW, Johnson DI. 2007a. Use of bimolecular fluorescence complementation to study in vivo interactions between Cdc42p and Rdi1p of Saccharomyces cerevisiae. *Eukaryot Cell* **6**: 378-387.

Cole KC, McLaughlin HW, Johnson DI. 2007b. Use of bimolecular fluorescence complementation to study in vivo interactions between Cdc42p and Rdi1p of Saccharomyces cerevisiae. *Eukaryotic Cell* **6**: 378-387.

Conway MK, Grunwald D, Heideman W. 2012. Glucose, nitrogen, and phosphate repletion in Saccharomyces cerevisiae: common transcriptional responses to different nutrient signals. *G3 (Bethesda)* **2**: 1003-1017.

Cunningham KW, Fink GR. 1994. Calcineurin-dependent growth control in Saccharomyces cerevisiae mutants lacking PMC1, a homolog of plasma membrane Ca2+ ATPases. *J Cell Biol* **124**: 351-363.

Currie E, Guo X, Christiano R, Chitraju C, Kory N, Harrison K, Haas J, Walther TC, Farese RV, Jr. 2014. High confidence proteomic analysis of yeast LDs identifies additional droplet proteins and reveals connections to dolichol synthesis and sterol acetylation. *J Lipid Res* **55**: 1465-1477.

de Godoy LM, Olsen JV, Cox J, Nielsen ML, Hubner NC, Frohlich F, Walther TC, Mann M. 2008. Comprehensive mass-spectrometry-based proteome quantification of haploid versus diploid yeast. *Nature* **455**: 1251-1254.

De Groot PW, Hellingwerf KJ, Klis FM. 2003. Genome-wide identification of fungal GPI proteins. *Yeast* **20**: 781-796.

de Maziere AM, Hage WJ, Ubbels GA. 1996. A method for staining of cell nuclei in Xenopus laevis embryos with cyanine dyes for whole-mount confocal laser scanning microscopy. *J Histochem Cytochem* **44**: 399-402.

Demidov VV, Dokholyan NV, Witte-Hoffmann C, Chalasani P, Yiu HW, Ding F, Yu Y, Cantor CR, Broude NE. 2006. Fast complementation of split fluorescent protein triggered by DNA hybridization. *Proc Natl Acad Sci U S A* **103**: 2052-2056.

Du Y, Pattnaik AK, Song C, Yoo D, Li G. 2012. Glycosyl-phosphatidylinositol (GPI)-anchored membrane association of the porcine reproductive and respiratory syndrome virus GP4 glycoprotein and its co-localization with CD163 in lipid rafts. *Virology* **424**: 18-32.

Ellenberger TE, Brandl CJ, Struhl K, Harrison SC. 1992. The GCN4 basic region leucine zipper binds DNA as a dimer of uninterrupted alpha helices: crystal structure of the protein-DNA complex. *Cell* **71**: 1223-1237.

Fan JY, Cui ZQ, Wei HP, Zhang ZP, Zhou YF, Wang YP, Zhang XE. 2008. Split mCherry as a new red bimolecular fluorescence complementation system for visualizing protein-protein interactions in living cells. *Biochem Biophys Res Commun* **367**: 47-53.

Filonov GS, Verkhusha VV. 2013. A near-infrared BiFC reporter for in vivo imaging of protein-protein interactions. *Chem Biol* **20**: 1078-1086.

Gao Q, Binns DD, Kinch LN, Grishin NV, Ortiz N, Chen X, Goodman JM. 2017. Pet10p is a yeast perilipin that stabilizes lipid droplets and promotes their assembly. *J Cell Biol* **216**: 3199-3217.

Gasch AP, Spellman PT, Kao CM, Carmel-Harel O, Eisen MB, Storz G, Botstein D, Brown PO. 2000. Genomic expression programs in the response of yeast cells to environmental changes. *Mol Biol Cell* **11**: 4241-4257.

Gasch AP, Werner-Washburne M. 2002. The genomics of yeast responses to environmental stress and starvation. *Funct Integr Genomics* **2**: 181-192.

Gavin AC, Bosche M, Krause R, Grandi P, Marzioch M, Bauer A, Schultz J, Rick JM, Michon AM, Cruciat CM et al. 2002. Functional organization of the yeast proteome by systematic analysis of protein complexes. *Nature* **415**: 141-147.

Gehl C, Waadt R, Kudla J, Mendel RR, Hansch R. 2009. New GATEWAY vectors for high throughput analyses of protein-protein interactions by bimolecular fluorescence complementation. *Mol Plant* **2**: 1051-1058.

Ghaemmaghami S, Huh WK, Bower K, Howson RW, Belle A, Dephoure N, O'Shea EK, Weissman JS. 2003. Global analysis of protein expression in yeast. *Nature* **425**: 737-741.

Ghosh I, Hamilton AD, Regan L. 2000. Antiparallel leucine zipper-directed protein reassembly: Application to the green fluorescent protein. *J Am Chem Soc* **122**: 5658-5659.

Giaever G, Chu AM, Ni L, Connelly C, Riles L, Veronneau S, Dow S, Lucau-Danila A, Anderson K, Andre B et al. 2002. Functional profiling of the Saccharomyces cerevisiae genome. *Nature* **418**: 387-391.

Gietz RD, Schiestl RH, Willems AR, Woods RA. 1995. Studies on the transformation of intact yeast cells by the LiAc/SS-DNA/PEG procedure. *Yeast* **11**: 355-360.

Gimeno CJ, Ljungdahl PO, Styles CA, Fink GR. 1992. Unipolar cell divisions in the yeast S. cerevisiae lead to filamentous growth: regulation by starvation and RAS. *Cell* **68**: 1077-1090.

Glover JN, Harrison SC. 1995. Crystal structure of the heterodimeric bZIP transcription factor c-Fos-c-Jun bound to DNA. *Nature* **373**: 257-261.

Goncalves EC, Koh J, Zhu N, Yoo MJ, Chen S, Matsuo T, Johnson JV, Rathinasabapathi B. 2016. Nitrogen starvation-induced accumulation of triacylglycerol in the green algae: evidence for a role for ROC40, a transcription factor involved in circadian rhythm. *Plant J* **85**: 743-757.

Goodman JM. 2008. The gregarious lipid droplet. *J Biol Chem* **283**: 28005-28009.

Goodsell DS, Olson AJ. 2000. Structural symmetry and protein function. *Annu Rev Biophys Biomol Struct* **29**: 105-153.

Greenberg AS, Egan JJ, Wek SA, Garty NB, Blanchette-Mackie EJ, Londos C. 1991. Perilipin, a major hormonally regulated adipocyte-specific phosphoprotein associated with the periphery of lipid storage droplets. *J Biol Chem* **266**: 11341-11346.

Griesbeck O, Baird GS, Campbell RE, Zacharias DA, Tsien RY. 2001. Reducing the environmental sensitivity of yellow fluorescent protein. Mechanism and applications. *J Biol Chem* **276**: 29188-29194.

Grimme JM, Honda M, Wright R, Okuno Y, Rothenberg E, Mazin AV, Ha T, Spies M. 2010. Human Rad52 binds and wraps single-stranded DNA and mediates annealing via two hRad52-ssDNA complexes. *Nucleic Acids Res* **38**: 2917-2930.

Guo Y, Rebecchi M, Scarlata S. 2005. Phospholipase Cbeta2 binds to and inhibits phospholipase Cdelta1. *J Biol Chem* **280**: 1438-1447.

Habeler G, Natter K, Thallinger GG, Crawford ME, Kohlwein SD, Trajanoski Z. 2002. YPL.db: the Yeast Protein Localization database. *Nucleic Acids Res* **30**: 80-83.

Han Y, Wang S, Zhang Z, Ma X, Li W, Zhang X, Deng J, Wei H, Li Z, Zhang XE et al. 2014. In vivo imaging of protein-protein and RNA-protein interactions using novel far-red fluorescence complementation systems. *Nucleic Acids Res* **42**: e103.

Hashimoto K, Nishi H, Bryant S, Panchenko AR. 2011. Caught in self-interaction: evolutionary and functional mechanisms of protein homooligomerization. *Phys Biol* **8**: 035007.

Herrick-Davis K, Grinde E, Cowan A, Mazurkiewicz JE. 2013. Fluorescence correlation spectroscopy analysis of serotonin, adrenergic, muscarinic, and dopamine receptor dimerization: the oligomer number puzzle. *Mol Pharmacol* **84**: 630-642.

Herskowitz I, Jensen RE. 1991. Putting the HO gene to work: practical uses for mating-type switching. *Methods Enzymol* **194**: 132-146.

Hess ST, Girirajan TP, Mason MD. 2006. Ultra-high resolution imaging by fluorescence photoactivation localization microscopy. *Biophys J* **91**: 4258-4272.

Hink MA, Shah K, Russinova E, de Vries SC, Visser AJ. 2008. Fluorescence fluctuation analysis of Arabidopsis thaliana somatic embryogenesis receptor-like kinase and brassinosteroid insensitive 1 receptor oligomerization. *Biophys J* **94**: 1052-1062.

Hirst J, Barlow LD, Francisco GC, Sahlender DA, Seaman MN, Dacks JB, Robinson MS.

2011. The fifth adaptor protein complex. *PLoS Biol* **9**: e1001170.

Ho Y, Gruhler A, Heilbut A, Bader GD, Moore L, Adams SL, Millar A, Taylor P, Bennett K, Boutilier K et al. 2002. Systematic identification of protein complexes in Saccharomyces cerevisiae by mass spectrometry. *Nature* **415**: 180-183.

Hong M, Fitzgerald MX, Harper S, Luo C, Speicher DW, Marmorstein R. 2008. Structural basis for dimerization in DNA recognition by Gal4. *Structure* **16**: 1019-1026.

Horstman A, Tonaco IA, Boutilier K, Immink RG. 2014. A cautionary note on the use of split-YFP/BiFC in plant protein-protein interaction studies. *Int J Mol Sci* **15**: 9628-9643.

Hsieh K, Huang AH. 2005. Lipid-rich tapetosomes in Brassica tapetum are composed of oleosin-coated oil droplets and vesicles, both assembled in and then detached from the endoplasmic reticulum. *Plant J* **43**: 889-899.

Hu CD, Chinenov Y, Kerppola TK. 2002. Visualization of interactions among bZIP and Rel family proteins in living cells using bimolecular fluorescence complementation. *Mol Cell* **9**: 789-798.

Hu CD, Kerppola TK. 2003. Simultaneous visualization of multiple protein interactions in living cells using multicolor fluorescence complementation analysis. *Nat Biotechnol* **21**: 539-545.

Huang B, Perroud TD, Zare RN. 2004. Photon counting histogram: one-photon excitation. *Chemphyschem* **5**: 1523-1531.

Huang H, Kawamata T, Horie T, Tsugawa H, Nakayama Y, Ohsumi Y, Fukusaki E. 2015. Bulk RNA degradation by nitrogen starvation-induced autophagy in yeast. *EMBO J* **34**: 154-168.

Huh WK, Falvo JV, Gerke LC, Carroll AS, Howson RW, Weissman JS, O'Shea EK. 2003. Global analysis of protein localization in budding yeast. *Nature* **425**: 686-691.

Hynes TR, Yost E, Mervine S, Berlot CH. 2008. Multicolor BiFC analysis of competition among G protein beta and gamma subunit interactions. *Methods* **45**: 207-213.

Ito T, Chiba T, Ozawa R, Yoshida M, Hattori M, Sakaki Y. 2001. A comprehensive two-hybrid analysis to explore the yeast protein interactome. *Proc Natl Acad Sci U S A* **98**: 4569-4574.

Jach G, Pesch M, Richter K, Frings S, Uhrig JF. 2006. An improved mRFP1 adds red to bimolecular fluorescence complementation. *Nat Methods* **3**: 597-600.

Jacquier N, Choudhary V, Mari M, Toulmay A, Reggiori F, Schneiter R. 2011. Lipid droplets are functionally connected to the endoplasmic reticulum in

Saccharomyces cerevisiae. *J Cell Sci* **124**: 2424-2437.

Job D, Valiron O, Oakley B. 2003. Microtubule nucleation. *Curr Opin Cell Biol* **15**: 111-117.

Johansson P, Wiltschi B, Kumari P, Kessler B, Vonrhein C, Vonck J, Oesterhelt D, Grininger M. 2008. Inhibition of the fungal fatty acid synthase type I multienzyme complex. *Proc Natl Acad Sci U S A* **105**: 12803-12808.

Jones CB, Ott EM, Keener JM, Curtiss M, Sandrin V, Babst M. 2012. Regulation of membrane protein degradation by starvation-response pathways. *Traffic* **13**: 468-482.

Jones S, Thornton JM. 1995. Protein-protein interactions: a review of protein dimer structures. *Prog Biophys Mol Biol* **63**: 31-65.

Jorgensen CS, Ryder LR, Steino A, Hojrup P, Hansen J, Beyer NH, Heegaard NH, Houen G. 2003. Dimerization and oligomerization of the chaperone calreticulin. *Eur J Biochem* **270**: 4140-4148.

Kamada Y, Sekito T, Ohsumi Y. 2004. Autophagy in yeast: a TOR-mediated response to nutrient starvation. *Curr Top Microbiol Immunol* **279**: 73-84.

Kanagavijayan D, Rajasekharan R, Srinivasan M. 2016. Yeast MRX deletions have short chronological life span and more triacylglycerols. *Fems Yeast Res* **16**.

Kang PJ, Beven L, Hariharan S, Park HO. 2010. The Rsr1/Bud1 GTPase interacts with itself and the Cdc42 GTPase during bud-site selection and polarity establishment in budding yeast. *Mol Biol Cell* **21**: 3007-3016.

Kawai-Noma S, Pack CG, Tsuji T, Kinjo M, Taguchi H. 2009. Single mother-daughter pair analysis to clarify the diffusion properties of yeast prion Sup35 in guanidine-HCl-treated [PSI] cells. *Genes Cells* **14**: 1045-1054.

Kerppola TK. 2008. Bimolecular fluorescence complementation (BiFC) analysis as a probe of protein interactions in living cells. *Annu Rev Biophys* **37**: 465-487.

Kerppola TK. 2009. Visualization of molecular interactions using bimolecular fluorescence complementation analysis: Characteristics of protein fragment complementation. *Chem Soc Rev* **38**: 2876-2886.

Kerppola TK. 2013. Multicolor bimolecular fluorescence complementation (BiFC) analysis of protein interactions with alternative partners. *Cold Spring Harb Protoc* **2013**: 798-803.

Kim HJ, Kwon S, Nam SH, Jung JW, Kang M, Ryu J, Kim JE, Cheong JG, Cho CY, Kim S et al. 2017. Dynamic and coordinated single-molecular interactions at TM4SF5-

enriched microdomains guide invasive behaviors in 2- and 3-dimensional environments. *FASEB J* **31**: 1461-1481.

Klopffleisch K, Phan N, Augustin K, Bayne RS, Booker KS, Botella JR, Carpita NC, Carr T, Chen JG, Cooke TR et al. 2011. Arabidopsis G-protein interactome reveals connections to cell wall carbohydrates and morphogenesis. *Mol Syst Biol* **7**: 532.

Kodama Y, Hu CD. 2012. Bimolecular fluorescence complementation (BiFC): a 5-year update and future perspectives. *Biotechniques* **53**: 285-298.

Kremers GJ, Goedhart J, van Munster EB, Gadella TW, Jr. 2006. Cyan and yellow super fluorescent proteins with improved brightness, protein folding, and FRET Forster radius. *Biochemistry* **45**: 6570-6580.

Krogan NJ, Cagney G, Yu H, Zhong G, Guo X, Ignatchenko A, Li J, Pu S, Datta N, Tikuisis AP et al. 2006. Global landscape of protein complexes in the yeast Saccharomyces cerevisiae. *Nature* **440**: 637-643.

Lam MH, Snider J, Rehal M, Wong V, Aboualizadeh F, Drecun L, Wong O, Jubran B, Li M, Ali M et al. 2015. A Comprehensive Membrane Interactome Mapping of Sho1p Reveals Fps1p as a Novel Key Player in the Regulation of the HOG Pathway in S. cerevisiae. *J Mol Biol* **427**: 2088-2103.

Le Lay S, Hajduch E, Lindsay MR, Le Liepvre X, Thiele C, Ferre P, Parton RG, Kurzchalia T, Simons K, Dugail I. 2006. Cholesterol-induced caveolin targeting to lipid droplets in adipocytes: a role for caveolar endocytosis. *Traffic* **7**: 549-561.

Lee JA, Beigneux A, Ahmad ST, Young SG, Gao FB. 2007. ESCRT-III dysfunction causes autophagosome accumulation and neurodegeneration. *Curr Biol* **17**: 1561-1567.

Lee LY, Fang MJ, Kuang LY, Gelvin SB. 2008. Vectors for multi-color bimolecular fluorescence complementation to investigate protein-protein interactions in living plant cells. *Plant Methods* **4**: 24.

Lee LY, Wu FH, Hsu CT, Shen SC, Yeh HY, Liao DC, Fang MJ, Liu NT, Yen YC, Dokladal L et al. 2012. Screening a cDNA library for protein-protein interactions directly in planta. *Plant Cell* **24**: 1746-1759.

Lee OH, Kim H, He Q, Baek HJ, Yang D, Chen LY, Liang J, Chae HK, Safari A, Liu D et al. 2011. Genome-wide YFP fluorescence complementation screen identifies new regulators for telomere signaling in human cells. *Mol Cell Proteomics* **10**: M110 001628.

Lee YR, Park JH, Hahm SH, Kang LW, Chung JH, Nam KH, Hwang KY, Kwon IC, Han

YS. 2010. Development of Bimolecular Fluorescence Complementation Using Dronpa for Visualization of Protein-Protein Interactions in Cells. *Mol Imaging Biol* **12**: 468-478.

Li BZ, Cheng JS, Ding MZ, Yuan YJ. 2010. Transcriptome analysis of differential responses of diploid and haploid yeast to ethanol stress. *J Biotechnol* **148**: 194-203.

Lin MZ, McKeown MR, Ng HL, Aguilera TA, Shaner NC, Campbell RE, Adams SR, Gross LA, Ma W, Alber T et al. 2009. Autofluorescent proteins with excitation in the optical window for intravital imaging in mammals. *Chem Biol* **16**: 1169-1179.

Lipatova Z, Belogortseva N, Zhang XQ, Kim J, Taussig D, Segev N. 2012. Regulation of selective autophagy onset by a Ypt/Rab GTPase module. *Proc Natl Acad Sci U S A* **109**: 6981-6986.

Llopis J, McCaffery JM, Miyawaki A, Farquhar MG, Tsien RY. 1998. Measurement of cytosolic, mitochondrial, and Golgi pH in single living cells with green fluorescent proteins. *Proc Natl Acad Sci U S A* **95**: 6803-6808.

Longtine MS, McKenzie A, 3rd, Demarini DJ, Shah NG, Wach A, Brachat A, Philippsen P, Pringle JR. 1998. Additional modules for versatile and economical PCR-based gene deletion and modification in Saccharomyces cerevisiae. *Yeast* **14**: 953-961.

Lopez Garcia de Lomana A, Schauble S, Valenzuela J, Imam S, Carter W, Bilgin DD, Yohn CB, Turkarslan S, Reiss DJ, Orellana MV et al. 2015. Transcriptional program for nitrogen starvation-induced lipid accumulation in Chlamydomonas reinhardtii. *Biotechnol Biofuels* **8**: 207.

Lorenz MC, Heitman J. 1997. Yeast pseudohyphal growth is regulated by GPA2, a G protein alpha homolog. *EMBO J* **16**: 7008-7018.

MacKinnon R. 2003. Potassium channels. *FEBS Lett* **555**: 62-65.

Magliery TJ, Wilson CG, Pan W, Mishler D, Ghosh I, Hamilton AD, Regan L. 2005. Detecting protein-protein interactions with a green fluorescent protein fragment reassembly trap: scope and mechanism. *J Am Chem Soc* **127**: 146-157.

Makrantoni V, Dennison P, Stark MJ, Coote PJ. 2007. A novel role for the yeast protein kinase Dbf2p in vacuolar H+-ATPase function and sorbic acid stress tolerance. *Microbiology* **153**: 4016-4026.

Malengo G, Andolfo A, Sidenius N, Gratton E, Zamai M, Caiolfa VR. 2008. Fluorescence correlation spectroscopy and photon counting histogram on membrane proteins: functional dynamics of the glycosylphosphatidylinositol-anchored urokinase

plasminogen activator receptor. *J Biomed Opt* **13**: 031215.

Maluf NK, Fischer CJ, Lohman TM. 2003. A Dimer of Escherichia coli UvrD is the active form of the helicase in vitro. *J Mol Biol* **325**: 913-935.

Marianayagam NJ, Sunde M, Matthews JM. 2004. The power of two: protein dimerization in biology. *Trends Biochem Sci* **29**: 618-625.

Markgraf DF, Klemm RW, Junker M, Hannibal-Bach HK, Ejsing CS, Rapoport TA. 2014. An ER protein functionally couples neutral lipid metabolism on lipid droplets to membrane lipid synthesis in the ER. *Cell Rep* **6**: 44-55.

Marsh JA, Kalton HM, Gaber RF. 1998. Cns1 is an essential protein associated with the hsp90 chaperone complex in Saccharomyces cerevisiae that can restore cyclophilin 40-dependent functions in cpr7Delta cells. *Mol Cell Biol* **18**: 7353-7359.

Matz MV, Fradkov AF, Labas YA, Savitsky AP, Zaraisky AG, Markelov ML, Lukyanov SA. 1999. Fluorescent proteins from nonbioluminescent Anthozoa species. *Nat Biotechnol* **17**: 969-973.

Miller KE, Kim Y, Huh WK, Park HO. 2015. Bimolecular Fluorescence Complementation (BiFC) Analysis: Advances and Recent Applications for Genome-Wide Interaction Studies. *J Mol Biol* **427**: 2039-2055.

Miller S, Lesk AM, Janin J, Chothia C. 1987. The accessible surface area and stability of oligomeric proteins. *Nature* **328**: 834-836.

Miyawaki A, Llopis J, Heim R, McCaffery JM, Adams JA, Ikura M, Tsien RY. 1997. Fluorescent indicators for Ca2+ based on green fluorescent proteins and calmodulin. *Nature* **388**: 882-887.

Miyawaki A, Nagai T, Mizuno H. 2003. Mechanisms of protein fluorophore formation and engineering. *Curr Opin Chem Biol* **7**: 557-562.

Mohamed AH, Chirala SS, Mody NH, Huang WY, Wakil SJ. 1988. Primary structure of the multifunctional alpha subunit protein of yeast fatty acid synthase derived from FAS2 gene sequence. *J Biol Chem* **263**: 12315-12325.

Muller JD, Chen Y, Gratton E. 2000. Resolving heterogeneity on the single molecular level with the photon-counting histogram. *Biophys J* **78**: 474-486.

Murozuka E, Hanisch S, Pomorski TG, Jahn TP, Schjoerring JK. 2013. Bimolecular fluorescence complementation and interaction of various Arabidopsis major intrinsic proteins expressed in yeast. *Physiol Plant* **148**: 422-431.

Murphy DJ, Vance J. 1999. Mechanisms of lipid-body formation. *Trends Biochem Sci* **24**:

109-115.

Nagai T, Ibata K, Park ES, Kubota M, Mikoshiba K, Miyawaki A. 2002. A variant of yellow fluorescent protein with fast and efficient maturation for cell-biological applications. *Nat Biotechnol* **20**: 87-90.

Nagai T, Sawano A, Park ES, Miyawaki A. 2001. Circularly permuted green fluorescent proteins engineered to sense Ca2+. *Proc Natl Acad Sci U S A* **98**: 3197-3202.

Nagiec MM, Wells GB, Lester RL, Dickson RC. 1993. A suppressor gene that enables Saccharomyces cerevisiae to grow without making sphingolipids encodes a protein that resembles an Escherichia coli fatty acyltransferase. *J Biol Chem* **268**: 22156-22163.

Nickerson A, Huang T, Lin LJ, Nan X. 2014. Photoactivated localization microscopy with bimolecular fluorescence complementation (BiFC-PALM) for nanoscale imaging of protein-protein interactions in cells. *PLoS One* **9**: e100589.

Niedziela-Majka A, Chesnik MA, Tomko EJ, Lohman TM. 2007. Bacillus stearothermophilus PcrA monomer is a single-stranded DNA translocase but not a processive helicase in vitro. *J Biol Chem* **282**: 27076-27085.

Nishi H, Hashimoto K, Madej T, Panchenko AR. 2013. Evolutionary, physicochemical, and functional mechanisms of protein homooligomerization. *Prog Mol Biol Transl Sci* **117**: 3-24.

Nooren IM, Thornton JM. 2003. Structural characterisation and functional significance of transient protein-protein interactions. *J Mol Biol* **325**: 991-1018.

O'Connell JD, Tsechansky M, Royall A, Boutz DR, Ellington AD, Marcotte EM. 2014. A proteomic survey of widespread protein aggregation in yeast. *Mol Biosyst* **10**: 851-861.

Oelkers P, Cromley D, Padamsee M, Billheimer JT, Sturley SL. 2002. The DGA1 gene determines a second triglyceride synthetic pathway in yeast. *J Biol Chem* **277**: 8877-8881.

Ohad N, Shichrur K, Yalovsky S. 2007. The analysis of protein-protein interactions in plants by bimolecular fluorescence complementation. *Plant Physiol* **145**: 1090-1099.

Ohashi K, Kiuchi T, Shoji K, Sampei K, Mizuno K. 2012. Visualization of cofilin-actin and Ras-Raf interactions by bimolecular fluorescence complementation assays using a new pair of split Venus fragments. *Biotechniques* **52**: 45-50.

Olofsson SO, Bostrom P, Andersson L, Rutberg M, Perman J, Boren J. 2009. Lipid

droplets as dynamic organelles connecting storage and efflux of lipids. *Biochim Biophys Acta* **1791**: 448-458.

Olzmann JA, Richter CM, Kopito RR. 2013. Spatial regulation of UBXD8 and p97/VCP controls ATGL-mediated lipid droplet turnover. *Proc Natl Acad Sci U S A* **110**: 1345-1350.

Onodera J, Ohsumi Y. 2005. Autophagy is required for maintenance of amino acid levels and protein synthesis under nitrogen starvation. *J Biol Chem* **280**: 31582-31586.

Orij R, Urbanus ML, Vizeacoumar FJ, Giaever G, Boone C, Nislow C, Brul S, Smits GJ. 2012. Genome-wide analysis of intracellular pH reveals quantitative control of cell division rate by pH(c) in Saccharomyces cerevisiae. *Genome Biol* **13**: R80.

Pack CG, Nishimura G, Tamura M, Aoki K, Taguchi H, Yoshida M, Kinjo M. 1999. Analysis of interaction between chaperonin GroEL and its substrate using fluorescence correlation spectroscopy. *Cytometry* **36**: 247-253.

Pack CG, Yukii H, Toh-e A, Kudo T, Tsuchiya H, Kaiho A, Sakata E, Murata S, Yokosawa H, Sako Y et al. 2014. Quantitative live-cell imaging reveals spatio-temporal dynamics and cytoplasmic assembly of the 26S proteasome. *Nat Commun* **5**: 3396.

Packter NM, Olukoshi ER. 1995. Ultrastructural studies of neutral lipid localisation in Streptomyces. *Arch Microbiol* **164**: 420-427.

Parrou JL, Enjalbert B, Plourde L, Bauche A, Gonzalez B, Francois J. 1999. Dynamic responses of reserve carbohydrate metabolism under carbon and nitrogen limitations in Saccharomyces cerevisiae. *Yeast* **15**: 191-203.

Pastor-Cantizano N, Montesinos JC, Bernat-Silvestre C, Marcote MJ, Aniento F. 2016. p24 family proteins: key players in the regulation of trafficking along the secretory pathway. *Protoplasma* **253**: 967-985.

Pedelacq JD, Cabantous S, Tran T, Terwilliger TC, Waldo GS. 2006. Engineering and characterization of a superfolder green fluorescent protein. *Nat Biotechnol* **24**: 79-88.

Pingoud A, Jeltsch A. 2001. Structure and function of type II restriction endonucleases. *Nucleic Acids Res* **29**: 3705-3727.

Pittet M, Conzelmann A. 2007. Biosynthesis and function of GPI proteins in the yeast Saccharomyces cerevisiae. *Biochim Biophys Acta* **1771**: 405-420.

Pol A, Martin S, Fernandez MA, Ferguson C, Carozzi A, Luetterforst R, Enrich C, Parton RG. 2004. Dynamic and regulated association of caveolin with lipid bodies: modulation of lipid body motility and function by a dominant negative mutant.

Mol Biol Cell **15**: 99-110.

Qiu D, Parada P, Marcos AG, Cardenas D, Remacha M, Ballesta JP. 2006. Different roles of P1 and P2 Saccharomyces cerevisiae ribosomal stalk proteins revealed by cross-linking. *Mol Microbiol* **62**: 1191-1202.

Rajakumari S, Grillitsch K, Daum G. 2008. Synthesis and turnover of non-polar lipids in yeast. *Prog Lipid Res* **47**: 157-171.

Randez-Gil F, Sanz P, Entian KD, Prieto JA. 1998. Carbon source-dependent phosphorylation of hexokinase PII and its role in the glucose-signaling response in yeast. *Mol Cell Biol* **18**: 2940-2948.

Raychaudhuri S, Young BP, Espenshade PJ, Loewen C, Jr. 2012. Regulation of lipid metabolism: a tale of two yeasts. *Curr Opin Cell Biol* **24**: 502-508.

Remy I, Michnick SW. 2004a. A cDNA library functional screening strategy based on fluorescent protein complementation assays to identify novel components of signaling pathways. *Methods* **32**: 381-388.

Remy I, Michnick SW. 2004b. Regulation of apoptosis by the Ft1 protein, a new modulator of protein kinase B/Akt. *Mol Cell Biol* **24**: 1493-1504.

Rigler R, Mets Ü, Widengren J, Kask P. 1993. Fluorescence correlation spectroscopy with high count rate and low background: analysis of translational diffusion. *European Biophysics Journal* **22**: 169-175.

Rizzo MA, Springer GH, Granada B, Piston DW. 2004. An improved cyan fluorescent protein variant useful for FRET. *Nat Biotechnol* **22**: 445-449.

Rue SM, Mattei S, Saksena S, Emr SD. 2008. Novel Ist1-Did2 complex functions at a late step in multivesicular body sorting. *Mol Biol Cell* **19**: 475-484.

Saffarian S, Li Y, Elson EL, Pike LJ. 2007. Oligomerization of the EGF receptor investigated by live cell fluorescence intensity distribution analysis. *Biophys J* **93**: 1021-1031.

Saka Y, Hagemann AI, Piepenburg O, Smith JC. 2007. Nuclear accumulation of Smad complexes occurs only after the midblastula transition in Xenopus. *Development* **134**: 4209-4218.

Saksena S, Wahlman J, Teis D, Johnson AE, Emr SD. 2009. Functional reconstitution of ESCRT-III assembly and disassembly. *Cell* **136**: 97-109.

Schneider CA, Rasband WS, Eliceiri KW. 2012. NIH Image to ImageJ: 25 years of image analysis. *Nat Methods* **9**: 671-675.

Schulze U, Liden G, Nielsen J, Villadsen J. 1996. Physiological effects of nitrogen

starvation in an anaerobic batch culture of Saccharomyces cerevisiae. *Microbiology* **142 (Pt 8)**: 2299-2310.

Seedorf M, Damelin M, Kahana J, Taura T, Silver PA. 1999. Interactions between a nuclear transporter and a subset of nuclear pore complex proteins depend on Ran GTPase. *Mol Cell Biol* **19**: 1547-1557.

Seedorf M, Silver PA. 1997. Importin/karyopherin protein family members required for mRNA export from the nucleus. *Proc Natl Acad Sci U S A* **94**: 8590-8595.

Sekar RB, Periasamy A. 2003. Fluorescence resonance energy transfer (FRET) microscopy imaging of live cell protein localizations. *J Cell Biol* **160**: 629-633.

Shaner NC, Campbell RE, Steinbach PA, Giepmans BN, Palmer AE, Tsien RY. 2004. Improved monomeric red, orange and yellow fluorescent proteins derived from Discosoma sp. red fluorescent protein. *Nat Biotechnol* **22**: 1567-1572.

Shcherbo D, Merzlyak EM, Chepurnykh TV, Fradkov AF, Ermakova GV, Solovieva EA, Lukyanov KA, Bogdanova EA, Zaraisky AG, Lukyanov S et al. 2007. Bright far-red fluorescent protein for whole-body imaging. *Nat Methods* **4**: 741-746.

Sherman F. 2002. Getting started with yeast. *Methods Enzymol* **350**: 3-41.

Shyu YJ, Hu CD. 2008. Fluorescence complementation: an emerging tool for biological research. *Trends Biotechnol* **26**: 622-630.

Shyu YJ, Liu H, Deng X, Hu CD. 2006. Identification of new fluorescent protein fragments for bimolecular fluorescence complementation analysis under physiological conditions. *Biotechniques* **40**: 61-66.

Sinturel F, Brechemier-Baey D, Kiledjian M, Condon C, Benard L. 2012. Activation of 5'-3' exoribonuclease Xrn1 by cofactor Dcs1 is essential for mitochondrial function in yeast. *Proc Natl Acad Sci U S A* **109**: 8264-8269.

Sjohamn J, Bath P, Neutze R, Hedfalk K. 2016. Applying bimolecular fluorescence complementation to screen and purify aquaporin protein:protein complexes. *Protein Sci* **25**: 2196-2208.

Sjohamn J, Hedfalk K. 2014. Unraveling aquaporin interaction partners. *Biochim Biophys Acta* **1840**: 1614-1623.

Snider J, Hanif A, Lee ME, Jin K, Yu AR, Graham C, Chuk M, Damjanovic D, Wierzbicka M, Tang P et al. 2013. Mapping the functional yeast ABC transporter interactome. *Nat Chem Biol* **9**: 565-572.

Solsbacher J, Maurer P, Bischoff FR, Schlenstedt G. 1998. Cse1p is involved in export of yeast importin alpha from the nucleus. *Mol Cell Biol* **18**: 6805-6815.

Song Q, Kumar A. 2012. An Overview of Autophagy and Yeast Pseudohyphal Growth: Integration of Signaling Pathways during Nitrogen Stress. *Cells* **1**: 263-283.

Song YB, Park CO, Jeong JY, Huh WK. 2014. Monitoring G protein-coupled receptor activation using an adenovirus-based beta-arrestin bimolecular fluorescence complementation assay. *Anal Biochem* **449**: 32-41.

Sorger D, Daum G. 2002. Synthesis of triacylglycerols by the acyl-coenzyme A:diacyl-glycerol acyltransferase Dga1p in lipid particles of the yeast Saccharomyces cerevisiae. *J Bacteriol* **184**: 519-524.

Stamatas GN, Southall M, Kollias N. 2006. In vivo monitoring of cutaneous edema using spectral imaging in the visible and near infrared. *J Invest Dermatol* **126**: 1753-1760.

Stoops JK, Wakil SJ. 1978. The isolation of the two subunits of yeast fatty acid synthetase. *Biochem Biophys Res Commun* **84**: 225-231.

Subach FV, Patterson GH, Manley S, Gillette JM, Lippincott-Schwartz J, Verkhusha VV. 2009. Photoactivatable mCherry for high-resolution two-color fluorescence microscopy. *Nat Methods* **6**: 153-159.

Sung MK, Ha CW, Huh WK. 2008. A vector system for efficient and economical switching of C-terminal epitope tags in Saccharomyces cerevisiae. *Yeast* **25**: 301-311.

Sung MK, Huh WK. 2007. Bimolecular fluorescence complementation analysis system for in vivo detection of protein-protein interaction in Saccharomyces cerevisiae. *Yeast* **24**: 767-775.

Sung MK, Lim G, Yi DG, Chang YJ, Yang EB, Lee K, Huh WK. 2013. Genome-wide bimolecular fluorescence complementation analysis of SUMO interactome in yeast. *Genome Res* **23**: 736-746.

Sung S, Li F, Park YB, Kim JS, Kim AK, Song OK, Kim J, Che J, Lee SE, Cho Y. 2014. DNA end recognition by the Mre11 nuclease dimer: insights into resection and repair of damaged DNA. *EMBO J* **33**: 2422-2435.

Tarassov K, Messier V, Landry CR, Radinovic S, Serna Molina MM, Shames I, Malitskaya Y, Vogel J, Bussey H, Michnick SW. 2008. An in vivo map of the yeast protein interactome. *Science* **320**: 1465-1470.

Tauchi-Sato K, Ozeki S, Houjou T, Taguchi R, Fujimoto T. 2002. The surface of lipid droplets is a phospholipid monolayer with a unique Fatty Acid composition. *J Biol Chem* **277**: 44507-44512.

Tromberg BJ, Shah N, Lanning R, Cerussi A, Espinoza J, Pham T, Svaasand L, Butler J. 2000. Non-invasive in vivo characterization of breast tumors using photon migration spectroscopy. *Neoplasia* **2**: 26-40.

Tsien RY. 1998. The green fluorescent protein. *Annu Rev Biochem* **67**: 509-544.

Vashist S, Cushman M, Shorter J. 2010. Applying Hsp104 to protein-misfolding disorders. *Biochem Cell Biol* **88**: 1-13.

Waadt R, Schmidt LK, Lohse M, Hashimoto K, Bock R, Kudla J. 2008. Multicolor bimolecular fluorescence complementation reveals simultaneous formation of alternative CBL/CIPK complexes in planta. *Plant J* **56**: 505-516.

Walther TC, Farese RV, Jr. 2012. Lipid droplets and cellular lipid metabolism. *Annu Rev Biochem* **81**: 687-714.

Wang II, Huang II. 2000. Adenovirus technology for gene manipulation and functional studies. *Drug Discov Today* **5**: 10-16.

Wendler P, Shorter J, Plisson C, Cashikar AG, Lindquist S, Saibil HR. 2007. Atypical AAA+ subunit packing creates an expanded cavity for disaggregation by the protein-remodeling factor Hsp104. *Cell* **131**: 1366-1377.

Wieland F, Siess EA, Renner L, Verfurth C, Lynen F. 1978. Distribution of yeast fatty acid synthetase subunits: three-dimensional model of the enzyme. *Proc Natl Acad Sci U S A* **75**: 5792-5796.

Wolins NE, Rubin B, Brasaemle DL. 2001. TIP47 associates with lipid droplets. *J Biol Chem* **276**: 5101-5108.

Yang Y, Dou SX, Ren H, Wang PY, Zhang XD, Qian M, Pan BY, Xi XG. 2008. Evidence for a functional dimeric form of the PcrA helicase in DNA unwinding. *Nucleic Acids Res* **36**: 1976-1989.

Yonehara M, Minami Y, Kawata Y, Nagai J, Yahara I. 1996. Heat-induced chaperone activity of HSP90. *J Biol Chem* **271**: 2641-2645.

Yoshikawa K, Tanaka T, Ida Y, Furusawa C, Hirasawa T, Shimizu H. 2011. Comprehensive phenotypic analysis of single-gene deletion and overexpression strains of Saccharomyces cerevisiae. *Yeast* **28**: 349-361.

Yu H, Braun P, Yildirim MA, Lemmens I, Venkatesan K, Sahalie J, Hirozane-Kishikawa T, Gebreab F, Li N, Simonis N et al. 2008. High-quality binary protein interaction map of the yeast interactome network. *Science* **322**: 104-110.

Zacharias DA, Violin JD, Newton AC, Tsien RY. 2002. Partitioning of lipid-modified monomeric GFPs into membrane microdomains of live cells. *Science* **296**: 913-

916.

Zeng X, Danquah MK, Chen XD, Lu Y. 2011. Microalgae bioengineering: From CO2 fixation to biofuel production. *Renewable and Sustainable Energy Reviews* **15**: 3252-3260.

Zhang T, Peli-Gulli MP, Yang H, De Virgilio C, Ding J. 2012. Ego3 functions as a homodimer to mediate the interaction between Gtr1-Gtr2 and Ego1 in the ego complex to activate TORC1. *Structure* **20**: 2151-2160.

Zhang X, Beuron F, Freemont PS. 2002. Machinery of protein folding and unfolding. *Curr Opin Struct Biol* **12**: 231-238.

Zhou J, Lin J, Zhou C, Deng X, Xia B. 2011. An improved bimolecular fluorescence complementation tool based on superfolder green fluorescent protein. *Acta Biochim Biophys Sin (Shanghai)* **43**: 239-244.

Zordan RE, Beliveau BJ, Trow JA, Craig NL, Cormack BP. 2015. Avoiding the ends: internal epitope tagging of proteins using transposon Tn7. *Genetics* **200**: 47-58.

국문 초록
효모에서의 단백질 호모머 형성에 대한 글로벌 분석

세포 내에서 단백질 간 상호 작용의 발생 및 발생 장소, 그리고 동적 변화에 대한 연구는 단백체학의 기능적 연구에서 매우 중요한 위치를 차지한다. 때문에 지난 수십 년에 걸쳐 생물학 분야에서는 단백질 상호 작용을 감지할 수 있는 다양한 분석 방법들이 개발되어 왔다. 이분자 형광 상보 기법(Bimolecular fluorescence complementation, BiFC)는 살아있는 세포 내에서 목표 단백질의 구조 및 기능에 최소한의 변형 만을 가하면서 단백질 간 상호 작용을 확인하고, 상호 작용의 발생 장소 역시 시각화할 수 있다는 점에서 다른 방법들에 비교했을 때 큰 장점을 가진다.

이전 연구에서, 이분자 형광 상보 기법을 게놈 수준에서 단백질 간 상호 작용 연구에 적용할 수 있도록 하기 위해서 본 연구실에서는 Venus 단백질의 N 말단 절편인 VN이 효모 단백질의 C 말단에 부착되어 내생 프로모터의 조절 하에 발현되는 효모 균주들의 모음인 VN 라이브러리를 제작한 바 있다. 이 라이브러리는 효모의 전체 단백체의 약 95%에 달하는 총 5,911 개의 균주로 구성되어 있으며 이를 이용하여 효모의 SUMO 상호 작용 단백질들을 성공적으로 분리해 내었다. 본 연구에서는, 앞서 제작된 VN 라이브러리와 함께 이분자 형광 상보 기법에 적용할 수 있도록 VC 라이브러리의 제작을 시도하였다. 효모 단백질의 C 말단에 Venus 단백질의 C 말단 절편인 VC가 부착되어 내생 프로모터 조절 하에 발현이 되도록 만들어진 메이팅 타입 알파 효모 균주 총 5,671개의 제작에 성공하였고, 이는 효모의 전체 단백체 중 약 91%에 달하는 수치이다. 완성된 VC 라이브러리의 신뢰성 및 용이성을 확인하기 위해 VN 라이브러리와 함께 이분자 형광 상보 기법에 적용하여 효모 내에 존재하고 있는 동종 복합체를 이루는 단백질들을 관찰하였다. 이 시도를 통하여 우리는 186개의 동종 복합체 형성 단백질을 찾아내는 데 성공하였으며, 이 중의 104개는 기존의 연구들에서는 관찰된 바 없는 새로운 동종 복합체 형성 단백질들이다. 동종 복합체 형성 단백질들의 세포 내 위치, 유의미하게 높은 비중으로 관찰되는 GO (Gene ontology) 등을 분석하였으며, 효모의 필수 영양 요소 중 하나인 질소가 고갈되었을 때 각각의 동종 복합체 형성 단백질들이 어떠한 변화 양상을 보이는지를 함께 분석하였다. 또한, 186개의 단백질 중 lipid droplet 에 존재하는 Pet10 단백질에 대해서는 질소 고갈 상황에서의 본 단백질의 동종 복합체 형성의 증가가 효모 세포 내의 중성 지방의 증가와 연관이 있음을 확인하였다. 본 연구를 통해서 신중하고 다양한 방법으로 확인된 VC 라이브러리의 신뢰도 및 사용의 용이성은 향후 이를 이용한 이분자 형광 상보 기법을 통한 단백질 간 상호 작용의 연

구 시스템이 자연적인 세포 내에서의 단백질 간 상호 작용을 보다 체계적으로 분석하고 다양한 interactome을 얻는 것에 있어 귀중한 연구 자원이 될 것을 시사하고 있다.

주요어: 이분자 형광 상보 기법, 단백질 상호 작용, 단백질 호모머, Saccharomyces cerevisiae, Pet10, 지질 대사.

학번: 2010-20309